

CARBON DIOXIDE-SELECTIVE MEMBRANES AND THEIR  
APPLICATIONS IN HYDROGEN PROCESSING

DISSERTATION

Presented in Partial Fulfillment of the Requirement for  
the Degree Doctor of Philosophy in the Graduate  
School of The Ohio State University

By

Jian Zou, M.S.

\*\*\*\*\*

The Ohio State University

2007

Dissertation Committee:

Professor W.S. Winston Ho, Advisor

Professor Kurt W. Koelling

Professor Barbara Wyslouzil

Approved by

---

Advisor

Chemical Engineering Graduate Program

## ABSTRACT

Fuel cells, which are regarded as a promising energy conversion approach in the 21st century, are now receiving increasing attention worldwide. In most cases, hydrogen is the preferred fuel for fuel cells, especially for proton-exchange membrane fuel cells (PEMFCs). One key issue in the development of PEMFC is how to generate hydrogen from the available hydrocarbon fuels. Most feasible strategies consist of a reforming step followed by the water gas shift (WGS) reaction. The resulting synthesis gas (syngas) still consists of 0.5 – 1.0% CO, which needs to be reduced to less than 10 ppm to meet the requirement of PEMFCs. Therefore, a further CO clean-up step is usually used to decrease CO concentration.

In the present work, new CO<sub>2</sub>-selective membranes were synthesized and their applications for fuel cell fuel processing and synthesis gas purification were investigated. In order to enhance CO<sub>2</sub> transport across membranes, the synthesized membranes contained both mobile and fixed site carriers in crosslinked poly(vinyl alcohol). The effects of crosslinking, membrane composition, feed pressure, water content, and temperature on transport properties were investigated. The membranes have shown a high permeability and a good CO<sub>2</sub>/H<sub>2</sub> selectivity and maintained their separation performance up to 170°C. One type of these membranes showed a permeability of 8000

Barrers (1 Barrer =  $10^{-10}$  cm<sup>3</sup> (STP).cm / (cm<sup>2</sup>.s.cm.Hg)) and a CO<sub>2</sub>/H<sub>2</sub> selectivity of 290 at 110°C. This membrane had a permeability of 1200 Barrers and a CO<sub>2</sub>/H<sub>2</sub> selectivity of 33 even at 170°C. The applications of the synthesized membranes were demonstrated in a CO<sub>2</sub>-removal experiment, in which the CO<sub>2</sub> concentration in retentate was decreased from 17% to less than 10 ppm.

With such membranes, there are several options to reduce the CO concentration of syngas. One option is to develop a WGS membrane reactor, in which both the low temperature WGS reaction and the CO<sub>2</sub>-removal take place. Another option is to use a proposed process consisting of a CO<sub>2</sub>-removal membrane module followed by a conventional low-temperature WGS reactor. A third option is to use methanation after the CO<sub>2</sub>-removal, one of the most widely used processes for the CO clean-up step. Experimental results showed that CO concentration was reduced to below 10 ppm with all three approaches. In the membrane reactor, a CO concentration of less than 10 ppm and a H<sub>2</sub> concentration of greater than 50% (on the dry basis) were achieved at various flow rates of a simulated autothermal reformat. In the proposed CO<sub>2</sub>-removal/WGS process, with more than 99.5 % CO<sub>2</sub> removed from the synthesis gas, the reversible WGS was shifted forward so that the CO concentration was decreased from 1.2% to less than 10 ppm (dry), which is the requirement for PEMFC. The WGS reactor had a gas hourly space velocity of 7650 h<sup>-1</sup> at 150°C and the H<sub>2</sub> concentration in the outlet was more than 54.7% (dry).

The applications of the synthesized CO<sub>2</sub>-selective membranes for high-pressure synthesis gas purification were also studied. Synthesis gas is the primary source for hydrogen as well as an intermediate for a broad range of chemicals. The separation of CO<sub>2</sub> from synthesis gas is a critical step to obtain high purity hydrogen in many industrial plants, especially refinery plants. We studied the synthesized polymeric CO<sub>2</sub>-selective membranes for synthesis gas purification at feed pressures higher than 200 psia and temperatures ranging from 100 to 150°C. The effects of feed pressure, microporous support, temperature, and permeate pressure were investigated using a simulated synthesis gas containing 20% carbon dioxide and 80% hydrogen. The membranes synthesized showed best CO<sub>2</sub> permeability and CO<sub>2</sub>/H<sub>2</sub> selectivity at 110°C. At a feed pressure of 220 psia, the CO<sub>2</sub> permeability and CO<sub>2</sub>/H<sub>2</sub> selectivity reached 756 Barrers and 42, respectively, whereas at a feed pressure of 440 psia, the CO<sub>2</sub> permeability was 391 Barrers and the CO<sub>2</sub>/H<sub>2</sub> selectivity was about 25.

Dedicated to my wife and my parents

## ACKNOWLEDGMENTS

I wish to thank my advisor, Dr. W. S. Winston Ho, for his support and guidance during all these years. Without his support and guidance, it would have been impossible for me to finish my doctoral research and dissertation. His dedication to work and research has always inspired me.

I am grateful to many faculty of the Department of Chemical and Biomolecular Engineering including Dr. Jeffrey J. Chalmers, Dr. Kurt W. Koelling, Dr. L. James Lee, Dr. Umit S. Ozkan, and Dr. Barbara Wyslouzil, who served as my qualifying exam, candidacy exam, or dissertation committee members and generously provided their time and valuable input about my research and dissertation. I am also grateful to Dr. Liang-Shih Fan, who has given me invaluable inspirations for my research.

I also thank my colleagues, Jin Huang, He Bai, Chi Yen, Bishnu Mandal, Hsien-Chen Ma, Philip Chang, Yit-Hong Tee, and Gaurav Shil, for their generous help and stimulating discussions. I wish to thank Cameron Begg for the training and technical support that he gave me for scanning electron microscopy. I also appreciate the help from Leigh Evrard and Paul Green, who helped me set up the experimental equipment. I would also like to thank Rick Watson for measuring the surface areas of the catalyst.

I am grateful to Süd-Chemie Inc. for the detailed technical support on the water gas shift catalyst. I am indebted to many tutors at the Center for the Study and Teaching of Writing, who patiently helped me in correcting my grammar and stylistic errors in my manuscripts and dissertation.

This research was supported by the U.S. Department of Energy (Grant/Contract No. DE-FC36-03AL68510), the Ohio Department of Development (Wright Center of Innovation Grant No. 342-0561), The Ohio State University, and Shell Oil Company. I would like to thank Chris Plotz and BHA Technologies, Inc., Debbie de la Cruz and GE Infrastructure, Dr. Norman N. Li and NL Chemical Technology, Inc. for giving us the BHA microporous Teflon supports, GE E500A and A1 microporous polysulfone supports, and NL microporous polysulfone supports, respectively.

## VITA

August 8, 1975 ..... Born - Leshan, Sichuan Province, China

1997 ..... B.S. Polymerization Engineering, Beijing University of  
Chemical Technology, Beijing, China

2000 ..... M.S. Materials Science, Beijing University of Chemical  
Technology, Beijing, China

2002 - present ..... Graduate Research Associate, The Ohio State University

## PUBLICATIONS

### Research Publications

1. J. Zou, W.S.W. Ho, CO<sub>2</sub>-selective polymeric membranes containing amines in crosslinked poly(vinyl alcohol), *Journal of Membrane Science* 286 (2006) 310-321
2. Y.H. Tee, J. Zou, W.S.W. Ho, CO<sub>2</sub>-selective membranes containing dimethylglycine mobile carriers and polyethylenimine fixed carrier, *Journal of Chinese Institute of Chemical Engineers*, 37 (2006) 37-47
3. B. Sun, J. Zou, Poly(vinyl alcohol)-based polyelectrolyte pervaporation membranes, *Annals of the New York Academy of Sciences*, 984 (2003) 386-400

4. J. Li, C. Chen, B. Han, Y. Peng, J. Zou, W. Jiang, Laboratory and pilot-scale study on dehydration of benzene by pervaporation, *Journal of Membrane Science*, 203 (2002) 127-136
5. C. Chen, B. Han, J. Li, T. Shang, J. Zou, W. Jiang, A new model on the diffusion of small molecule penetrants in dense polymer membranes, *Journal of Membrane Science*, 187 (2001) 109-118
6. J. Zou, B. Sun, C. Chen, Studies on poly(vinyl alcohol)-based polyelectrolyte pervaporation membranes. (I) synthesis of polyelectrolytes, *Membrane Science and Technology* (written in Chinese) 21 (2001) 21-24
7. J. Zou, B. Sun, C. Chen, Polyelectrolyte membranes for pervaporation, *Polymer Bulletin* (written in Chinese) 55 (2001) 44-52

### **FIELD OF STUDY**

Major Field: Chemical Engineering

## TABLE OF CONTENTS

	Page
Abstract .....	ii
Dedication .....	v
Acknowledgments .....	vi
Vita .....	viii
List of Tables .....	xiii
List of Figures .....	xvi
List of Symbols .....	xx
Chapters:	
1. Introduction .....	1
2. Synthesis of new carbon dioxide-selective membranes .....	7
2.1 Introduction .....	7
2.2 Experimental .....	13
2.3 Results and discussion .....	18
2.4 Conclusions .....	36
3. Carbon dioxide-selective membrane reactors.....	67
3.1 Introduction .....	67
3.2 Experimental .....	73

3.3	Thermodynamic analysis .....	77
3.4	Results and discussion .....	78
3.5	Conclusions .....	85
4.	Hydrogen purification by carbon dioxide-removal membrane followed by water gas shift reaction .....	95
4.1	Introduction .....	95
4.2	Thermodynamic analysis .....	96
4.3	Experimental .....	98
4.4	Results and discussion .....	100
4.5	Conclusions .....	105
5.	Carbon dioxide-selective membranes for high pressure applications .....	114
5.1	Introduction .....	114
5.2	Experimental .....	116
5.3	Results and discussions .....	117
5.4	Conclusions .....	127
6.	Summary and future work .....	138
6.1	Summary .....	138
6.2	Future work .....	140
	Appendix A .....	142

List of References ..... 160

## LIST OF TABLES

Table	Page
2.1	Effects of percentage of KOH and AIBA-K on separation performance ..... 25
2.2	Effects of types of fixed-site carriers on separation performance ..... 27
2.3	Separation performance vs. feed gas water content ..... 30
2.4	Comparison of membrane performance with literature results ..... 34
3.1	Process gas composition (dry basis) and conditions for WGS / methanation in an ammonia plant ..... 68
3.2	Equilibrium constants for methanation ..... 69
3.3	WGS reaction constant from different equations ..... 78
3.4	Retentate CO concentration vs. temperature for membrane reactor experiments ..... 84
4.1	Results of CO <sub>2</sub> removal / water gas shift process ..... 103
4.2	Results of CO <sub>2</sub> removal / methanation process ..... 104
5.1	Microporous supports investigated ..... 119
5.2	Flux vs. partial pressure difference for a membrane on the microporous Teflon support ..... 120
5.3	Flux vs. partial pressure difference for a membrane on the E500A microporous polysulfone support ..... 122
5.4	Summary of key data at 110°C (Feed: 20% CO <sub>2</sub> and 80% H <sub>2</sub> ) ..... 125

5.5	Comparison of separation performance with membranes reported in the literature .....	126
A.1	Casting solution composition of a formaldehyde-crosslinked membrane .....	143
A.2	Casting solution composition of a glutaraldehyde-crosslinked membrane .....	144
A.3	Casting solution composition of a maleic anhydride-crosslinked membrane .....	145
A.4	Solution composition of crosslinking PVA with divinyl sulfone .....	145
A.5	Separation results of a maleic acid-crosslinked membrane at various temperatures .....	146
A.6	Separation results of a glutaraldehyde-crosslinked membrane at various temperatures .....	147
A.7	Separation results of a formaldehyde-crosslinked membrane at various temperatures .....	148
A.8	Separation results of a formaldehyde-crosslinked membrane .....	150
A.9	Separation results of a formaldehyde-crosslinked membrane at various temperatures .....	151
A.10	Separation results of a formaldehyde-crosslinked membrane .....	152
A.11	Separation results of a formaldehyde-crosslinked membrane containing polyethylenimine at various temperatures .....	152
A.12	Separation results of a formaldehyde-crosslinked membrane	

	at various temperatures .....	153
A.13	Casting solution composition of a glutaraldehyde-crosslinked membrane for high-pressure CO <sub>2</sub> /H <sub>2</sub> separation .....	154
A.14	Maximum water rate for a dry gas flowrate of 30 cm <sup>3</sup> /min .....	155
A.15	Separation results of a glutaraldehyde-crosslinked membrane at high pressures .....	156
A.16	Separation results of a membrane on BHA Teflon support at high pressures .....	157
A.17	Separation results of a membrane on BHA Teflon support at high pressures .....	158
A.18	Separation results of a membrane on NL-2 microporous polysulfone support at high pressures .....	159

## LIST OF FIGURES

Figure	Page
1.1 Steps and current options for on-site and on-board processing to produce H <sub>2</sub> for PEMFCs .....	6
2.1 Schematic of facilitated transport membranes .....	38
2.2 Schematic of gas permeation apparatus .....	39
2.3 SEM image of the cross-section of the membrane synthesized .....	40
2.4 SEM image of the cross-section of the membrane synthesized .....	41
2.5 Chemical structure of poly(vinyl alcohol) and crosslinking agents .....	42
2.6 Diagram of the crosslinking reaction of poly(vinyl alcohol) with formaldehyde .....	43
2.7 FTIR ATR spectra of PVA membranes .....	44
2.8 FTIR ATR spectra of PVA membranes .....	45
2.9 Diagram of the crosslinking reaction of poly(vinyl alcohol) with glutaraldehyde .....	46
2.10 DSC curve of poly(vinyl alcohol) (M <sub>w</sub> = 89,000 – 98,000, hydrolysis degree > 99%) .....	47
2.11 DSC curve of poly(allylamine) [prepared from poly(allylamine) hydrochloride, M <sub>w</sub> = 68,000] .....	48
2.12 DSC curve of formaldehyde-crosslinked membrane	

	[50% PVA/60mol% crosslinked with formaldehyde, 20.3% AIBA-K, 18.7% KOH, 11% poly(allylamine)] .....	49
2.13	DSC curve of formaldehyde-crosslinked membrane [50% PVA/60mol% crosslinked with glutaraldehyde, 20.3% AIBA-K, 18.7% KOH, 11% poly(allylamine)] .....	50
2.14	Diagram of the crosslinking reaction of poly(vinyl alcohol) with maleic anhydride .....	51
2.15	Diagram of the crosslinking reaction of poly(vinyl alcohol) with divinyl sulfone .....	52
2.16	Schematic of CO <sub>2</sub> transport mechanism in the membranes synthesized .....	53
2.17	Chemical structure of carriers for CO <sub>2</sub> transport .....	54
2.18	Effect of feed pressure on CO <sub>2</sub> flux and permeability .....	55
2.19	Effect of feed pressure on H <sub>2</sub> flux .....	56
2.20	Effect of feed pressure on CO <sub>2</sub> /H <sub>2</sub> selectivity .....	57
2.21	CO <sub>2</sub> permeability vs. water content on the sweep side .....	58
2.22	CO <sub>2</sub> /H <sub>2</sub> selectivity vs. water content on the sweep side.....	59
2.23	CO <sub>2</sub> and H <sub>2</sub> permeabilities vs. temperature .....	60
2.24	CO <sub>2</sub> /H <sub>2</sub> and CO <sub>2</sub> /N <sub>2</sub> selectivities vs. temperature .....	61
2.25	CO <sub>2</sub> and H <sub>2</sub> permeabilities vs. temperature .....	62
2.26	CO <sub>2</sub> /H <sub>2</sub> and CO <sub>2</sub> /N <sub>2</sub> selectivities vs. temperature .....	63

2.27	CO <sub>2</sub> /CO selectivity vs. temperature .....	64
2.28	CO <sub>2</sub> permeability and CO <sub>2</sub> /H <sub>2</sub> selectivity vs. temperature .....	65
2.29	CO <sub>2</sub> permeability and CO <sub>2</sub> /H <sub>2</sub> selectivity vs. time .....	66
3.1	Schematic of the test unit for membrane reactors .....	86
3.2	Schematic of the water gas shift membrane reactor .....	87
3.3	Retentate gas composition during catalyst reduction .....	88
3.4	Retentate gas composition during catalyst reduction .....	89
3.5	Retentate gas composition during catalyst reduction .....	90
3.6	Retentate CO concentration vs. feed water concentration in the circular membrane reactor .....	91
3.7	Retentate CO concentration vs. feed flow rate in the rectangular WGS membrane reactor .....	92
3.8	Equilibrium CO concentration without CO <sub>2</sub> removal vs. temperature .....	93
3.9	Retentate H <sub>2</sub> concentration vs. feed flow rate in the rectangular membrane reactor .....	94
4.1	Schematic of the CO <sub>2</sub> -removal membrane / Water gas shift process .....	107
4.2	Equilibrium CO concentration of WGS reaction vs. temperature for the synthesis gas feed from autothermal reforming of gasoline with air .....	108
4.3	Equilibrium CO concentration of WGS reaction vs. temperature with for the synthesis gas feed after CO <sub>2</sub> removal .....	109

4.4	CO <sub>2</sub> concentration in retentate vs. feed flow rate in the rectangular cell .....	110
4.5	CO <sub>2</sub> concentration in retentate vs. feed flow rate in the rectangular cell .....	111
4.6	H <sub>2</sub> concentration in retentate vs. feed flow rate in the rectangular cell .....	112
4.7	Equilibrium CO concentration of WGS reaction after CO <sub>2</sub> removal vs. temperature .....	113
5.1	Effect of feed pressure on CO <sub>2</sub> permeability .....	129
5.2	Effect of feed pressure on CO <sub>2</sub> /H <sub>2</sub> selectivity .....	130
5.3	Maximum water content vs. temperature .....	131
5.4	Effect of temperature on CO <sub>2</sub> permeability .....	132
5.5	Effect of temperature on CO <sub>2</sub> /H <sub>2</sub> selectivity .....	133
5.6	Effect of temperature on CO <sub>2</sub> flux and H <sub>2</sub> flux .....	134
5.7	Effect of temperature on CO <sub>2</sub> permeability .....	135
5.8	Effect of temperature on CO <sub>2</sub> /H <sub>2</sub> and CO <sub>2</sub> /N <sub>2</sub> selectivities .....	136
5.9	Effects of permeate pressure on CO <sub>2</sub> permeability and CO <sub>2</sub> /H <sub>2</sub> selectivity.....	137

## LIST OF SYMBOLS

$C_A$	CO <sub>2</sub> concentration
$C_{AB}$	CO <sub>2</sub> – carrier reaction product concentration
$D_A$	diffusivity coefficient for CO <sub>2</sub>
$D_{AB}$	diffusivity coefficient for CO <sub>2</sub> – carrier reaction product
$H_A$	Henry's law constant for unreacted CO <sub>2</sub> in the membrane
$H_{AB}$	Henry's law constant for CO <sub>2</sub> – carrier reaction product
$H_{A p_1}$	Henry's law constant for unreacted CO <sub>2</sub> in the membrane at $p_1$
$H_{A p_2}$	Henry's law constant for unreacted CO <sub>2</sub> in the membrane at $p_2$
$H_{AB p_1}$	Henry's law constant for CO <sub>2</sub> -carrier reaction product concentration at $p_1$
$H_{AB p_2}$	Henry's law constant for CO <sub>2</sub> -carrier reaction product concentration at $p_2$
$K$	reaction equilibrium constant
$k_f$	rate constant of the forward reaction between CO <sub>2</sub> and carrier
$k_r$	rate constant of the reverse reaction between CO <sub>2</sub> and carrier
$l$	membrane thickness
$N_i$	steady-state flux of component $i$
$P_i$	permeability of component $i$
$p$	pressure

$p_1$	CO <sub>2</sub> partial pressure on high pressure side of membrane
$p_2$	CO <sub>2</sub> partial pressure on low pressure side of membrane
$p_{1c}$	critical CO <sub>2</sub> partial pressure at which carrier saturation occurs
$p_{1m}$	CO <sub>2</sub> partial pressure in the membrane on high pressure side of membrane
$p_{2m}$	CO <sub>2</sub> partial pressure in the membrane on low pressure side of membrane
$R$	ideal gas constant
$R_f$	mass transfer resistance due to the forward reactions between CO <sub>2</sub> and carrier
$R_r$	mass transfer resistance due to the reverse reactions between CO <sub>2</sub> and carrier
$R_t$	total mass transfer resistance for CO <sub>2</sub> across membrane
$T$	temperature
$x_i$	mole fractions of components $i$ in retentate stream
$y_i$	mole fractions of components $i$ in permeate stream
Greek letters	
$\alpha_{ij}$	selectivity of component $i$ over component $j$
$\Delta H$	heat of reaction
$\Delta p_i$	partial pressure difference of component $i$

## **CHAPTER 1**

### **INTRODUCTION**

The separation of carbon dioxide from other gases, such as hydrogen, nitrogen, carbon monoxide, and methane, has various potential applications, including the purification of synthesis gas to obtain high purity hydrogen for fuel cells, the removal of carbon dioxide from natural gas for natural gas sweetening, the separation of carbon dioxide from flue gas for the greenhouse gas sequestration, and the removal of carbon dioxide from breathing air in spacecrafts or spacesuits. Conventional CO<sub>2</sub> separation processes, like amine scrubbing, are highly energy-consuming, and they require regeneration steps and additional chemicals (Dortmundt and Doshi, 1999). Their applications were also limited in certain areas, such as onboard hydrogen production, offshore natural gas sweetening, and the life support system in a spacecraft, due to their system complexity and large sizes and weights. Membrane separation provides one prospective approach to capturing and concentrating CO<sub>2</sub> with reduced energy consumption, enhanced weight and space efficiency, and operational simplicity.

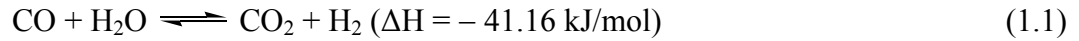
The primary objectives of this dissertation are to develop new CO<sub>2</sub>-selective membranes and to use these membranes to obtain high purity hydrogen for fuel cells and the petrochemical industry. Fuel cells, which are regarded as a promising energy

conversion approach, are now receiving increasing attention worldwide. Fuel cells are electrochemical devices that convert the chemical energy of a fuel directly into electricity and intrinsically energy-efficient and environment-friendly. They can achieve a system efficiency as high as 70 – 80% (including heat utilization) in electric power plants by using solid oxide fuel cells (versus the current efficiency of 30 – 37% with combustion) and 40 – 50% efficiency for transportation by using proton-exchange membrane fuel cells (versus the current efficiency of 20 – 35% with internal combustion engines) (Song, 2002).

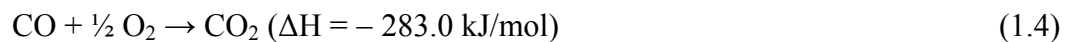
There are mainly five types of fuel cells: phosphoric acid, proton-exchange membrane, molten carbonate, solid oxide, and alkaline fuel cells. Among all these types of fuel cells, the proton-exchange membrane fuel cell (PEMFC) is considered as the best candidate for automotives and small stationary power generators due to its high power density, low operation temperature, and fast startup (Ghenciu, 2002; Song, 2002).

Hydrogen, natural gas, and methanol can be used as fuels for fuel cells. Yet in most cases, hydrogen is the preferred fuel for fuel cells, especially for PEMFCs, because hydrogen has the highest reactivity and a clean emission (Dicks, 1996; Song, 2002). Hydrogen is currently generated on large scale from hydrocarbon fuels, such as natural gas. Most commercially used strategies to generate hydrogen from hydrocarbon fuels consist of a reforming reaction, followed by the water gas shift (WGS) reaction (Eq. 1.1). The reforming reaction converts hydrocarbon fuels, such as natural gas, gasoline, and diesel, to synthesis gas containing hydrogen, carbon monoxide, and carbon dioxide, while the WGS reaction converts carbon monoxide into hydrogen. In modern hydrogen plants,

two stages of WGS reaction are usually used. Iron based catalysts are used in the first stage at high inlet temperature (typically in the range of 370 – 400°C). In the second stage, copper based catalysts are used at much lower inlet temperature (typically in the range of 170 – 220°C) in order to obtain high conversion. Cu/ZnO/Al<sub>2</sub>O<sub>3</sub> is the most widely used commercial low-temperature WGS catalyst.



The resulting synthesis gas (syngas) from WGS still consists of a significant amount of CO, usually about 0.5 to 1%, which is controlled by the equilibrium of the reversible WGS reaction (Twigg, 1989). However, even a small amount of CO deteriorates the platinum electrode and thus the fuel cell performance. CO concentration in the fuel feed usually needs be reduced to less than 10 parts per million (ppm) (Song, 2002). So a further CO clean-up step is usually used to decrease CO concentration to meet the requirement of PEMFCs. Fig. 1.1 shows the steps and some of current options for on-site and on-board processing to produce H<sub>2</sub> for PEMFCs. For the CO clean-up step, several methods are used or under development, including methanation (Eqs. 1.2 and 1.3), preferential oxidation (Eq. 1.4), pressure swing absorption, sorption-enhanced hydrogen production, and membrane separation.



Gas separation membrane provides economical and effective options to remove CO<sub>2</sub> and to improve the hydrogen processing for fuel cells. The present work was on synthesizing novel CO<sub>2</sub>-selective membranes and using such membranes to develop new approaches for hydrogen processing for fuel cells.

With the membranes synthesized in this work, there are several options for the CO clean-up. One option is to develop a WGS membrane reactor. A membrane reactor combines a reactor with a semi-permeable membrane that extracts product(s) of the reaction in one unit. In our case, the WGS reaction takes place in the reactor, and our CO<sub>2</sub>-selective membrane removes CO<sub>2</sub> from the reactor at the same time. By removing CO<sub>2</sub>, one of the products, the reversible WGS can be shifted forward so that the CO concentration can be further decreased. This application requires membrane to maintain its high separation performance and thermal stability to 150 to 180°C. Another option is to use a novel two-stage WGS process that I proposed. This process consists of a CO<sub>2</sub>-removal membrane module followed by a conventional low-temperature WGS (LTWGS) reactor. The conventional low-temperature WGS reactor runs at a temperature ranging from 150 to 160°C, which is the most suitable temperature range for LTWGS, to decrease CO concentration to ppm levels. A third option is to use methanation after the CO<sub>2</sub>-removal with our membranes. These options were investigated and compared.

The applications of the synthesized CO<sub>2</sub>-selective membranes for high-pressure synthesis gas purification were also studied. Synthesis gas is the primary source for hydrogen as well as an intermediate for a broad range of chemicals. The separation of CO<sub>2</sub> from synthesis gas is a critical step to obtain high purity hydrogen in many industrial

plants, especially refinery plants. In comparison with removing H<sub>2</sub> from synthesis gas, removing CO<sub>2</sub> is more advantageous because a high-purity H<sub>2</sub> product is recovered at the feed gas pressure, thereby eliminating expensive recompression of H<sub>2</sub> for the subsequent process. High flux and CO<sub>2</sub>/H<sub>2</sub> selectivity more than 30 are required for the membranes, since higher flux means less membrane area and less equipment investment and higher CO<sub>2</sub>/H<sub>2</sub> selectivity means less H<sub>2</sub> loss. Using polymeric CO<sub>2</sub>-selective membranes for synthesis gas purification was studied in this dissertation. The effects of feed pressure, microporous support, temperature, and permeate pressure were investigated using a simulated synthesis gas containing 20% carbon dioxide and 80% hydrogen.

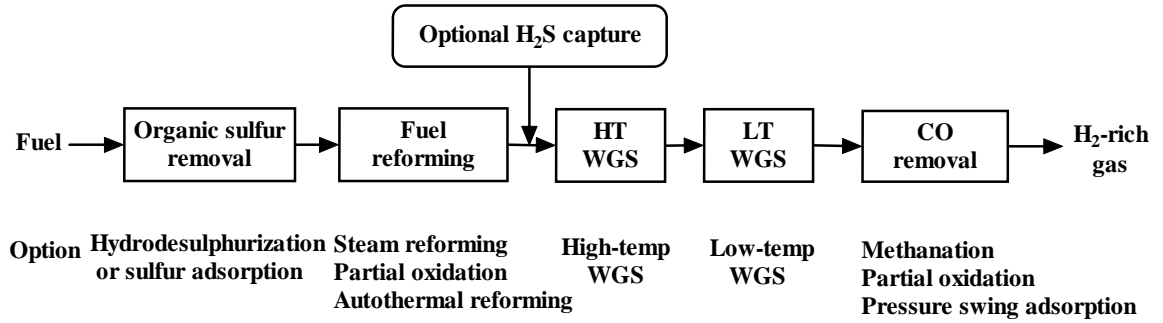


Figure 1.1: Steps and current options for on-site and on-board processing to produce  $H_2$  for PEMFCs. (Song, 2002)

## CHAPTER 2

### SYNTHESIS OF NEW CARBON DIOXIDE-SELECTIVE MEMBRANES

#### 2.1 Introduction

The separation of CO<sub>2</sub> from other gases, such as H<sub>2</sub>, N<sub>2</sub>, CO, and CH<sub>4</sub>, plays important roles in various industries, especially petroleum and chemical industries. The applications of CO<sub>2</sub> separation include the purification of synthesis gas to obtain high purity hydrogen for fuel cells, the removal of CO<sub>2</sub> from natural gas for natural gas sweetening, the separation of CO<sub>2</sub> from flue gas for the greenhouse gas sequestration, and the removal of CO<sub>2</sub> from breathing air in submarines, spacecrafts, or spacesuits. The separation of CO<sub>2</sub> from a gas mixture can be achieved via various separation processes.

Conventional CO<sub>2</sub> separation processes include adsorption of CO<sub>2</sub> onto a solid, such as zeolite and activated carbon, and absorption into a liquid, such as aqueous alkanolamine solutions and promoted hot potassium carbonate solutions. However, these conventional processes are highly energy-consuming and require regeneration steps and additional chemicals. Their applications were also limited in certain areas, such as on-board hydrogen production, off-shore natural gas sweetening, and life support systems in spacecrafts and submarines, due to their system complexity and large size. Over the last

40 years, separations using synthetic membranes have been widely adopted for environmental and energy applications in numerous industries. Using membrane for CO<sub>2</sub> separation provides one promising approach to capturing and concentrating CO<sub>2</sub> with reduced energy consumption, enhanced weight and space efficiency, and operational simplicity.

There are two parameters to characterize the separation performance of a membrane. One is the selectivity (or the separation factor), which is defined as

$$\alpha_{ij} = \frac{y_i / y_j}{x_i / x_j} \quad (2.1)$$

Another parameter is the permeability  $P_i$ , which is defined as

$$P_i = \frac{N_i}{\Delta p_i / l} \quad (2.2)$$

The common unit of  $P_i$  is Barrer, which is  $10^{-10} \text{ cm}^3 \text{ (STP) cm} / (\text{cm}^2 \text{ s cmHg})$ . ( $P_i / l$ ) is referred to as the permeance, and its common unit is the gas permeation unit (GPU), which is  $10^{-6} \text{ cm}^3 \text{ (STP)} / (\text{cm}^2 \text{ s cmHg})$ . If the downstream pressure is negligible compared to the upstream pressure, the selectivity can be expressed as

$$\alpha_{ij} = \frac{P_i}{P_j} = \left( \frac{D_i}{D_j} \right) \left( \frac{S_i}{S_j} \right) \quad (2.3)$$

where  $D_i / D_j$  is the diffusivity selectivity, which is the ratio of the diffusivity coefficients of components  $i$  and  $j$ . The solubility selectivity,  $S_i / S_j$ , is the ratio of the solubility of components  $i$  and  $j$  (Ho and Sirkar, 1992).

For the CO<sub>2</sub> separation membranes, two separation mechanisms are mainly used. One mechanism is the solution-diffusion mechanism. The separation of CO<sub>2</sub> from other gases is achieved by the solution-diffusion rate differences between CO<sub>2</sub> and the other gases across the membranes. But, with these types of membranes, an increase in selectivity is often accompanied by a decrease in flux, and vice versa (Gottschlich et al., 1988). For the application of CO<sub>2</sub>/H<sub>2</sub> separation, it is challenging to achieve a high CO<sub>2</sub>/H<sub>2</sub> selectivity since H<sub>2</sub> usually exhibits an unfavorably higher diffusivity coefficient than CO<sub>2</sub> does. As a result, in most conventional polymeric membranes, the CO<sub>2</sub>/H<sub>2</sub> selectivities are usually less than one (Lin and Freeman, 2005a).

Facilitated transport membranes offer an attractive method of achieving high selectivity while also maintaining high flux. This type of membrane is based on facilitated transport, which combines diffusion with the reversible reaction of a targeted component with reactive carriers inside the membrane. There are two main types of reactive carriers: the mobile carrier, which can move freely across the membrane, and the fixed-site carrier or fixed carrier, which only has limited mobility around its equilibrium position. Fig. 2.1 is a schematic diagram of the membranes with these two types of carriers. In a mobile carrier membrane, the mobile carriers react with the targeted component on the feed side of the membrane, move across the membrane, and release this component on the permeate side. The carrier-component complex diffuses in parallel with the molecular diffusion of the component. As a result, the diffusion of this component is augmented or facilitated. The other components, which do not react with the reactive carriers, diffuse across the membrane down their concentration gradients via only the solution-diffusion mechanism. In a fixed-site carrier membrane, the targeted

component reacts at one carrier site and then hops to the next unreacted carrier site along the direction of the concentration gradient via the “hopping” mechanism (Cussler et al., 1989). Compared with the conventional membranes based on the solution-diffusion mechanism, facilitated transport membranes have several advantages:

- They are often highly selective, especially at low concentration driving forces.
- High permeability can be achieved when the concentration driving force is very low.
- They can maintain both high permeability and high selectivity at the same time.

These advantages have made facilitated transport membranes very attractive in certain areas, such as the removal of CO<sub>2</sub> from synthesis gas containing H<sub>2</sub>, CO, and CO<sub>2</sub>. The facilitated transport membranes can achieve very high CO<sub>2</sub>/H<sub>2</sub> selectivities.

Yet, facilitated transport membranes have a characteristic, which is known as the carrier saturation phenomenon. When the partial pressure of the targeted component is equal to or higher than a critical value, the carrier saturation occurs, in which the concentration of the component-carrier complex attains its maximum value and becomes a constant (Ho and Dalrymple, 1994; Way and Noble, 1992). In other words, further increase in the partial pressure of the component will not increase the concentration of the component-carrier complex; therefore, the flux will remain constant.

Facilitated transport membranes have been studied for a long time. The earliest report was on the facilitated transport of oxygen through the hemoglobin solutions (Scholander, 1960). Since then, new membranes and new applications have emerged in many areas. Today, the potential applications of facilitated transport membranes include acid gas removal, heavy metal recovery, bio separations, O<sub>2</sub> / N<sub>2</sub> separation, and olefin / paraffin separation.

Facilitated transport CO<sub>2</sub>-selective membranes reported in the literature include supported liquid membranes (SLMs), ion-exchange membranes, and membranes with reactive carriers bonded in the matrices of membranes. For supported liquid membranes, Ward and Robb (1967) immobilized an aqueous bicarbonate-carbonate solution into a porous support and obtained a CO<sub>2</sub>/O<sub>2</sub> separation factor of 1,500. Meldon et al. (1977) investigated the facilitated transport of CO<sub>2</sub> through an immobilized alkaline liquid film. Their experimental results confirmed that weak acid buffers significantly increased the CO<sub>2</sub> transport. However, such SLMs have two major problems: loss of solvent, and loss or degradation of carriers. The loss of solvent is caused by its evaporation especially at a high temperature and / or caused by its permeation through a microporous support under a high trans-membrane pressure. The loss of carrier occurs when the carrier solution is forced to permeate through the support ('washout'), and the degradation of carriers is led by the irreversible reaction of the carrier with impurities or the feed gas stream (LeBlanc et al., 1980; Way et al., 1987).

Ion-exchange facilitated transport membranes was first reported by LeBlanc et al. (1980) to address the instability issue of SLMs. In the ion-exchange membranes, ionic carriers were retained inside the membranes by electrostatic forces; therefore, minimizing the washout of carriers. Way et al. (1987) and Yamaguchi et al. (1996) used perfluorosulfonic acid ionomer cation-exchange membranes containing amines as the carriers. The ion-exchange membrane used by Langevin et al. (1993) was sulfonated styrene-divinylbenzene in a fluorinated matrix, and the transport model based on the Nernst-Planck equation was developed. Matsuyama et al. (1994; 1996) grafted acrylic acid and methacrylic acid on different substrates and used various diamines, diethylenetriamine and triethylenetetramine as the carriers. They also blended poly(acrylic acid) with poly(vinyl alcohol) to prepare membranes and introduced monoprotinated ethylenediamine into the membranes by ion-exchange and used it as the carrier (Matsuyama et al., 2001). Other approaches were also proposed to solve these instability problems of SLMs. Quinn et al. (1995) developed membranes consisting of molten salt hydrates, which were nonvolatile and immobilized in microporous polypropylene supports. Teramoto et al. (2001; 2002; 2004) developed a “bulk flow liquid membrane”, in which a carrier solution was forced to permeate through the membrane and then was recycled continuously.

Membranes with reactive carriers bonded in the membrane matrices were reported by several researchers and were believed to have better stability than SLMs. Yamaguchi et al. (1995) developed membranes with poly(allylamine) and compared them with ion-exchange membranes containing amines as the counterions. Matsuyama et al. (1999) heat-treated poly(vinyl alcohol)-polyethylenimine membranes to improve their stability

and to increase the amount of polyethylenimine retained inside the membranes, which increased the water content, therefore increasing the diffusivity of the carrier complex. Quinn and Laciak (1997) developed polyelectrolyte membranes based on poly(vinylbenzyltrimethylammonium fluoride) (PVBTAf) and achieved a CO<sub>2</sub>/H<sub>2</sub> selectivity of 87 at 23°C. They also blended fluoride-containing organic and inorganic salts, like CsF, into the PVBAT membranes and obtained a CO<sub>2</sub> permeance more than four times of that of PVBAT (Quinn et al., 1997). Ho and his co-workers synthesized crosslinked poly(vinyl alcohol) membranes containing polyamines as fixed carriers and aminoacid salts as mobile carriers (Ho, 1997; 2000; Tee et al., 2006). They reported membranes containing dimethylglycine (DMG) salts and polyethylenimine (PEI), and found that both CO<sub>2</sub> permeability and CO<sub>2</sub>/H<sub>2</sub> selectivity of the membranes increased as temperature increased in the temperature range of 50 – 100°C (Tee et al., 2006).

Models for facilitated transport on different systems have been developed and studied by many researchers (Cussler et al., 1989; Donaldson and Lapinas, 1982; Gottschlich et al., 1988; Ho and Dalrymple, 1994; Hong et al., 1996; Kang et al., 1996; Noble, 1990; 1991; 1992; Smith and Quinn, 1979; Ward, 1970).

## 2.2 Experimental

### 2.2.1 Materials

Poly(vinyl alcohol) (99+% hydrolyzed powder, M<sub>w</sub> = 89,000 – 98,000) was obtained from Sigma-Aldrich (St. Louis, MO). Poly(allylamine hydrochloride) (M<sub>w</sub> = 60,000) was purchased from Polysciences Inc. (Warrington, PA). 2-Aminoisobutyric

acid, formaldehyde (37 wt% aqueous solution), glutaraldehyde (50 wt% aqueous solution), maleic anhydride, divinyl sulfone, and potassium hydroxide were purchased from Sigma-Aldrich and used without further purification. Microporous Teflon supports (thickness: 60  $\mu\text{m}$ , average pore size: 0.2  $\mu\text{m}$ ) were donated by BHA Technologies (Kansas City, MS). GE E500A microporous polysulfone supports (thickness: about 60  $\mu\text{m}$  excluding an non-woven fabric support, average pore size: 0.05  $\mu\text{m}$ ) and GE A1 microporous polysulfone supports (thickness: about 60  $\mu\text{m}$  excluding an non-woven fabric support, average pore size: 0.009  $\mu\text{m}$ ) were given by GE Infrastructure (Vista, CA). Two feed gases with certified compositions were purchased from Praxair Inc. (Danbury, CT) for the gas permeation tests: one consisting of 20%  $\text{CO}_2$ , 40%  $\text{H}_2$ , and 40%  $\text{N}_2$ , and the other consisting of 17%  $\text{CO}_2$ , 1.0%  $\text{CO}$ , 45%  $\text{H}_2$ , and 37%  $\text{N}_2$  (all on dry basis).

### 2.2.2 Membrane preparation

Polymeric  $\text{CO}_2$ -selective membranes with the thin-film-composite structure were prepared by casting an aqueous solution onto microporous supports. The microporous supports used in the study were mainly the BHA Teflon<sup>®</sup> (a trademark of DuPont, Delaware) supports (thickness: 60  $\mu\text{m}$ , average pore size: 0.2  $\mu\text{m}$ , BHA Technologies, Kansas City, MS), GE E500A microporous polysulfone supports (thickness: about 60  $\mu\text{m}$  excluding an non-woven fabric support, average pore size: 0.05  $\mu\text{m}$ , GE Infrastructure Vista, CA), and GE A1 microporous polysulfone supports (thickness: about 60  $\mu\text{m}$  excluding an non-woven fabric support, average pore size: 0.009  $\mu\text{m}$ , GE Infrastructure Vista, CA). The aqueous solution was prepared by mixing water with poly(vinyl alcohol),

formaldehyde (crosslinking agent), potassium hydroxide, 2-aminoisobutyric acid (AIBA) potassium salt, and poly(allylamine). The exact amount of these chemicals is listed in Table A.1 of Appendix A. PVA was first dissolved in water at 80°C under stirring. A stoichiometric amount of formaldehyde and a certain amount of potassium hydroxide were added into the PVA aqueous solution to achieve a 60 mol% degree of crosslinking. The PVA / formaldehyde / KOH solution was heated at about 80°C for 16 hours under stirring. Separately, an amino acid salt solution was prepared by adding a stoichiometric amount of potassium hydroxide into an aqueous 2-aminoisobutyric acid (AIBA) solution with mixing. A proper amount of the AIBA-potassium solution was then added into the PVA / formaldehyde / KOH solution with stirring for 30 minutes.

Free poly(allylamine) was obtained by mixing poly(allylamine hydrochloride) with potassium hydroxide (1.2 equiv.) in methanol overnight. The resulting potassium chloride was precipitated from the solution. Then methanol was evaporated at room temperature and replaced with water as the solvent. A proper amount of aqueous poly(allylamine) solution was added slowly into the PVA / formaldehyde / KOH / AIBA-K solution with stirring for about 30 minutes. Finally, the solution was centrifuged at 8000 rpm for five minutes before casting. The thickness of coating was controlled by using a GARDCO adjustable micrometer film applicator (Paul N. Gardner Company, Pompano Beach, FL). The cast membranes were first dried at room temperature inside a hood overnight, ~ 16 hours, to remove most of the water. Then they were heated to 120°C inside a muffle furnace and kept at this temperature for six hours. The heat-treatment ensured the complete removal of water and crosslinking reaction of PVA with the crosslinking agent.

A Mitutoyo Electronic Indicator (Model: 543-252B, Mitutoyo America Corporation, Aurora, IL) was used to measure the membrane thickness with an accuracy of about  $\pm 0.5 \mu\text{m}$ . The thickness of the active membrane layer was also confirmed with scanning electron microscopic pictures. The active layer was dense and about 10 to 90  $\mu\text{m}$  thick after heat-treatment. The thickness of a membrane to be mentioned hereafter all refers to the thickness of the active layer.

### 2.2.3 Gas permeation measurements

The gas permeation measurements were conducted by using a permeation cell inside an oven (Bemco Inc., Simi Valley, CA) for the accurate control of temperature. The schematic diagram of the permeation apparatus is shown in Fig. 2.2. A circular stainless steel cell with an active membrane area of  $45.60 \text{ cm}^2$  was used for measuring transport properties of the membranes. In this cell, the feed and the sweep gas flows were counter-current. As mentioned earlier, two feed gases were used: one consisting of 20%  $\text{CO}_2$ , 40%  $\text{H}_2$ , and 40%  $\text{N}_2$ , and the other consisting of 17%  $\text{CO}_2$ , 1.0%  $\text{CO}$ , 45%  $\text{H}_2$ , and 37%  $\text{N}_2$ . The second composition was used to simulate the composition of the synthesis gas from autothermal reforming of gasoline with air. Argon was used as the sweep gas for the ease of gas chromatography (GC) analysis.

Gas flow rates were controlled by Brooks flow-meters (Brooks Instrument, Hatfield, PA). The feed and the sweep gas rates were kept at 30 and 30 cc/min, respectively, unless indicated otherwise. A proper amount of water was pumped into two vessels using two Varian Prostar 210 pumps (Varian Inc., Palo Alto, CA) to control the water contents of the feed gas and the sweep gas, respectively, before they entered the

permeation cell. The pressure of the retentate was controlled by a back-pressure regulator and measured with a pressure gauge. The pressure on the permeate side was set close to atmospheric pressure via a near-ambient pressure regulator and measured with a pressure gauge.

Both the retentate and permeate streams leaving the oven were cooled down to ambient temperature in their respective water knockout vessels, which removed the water condensed. The compositions for both the retentate and permeate gases were then analyzed using an Agilent 6890N gas chromatograph with two thermal conductivity detectors (TCDs) (Agilent Technologies, Palo Alto, CA). Helium and argon were used as the carrier gases for the front and back TCD detectors, respectively. The GC columns used were SUPELCO Carboxen<sup>®</sup> 1004 micro-packed columns (Sigma-Aldrich, St. Louis, MO). Each of the membrane permeation measurements was taken after the membrane had been exposed to the feed and permeate streams under a specific condition (temperature, pressure, and water rate) for at least six hours, which allowed for steady-state permeation.

#### 2.2.4 Membrane characterization

Scanning electron microscopic (SEM) images of membranes were taken using an XL-30 ESEM scanning electron microscope (FEI Company, Hillsboro, OR). The SEM samples were freeze-fractured in liquid nitrogen, dried in a vacuum oven, and then coated with gold. The chemical structure of the membranes was characterized with a Nicolet 470 Fourier transform infrared (FTIR) spectrometer with an attenuated total reflectance (ATR) accessory (Thermo Electron Co., Waltham, MA) with Zn/Se crystal.

Thermal analysis of the membranes including differential scanning calorimetry (DSC) and thermal gravity analysis were conducted with PerkinElmer Diamond DSC and Pyris<sup>®</sup> 1 TGA (PerkinElmer Life and Analytical Sciences, Wellesley, MA), respectively. During the thermal analysis using DSC, aluminum pans with a volume of 30  $\mu\text{L}$  were used. The heating rate was 10 $^{\circ}\text{C}/\text{min}$ , and the temperature range was from  $-40^{\circ}\text{C}$  to 140 $^{\circ}\text{C}$ .  $T_{\text{mg}}$ , the middle point temperature, was used as the  $T_{\text{g}}$ , according to the ASTM D 3418 standard (Standard Test Method for Enthalpies of Fusion and Crystallization of Polymers by Differential Scanning Calorimetry).

## 2.3 Results and discussion

### 2.3.1 Membrane morphology

The membranes synthesized were consisted of a thin active layer and a porous support. The thin active layer contained both mobile and fixed carriers in crosslinked poly(vinyl alcohol). The porous support was microporous Teflon or polysulfone microporous membranes. This composite structure minimizes the mass transfer resistance while maximizes the mechanical strength. Figs. 2.3 and 2.4 show the scanning electron microscopic (SEM) images of the cross-section of a membrane on the GE E500A microporous polysulfone support. It can be seen that the membrane consisted of two portions. The top portion was a dense active layer, which provided separation, and the bottom portion was the microporous support, which provided mechanical strength. In Fig.

2.3, the polyester fabric of the polysulfone membrane is shown at the bottom of the image. The polyester fabric provided mechanical strength and flexibility to the membrane.

### 2.3.2 Membrane crosslinking

Poly(vinyl alcohol) (PVA) was chosen as the matrix of the active layer because of its good compatibility with both mobile and fixed carriers, high hydrophilicity, and good film forming ability. However, PVA without crosslinking dissolves in water easily at a temperature of 70°C or more (Pritchard, 1970). For certain applications, where a temperature higher than 100°C is preferred, crosslinking of PVA to improve its thermal stability is critical. The previous work on the membranes containing dimethylglycine (DMG) salts and polyethylenimine (PEI) in formaldehyde-crosslinked PVA showed that the membranes were only able to maintain good CO<sub>2</sub> permeability and CO<sub>2</sub>/H<sub>2</sub> selectivity up to 100°C (Tee et al., 2006). However, the thermal stability of these membranes needs improvement, since a working temperature of more than 150°C is required for applications such as water gas shift membrane reactors. In this work, formaldehyde and glutaraldehyde were mainly used the crosslinking agents. The crosslinking conditions of these two crosslinkers as well as other crosslinking agents including maleic anhydride and divinyl sulfone were investigated. The chemical structures of poly(vinyl alcohol) and these four crosslinkers are shown in Fig. 2.5.

Using formaldehyde to crosslink PVA has been used for a long time (Pritchard, 1970; Jegal and Lee, 1999; Li et al., 2002). The reaction can be easily conducted in aqueous solution with strong acids as catalyst. In aqueous acid solutions, the reaction

between formaldehyde and PVA forms cyclic formal rings between adjacent hydroxyl groups until 80% of the hydroxyl groups are substituted, and there is little tendency to form intermolecular acetal linkages (Pritchard, 1970). The acetal links formed are stable in neutral and basic solutions. In the present study, strong bases instead of strong acids were used as catalyst for this crosslinking, since the carriers used in the membranes were basic. The diagram of this reaction is depicted in Fig. 2.6. During the preparation of the casting solution for the membranes as described earlier in this chapter, the PVA / formaldehyde / KOH solution was heated at about 80°C for 16 hours under stirring. The viscosity of the solution increased significantly, which indicated some extent of the crosslinking of PVA. However, all components remained soluble in the solution. The acetal linkages formed during this step are presumably intramolecular acetal linkages. The cast membranes were first dried at room temperature inside a hood overnight to remove most of the water. Then they were heated to 120°C inside a muffle furnace and kept at this temperature for six hours. This heat-treatment ensured the complete removal of water and crosslinking reaction of PVA with formaldehyde, and presumably formed more intermolecular acetal linkages. Heat-treatments at temperatures of 140 and 160°C were also investigated, but some of the membranes that were heat-treated at 140 and 160°C for six hours could not hold feed side pressure; therefore, heat-treatment at 120°C was used for formaldehyde-crosslinked membranes.

Fourier transform infrared (FTIR) spectrometer was used to confirm the crosslinking of the membranes. Figs. 2.7 and 2.8 present the FTIR spectra of the membranes of pure PVA and the PVA crosslinked with formaldehyde. There were some peaks present in all these spectra, which can be attributed to the  $-CH_2-$  and  $-OH$  groups

of PVA. The strong and broad peak of  $3340\text{ cm}^{-1}$  was due to the O–H stretch. The peaks of  $2940$  and  $2910\text{ cm}^{-1}$  can be attributed to the stretching C–H. The peak of  $1100\text{ cm}^{-1}$  was due to the C–O stretching and O–H bending (Pritchard, 1970). On the other hand, there were some peaks only present in the spectra of crosslinked PVA. The peak of  $1590\text{ cm}^{-1}$  in the spectra of PVA crosslinked with formaldehyde was probably due to the stretching of C=O of formaldehyde. For the pure PVA membrane, there was no peak at  $1144\text{ cm}^{-1}$ , while for the membranes prepared from the PVA solution crosslinked with formaldehyde at  $80^\circ\text{C}$  for five minutes and 16 hours, the  $1144\text{ cm}^{-1}$  peak was present both before and after the heat-treatment. The peak of  $1144\text{ cm}^{-1}$  can be attributed to the –C–O–C– stretch (Jegal and Lee, 1999; Lambert et al., 1998), which confirms the formation of acetal linkages during the crosslinking.

Glutaraldehyde was also used as the crosslinking agent for PVA. Fig. 2.9 shows the reaction diagram. It should be noted that although this diagram only shows the intermolecular acetal linkages, intramolecular acetal linkages may also be present. In this study, bases, mostly potassium hydroxide, was used to catalyses this reaction. The procedure to prepare a casting solution was similar to the procedure to prepare formaldehyde-crosslinked membranes described previously in this chapter. The exact amount of the chemicals used is listed in Table A.2. During the preparation of the casting solution for the membranes, the solution of PVA / glutaraldehyde / KOH was heated at about  $80^\circ\text{C}$  for about 100 to 120 minutes under stirring before the AIBA-K solution was added. The reaction was found to be faster than that between formaldehyde and PVA. The viscosity of the solution increased sharply, which indicated the crosslinking of PVA. However, all components remained soluble in the solution. The cast membranes were

first dried at room temperature inside a hood overnight to remove most of the water. Then they were heated to 120°C inside a muffle furnace and kept at this temperature for six hours.

The crosslinking of PVA with formaldehyde and glutaraldehyde was confirmed by Differential Scanning Calorimetry (DSC). For pure PVA with a molecular weight of 89,000 to 98,000 and a hydrolysis degree more than 99%, the glass transition temperature,  $T_g$ , measured was 68°C as shown in Fig. 2.10. The sample was prepared by dissolving PVA in water, then casting the solution onto a Teflon plate, and drying it inside a vacuum oven at 80°C overnight. The glass transition temperature of pure poly(allylamine) measured was -23°C as shown in Fig. 2.11. This value agrees with the value of -26°C reported in literature (Kim et al., 2002; Shin et al., 2002). For formaldehyde-crosslinked PVA membrane [50% PVA / 60 mol% degree of crosslinking, 20.3% AIBA-K, 18.7% KOH, 11% poly(allylamine)], the glass transition temperature was 79°C as shown in Fig. 2.12. For glutaraldehyde-crosslinked PVA membrane [50% PVA / 15 mol% degree of crosslinking, 20.3% AIBA-K, 18.7% KOH, 11% poly(allylamine)], the glass transition temperature was 84°C as shown in Fig. 2.13. Compared with the pure PVA, the formaldehyde and glutaraldehyde crosslinked PVA membranes had higher glass transition temperatures, which suggest better thermal stability.

Crosslinking PVA with maleic anhydride was investigated. Fig. 2.14 shows the reaction diagram. Although this diagram only shows the intermolecular ester linkages, it should be noted that intramolecular ester linkages may also be present. In this study,

KOH was used to catalyze this reaction. Table A.3 lists the amount of each chemical used in the preparation of a maleic anhydride-crosslinked membrane. During the preparation of the casting solution for the membranes, PVA was dissolved in water at 80°C to make a 14 wt% solution. A stoichiometric amount of maleic anhydride equivalent to a crosslinking degree of 20 mol% was added into the solution. In 5 minutes, a KOH solution was added into the solution. The color of PVA solution didn't change. The solution was kept at 55°C for 55 minutes. Then the AIBA-K solution was added into the PVA solution slowly. The viscosity of the solution increased, but all components remained soluble in the solution. The cast membranes were first dried at room temperature inside a hood overnight to remove most of the water. Then they were heated to 120°C inside a muffle furnace and kept at this temperature for six hours. However, the maleic anhydride-crosslinked membranes showed worse thermal stability than the membranes crosslinked with formaldehyde and glutaraldehyde. Table A.5 shows that the CO<sub>2</sub>/H<sub>2</sub> selectivity of the maleic anhydride-crosslinked membrane dropped to less than 5 at 170°C, while the glutaraldehyde-crosslinked membrane still had a CO<sub>2</sub>/H<sub>2</sub> selectivity around 70 at this temperature shown in Table A.6. The formaldehyde-crosslinked membrane had a CO<sub>2</sub>/H<sub>2</sub> selectivity around 50 at this temperature shown in Table A.7.

Divinyl sulfone was also investigated as the crosslinking agent for PVA. Fig. 2.15 shows the reaction diagram. PVA was dissolved in water at 80°C to make a 14 wt% solution. A stoichiometric amount of divinyl sulfone equivalent to a crosslinking degree of 4.0 mol% was added into the solution. In 5 minutes, a KOH solution was added into the solution. The solution formed a jelly mass immediately, which suggested that the linkages could be mostly intermolecular and that the crosslinking reaction was fast and

complete. Table A.4 of Appendix A lists the amount of each chemical used in this experiment. Since a homogeneous solution was needed for membrane casting, divinyl sulfone was not further used as the crosslinking agent for PVA.

Of these four crosslinking agents, formaldehyde and glutaraldehyde were chosen as the crosslinking agents for PVA because these two crosslinkers provided better thermal stability than maleic anhydride did. The separation performance of the formaldehyde-crosslinked membranes will be reported mainly in this chapter, while the results of glutaraldehyde-crosslinked membranes will be reported in detail in Chapter 5.

### 2.3.3 Membrane compositions

In the synthesized membranes, both mobile carriers and fixed-site carriers were incorporated into the crosslinked PVA to facilitate the CO<sub>2</sub> transport across the membranes. The most used composition was 50 wt% PVA, 18.3 wt% KOH, 20.7 wt% AIBA-K, and 11.0 wt% poly(allylamine), unless otherwise indicated. Formaldehyde equivalent to a 60 mol% of crosslinking degree was added into the casting solution. Fig. 2.16 presents a schematic of the CO<sub>2</sub> transport mechanism in the membranes. The membranes contained both 2-aminoisobutyric acid-K and KHCO<sub>3</sub>-K<sub>2</sub>CO<sub>3</sub> (converted from KOH) as the mobile carriers, and poly(allylamine) as the fixed-site carrier for CO<sub>2</sub> transport. The chemical structures of both 2-aminoisobutyric acid (AIBA) and poly(allylamine) were illustrated in Fig. 2.17. 2-Aminoisobutyric acid is a sterically-hindered amine, and its reaction with CO<sub>2</sub> is depicted in Eq. 2.4 (Sartori et al., 1987). Poly(allylamine) contains un-hindered, primary amino groups, and their reactions are

shown in Eq. 2.5 (Sartori et al., 1987). The reaction mechanism of the CO<sub>2</sub> with KHCO<sub>3</sub>-K<sub>2</sub>CO<sub>3</sub> was presumably similar to that of hindered amine promoted potassium carbonate described in Eq. 2.6 (Sartori and Savage, 1983):



Membrane	Z2004-1-73	Z2004-1-77	Z2004-1-67-1
Testing	U1-2004-2-45	U1-2004-2-49	U1-2004-2-51
Membrane composition	50 wt% PVA (60 mol% formaldehyde crosslinked), 29.0 wt% AIBA-K, 10.0 wt% KOH, 11% poly(allylamine)	50 wt% PVA (60 mol% formaldehyde crosslinked), 24.8 wt% AIBA-K, 14.2 wt% KOH, 11% poly(allylamine)	50 wt% PVA (60 mol% formaldehyde crosslinked), 20.7 wt% AIBA-K, 18.3 wt% KOH, 11% poly(allylamine)
Thickness (μm)	49.7	33.2	60.7
α (CO <sub>2</sub> /H <sub>2</sub> )	297.3	78.6	242.2
Permeability (Barrers)	895.6	798.0	4732.8
Permeance (GPU)	18.02	24.04	77.97

Tested at T = 110°C; water rate = 0.03 cm<sup>3</sup>/min (both sides); feed pressure = 30.3 – 30.5 psia.

Table 2.1: Effects of percentage of KOH and AIBA-K on separation performance.

The membranes contained both 2-aminoisobutyric acid-K and  $\text{KHCO}_3\text{-K}_2\text{CO}_3$  (converted from KOH) as the mobile carriers. To investigate the contribution of each carrier to the total  $\text{CO}_2$  transport, we prepared the membranes with different percentages of AIBA-K and KOH. The effects of the percentage of each mobile carrier on the separation performance were presented in Table 2.1. As we can see from the table, all these membranes had the 50 wt% of PVA and 11 wt% of poly(allylamine). The membrane containing the highest percentage of KOH showed the highest  $\text{CO}_2$  permeance, while the membrane containing the lowest percentage of KOH showed the lowest  $\text{CO}_2$  permeance. This can be attributed to the higher diffusivity of  $\text{KHCO}_3 / \text{K}_2\text{CO}_3$  than that of AIBA-K.

The membranes contained poly(allylamine) as the fixed-site carrier for the  $\text{CO}_2$  transport. Another amine-containing polymer, poly(ethylenimine), was also studied as a fixed-site carrier for the  $\text{CO}_2$  transport. The results from the membranes containing poly(allylamine) and poly(ethylenimine), respectively, were summarized in Table 2.2. As we can see from the table, both membranes contained 50 wt% of PVA, 20.7 wt% of AIBA-K, and 18.3 wt% of KOH. The membrane containing 11.0 wt% of poly(allylamine) showed higher  $\text{CO}_2$  permeance and better  $\text{CO}_2/\text{H}_2$  selectivity than the membrane containing 11.0 wt% of polyethylenimine. The former had a  $\text{CO}_2/\text{H}_2$  selectivity of 33 even at  $170^\circ\text{C}$  shown in Table A.12, while the latter's  $\text{CO}_2/\text{H}_2$  selectivity dropped to less than 5 at  $150^\circ\text{C}$  shown in Table 2.2 and Table A.11. Therefore, poly(allylamine) was chosen as the fixed-site carrier for the membranes used in the study.

Membrane	Z2004-1-81	Z2004-1-114
Testing	U1-2004-2-57	U1-2004-2-89
Membrane composition	50 wt% PVA (60 mol% formaldehyde crosslinked), 20.7 wt% AIBA-K, 18.3 wt% KOH, 11% polyethylenimine	50 wt% PVA (60 mol% formaldehyde crosslinked), 20.7 wt% AIBA-K, 18.3 wt% KOH, 11% poly(allylamine)
Thickness ( $\mu\text{m}$ )	37.3	68.8
$\alpha$ ( $\text{CO}_2/\text{H}_2$ ) at 110°C	217.7	292.6
$\alpha$ ( $\text{CO}_2/\text{H}_2$ ) at 150°C	2.6	100.8
Permeance at 110°C (GPU)	46.46	86.51
Permeance at 150°C (GPU)	38.39	25.82

Tested at feed pressure = 28.2 – 30.5 psia.

Table 2.2: Effects of types of fixed-site carriers on separation performance.

The transport of  $\text{CO}_2$  across the membrane is enhanced by the facilitated transport with the reactions mentioned above, and the flux equation for the  $\text{CO}_2$  transport can be expressed as follows (Ho and Dalrymple, 1994):

$$N_A = D_A(C_{A|p1} - C_{A|p2})/l + D_{AB}(C_{AB|p1m} - C_{AB|p2m})/l \quad (2.7)$$

In this equation, the first term on the right-hand side is the flux contributed by physical solubility, while the second term is contributed by chemical reactions. The non-reacting gases, like  $\text{H}_2$ ,  $\text{N}_2$ ,  $\text{CO}$  and  $\text{CH}_4$ , do not have chemical association with the carriers and therefore can only be transported by diffusion, which is limited by their low solubility on

the highly polar sites in the membranes (Quinn et al., 1995). For these non-reacting gases, the flux equation for the diffusion step in the membrane is the first term on the right-hand side of Eq. 2.7 only.

#### 2.3.4 Effects of feed pressure on separation performance

The effects of feed pressure on CO<sub>2</sub> flux and permeability, H<sub>2</sub> flux, and CO<sub>2</sub>/H<sub>2</sub> selectivity were investigated using a membrane with a thickness of ~ 60 μm on the BHA microporous Teflon support. The feed gas consisted of 20% CO<sub>2</sub>, 40% H<sub>2</sub>, and 40% N<sub>2</sub>. Fig. 2.18 illustrates the effects of the feed pressure on CO<sub>2</sub> flux and permeability. As illustrated in this figure, CO<sub>2</sub> flux increased first linearly with the feed pressure and then approached a constant value. This can be explained with the carrier saturation phenomenon. As described by Ho and Dalrymple (1994), when the partial pressure of CO<sub>2</sub> is equal to or higher than a critical CO<sub>2</sub> partial pressure,  $p_{1c}$ , the carrier saturation occurs, in which the concentration of CO<sub>2</sub>-carrier reaction product attains its maximum value,  $C_{AB, max}$ , and becomes constant. In other words, further increase in the partial pressure of CO<sub>2</sub> will not increase the concentration of CO<sub>2</sub>-carrier reaction product. This can be expressed as follows:

$$C_{AB|p_1} = H_{AB|p_1} p_1 = C_{AB, max} = \text{constant} \quad \text{when } p_1 \geq p_{1c} \quad (2.8)$$

Compared with its facilitated transport, the physical solution and diffusion of CO<sub>2</sub> in the membrane is negligible. Therefore, the total CO<sub>2</sub> flux becomes constant eventually as the feed pressure increases.

As demonstrated in Fig. 2.18, CO<sub>2</sub> permeability decreased when the feed pressure increased. This can also be explained by using the carrier saturation phenomenon. In Eq. 2.2, in order to maintain the equality, increasing the CO<sub>2</sub> partial pressure,  $p_1$ , will not further increase the CO<sub>2</sub> flux, since all the carriers have already reacted with CO<sub>2</sub> and attained the maximum capacities. Thus, the CO<sub>2</sub> permeability will decrease.

Fig. 2.19 depicts the effect of feed pressure on H<sub>2</sub> flux. Unlike CO<sub>2</sub> flux, H<sub>2</sub> flux increased linearly with the feed pressure. This is because H<sub>2</sub> has no chemical association with carriers. Its sorption in the membrane can be described by the Henry's law, and its flux usually increases linearly with the feed pressure (Zolandz and Fleming, 1992).

Fig. 2.20 depicts the effect of feed pressure on CO<sub>2</sub>/H<sub>2</sub> selectivity. As depicted in this figure, the CO<sub>2</sub>/H<sub>2</sub> selectivity decreased as the pressure increased. Again, this can be explained using the carrier saturation phenomenon described earlier that CO<sub>2</sub> permeability reduces as the pressure increases. As a result, the selectivity is reduced as the pressure increases, since H<sub>2</sub> permeability does not subject to the carrier saturation phenomenon and usually does not change with pressure significantly.

### 2.3.5 Effects of water content on separation performance

In this study, both the feed and the sweep gases were fed with controlled amounts of water before they entered the permeation cell. The effects of water content on the membrane separation performance at 120°C and 150°C were investigated. The feed gas consisted of 20% CO<sub>2</sub>, 40% H<sub>2</sub>, and 40% N<sub>2</sub>. Fig. 2.21 depicts the CO<sub>2</sub> permeability as a function of the water concentration on the sweep side. As the water concentration on the

sweep side increased, CO<sub>2</sub> permeability increased almost linearly. When the water content was increased from 58 % to 93 % (mol), the CO<sub>2</sub> permeability at 120°C increased from 3,700 to as high as 8,200 Barrers, while the permeability at 150°C increasing from 920 to 2,700 Barrers. These increases were presumably due to two reasons: (1) higher water content on the sweep side raised the water retention inside the membrane, thus increased the mobility of both mobile and fixed carriers; (2) higher water content on the sweep side diluted the CO<sub>2</sub> permeated to the sweep side, thus increased the driving force for the CO<sub>2</sub> transport. The increase of CO<sub>2</sub> permeability with increasing gas water content was also reported by Quinn et al. (Quinn and Laciak, 1997; Quinn et al., 1997).

Fig. 2.22 shows the CO<sub>2</sub>/H<sub>2</sub> selectivity as a function of the water concentration on the sweep side at 120°C and 150°C. The CO<sub>2</sub>/H<sub>2</sub> selectivities at both temperatures rose as the water concentration on the sweep side increased. With a sweep water content of 93 mol%, the CO<sub>2</sub>/H<sub>2</sub> selectivities at 120°C and 150°C reached 450 and 270, respectively. The increase could be explained by the rise of CO<sub>2</sub> transport rate while the transport of H<sub>2</sub> was not affected much by the increase of the water content.

Feed water rate (cm <sup>3</sup> /min)	Feed water content (mol%)	CO <sub>2</sub> permeability (Barrer)	CO <sub>2</sub> /H <sub>2</sub> Selectivity
0.03	41	6950	398
0.06	59	9710	523

T = 120°C, feed pressure = 29.1 psia, sweep water rate = 0.12 cm<sup>3</sup>/min (85 mol%).

Table 2.3: Separation performance vs. feed gas water content.

The water content on the feed side also had significant effects on CO<sub>2</sub> permeability and CO<sub>2</sub>/H<sub>2</sub> selectivity as shown in Table 2.3. Both CO<sub>2</sub> permeability and CO<sub>2</sub>/H<sub>2</sub> selectivity increased as the water content in the feed stream was raised. This might be explained by that the higher water content on the feed side raised the water retention inside the membrane, therefore increased the mobility of both mobile and fixed carriers. As a result, the CO<sub>2</sub> transport was enhanced, while the transport of H<sub>2</sub> was not significantly affected.

In the present study, argon was used as the sweep gas only due to the ease of gas chromatography analysis. In real applications, N<sub>2</sub>, air, or steam can be used to sweep CO<sub>2</sub> on the low-pressure side of the membrane to obtain a high driving force for the separation. It is feasible to use steam alone as the sweep gas, therefore permeated CO<sub>2</sub> can be easily separated from steam and then be ready for sequestration. Steam can also enhance the separation performance for the reasons mentioned earlier.

#### 2.3.6 Effects of temperature on separation performance

The effects of temperature on CO<sub>2</sub> permeability, CO<sub>2</sub>/H<sub>2</sub>, CO<sub>2</sub>/N<sub>2</sub>, and CO<sub>2</sub>/CO selectivity were studied in the temperatures range of 100°C to 180°C using membranes on the BHA microporous Teflon support.

Fig. 2.23 illustrates the effects of temperature on CO<sub>2</sub> permeability and H<sub>2</sub> permeability from 110°C to 150°C with fixed water rates (feed: 0.03 cm<sup>3</sup>/min resulting in 41 mol% water vapor in the feed; sweep: 0.03 cm<sup>3</sup>/min resulting in 58 mol% water vapor in the sweep). As illustrated in this figure, CO<sub>2</sub> permeability decreased as temperature increased. This was presumably due to the reduction of water retention in the membrane as temperature increased, since the mobility of the mobile and fixed carriers and the reaction rates of CO<sub>2</sub> with the carriers were affected by the water content of the membrane as described before. The figure also shows that H<sub>2</sub> permeability only slightly decreased as temperature increased. This might be explained by the fact that H<sub>2</sub> transport was not affected by the facilitated transport, thus not affected significantly by the water retention in the membrane. In addition, as temperature increased, the effect of H<sub>2</sub> diffusivity increase was compromised by that of H<sub>2</sub> solubility reduction.

Fig. 2.24 shows the effects of temperature on CO<sub>2</sub>/H<sub>2</sub> and CO<sub>2</sub>/N<sub>2</sub> selectivities from 110°C to 150°C with fixed water rates (0.03 cm<sup>3</sup>/min for both sides resulting in 41 mol% water vapor in the feed and 58 mol% water vapor in the sweep, respectively). Both CO<sub>2</sub>/H<sub>2</sub> and CO<sub>2</sub>/N<sub>2</sub> selectivities reduced as temperature increased. This was due to the fact that CO<sub>2</sub> permeability decreased as temperature increased, while the transport of both H<sub>2</sub> and N<sub>2</sub> was not affected by temperature significantly.

As described earlier, increasing the sweep water content can effectively improve the separation performance; therefore, in order to maintain the separation performance at elevated temperature, the sweep water rate was increased gradually with increasing temperature. Figs. 2.25 and 2.26 show the effects of temperature with increasing sweep water rate, using the same membrane used in Figs. 2.23 and 2.24. Table A.12 lists the

water rates used in the sweep at different temperatures. As shown in Figs. 2.25 and 2.26, the CO<sub>2</sub> permeability, CO<sub>2</sub>/H<sub>2</sub> selectivity, and CO<sub>2</sub>/N<sub>2</sub> selectivity all reduced as temperature increased due to the reasons mentioned before. However, the membrane still showed good separation performance from 110°C to 160°C. At 150°C, the CO<sub>2</sub> permeability, CO<sub>2</sub>/H<sub>2</sub> selectivity, and CO<sub>2</sub>/N<sub>2</sub> selectivity were about 1,800 Barrers, 100, and 280, respectively. The CO<sub>2</sub>/H<sub>2</sub> selectivity reduced slightly as the temperature increased to 170°C, and it decreased significantly to less than 10 at 180°C presumably due to the significant swelling of the membrane, thus resulting in a sharp increase of H<sub>2</sub> permeability at this high temperature.

The CO<sub>2</sub>/CO selectivity of the membrane was investigated with a feed gas of 17% CO<sub>2</sub>, 1.0% CO, 45% H<sub>2</sub>, and 37% N<sub>2</sub> from 100°C to 170°C. As shown in Fig. 2.27, the selectivity decreased as temperature increased, which can be explained by the decrease of CO<sub>2</sub> permeability at elevated temperatures. However, even at 170°C, the CO<sub>2</sub>/CO selectivity was 160.

The effects of temperature on CO<sub>2</sub> permeability and CO<sub>2</sub>/H<sub>2</sub> selectivity were also investigated using another membrane consisting of 45.0 wt% PVA, 18.3 wt% KOH, 25.7 wt% AIBA-K, and 11.0 wt% poly(allylamine). Formaldehyde equivalent to a 60 mol% of crosslinking degree was added during the PVA solution preparation. The membrane had a thickness of 25.8 μm on the BHA microporous support. The feed gas consisted of 20% CO<sub>2</sub>, 40% H<sub>2</sub>, and 40% N<sub>2</sub>. Both the feed and sweep water rates were raised gradually at elevated temperatures shown in Table A.7 with their corresponding water contents. As we can see in Fig. 2.28, both CO<sub>2</sub> permeability and CO<sub>2</sub>/H<sub>2</sub> selectivity showed similar behaviors as shown in Figs. 2.25 and 2.26. However, the CO<sub>2</sub>

permeability and CO<sub>2</sub>/H<sub>2</sub> selectivity were higher than the values shown in Figs. 2.25 and 2.26. At 150°C, the CO<sub>2</sub> permeability and CO<sub>2</sub>/H<sub>2</sub> selectivity reached 2,500 Barrers and 80, respectively. The higher values in Fig. 2.28 were mainly attributed to the higher feed water rates used for this case as well as the higher carrier content in the membrane.

Membrane	T (°C)	CO <sub>2</sub> partial pressure (psia)	Feed gas (dry basis)	P <sub>CO2</sub> (Barrer)	α (CO <sub>2</sub> /H <sub>2</sub> )	α (CO <sub>2</sub> /N <sub>2</sub> )
Polyethyleneimine/poly(vinyl alcohol) (Matsuyama et al., 1999)	25	0.956	CO <sub>2</sub> /N <sub>2</sub>	850	N/A	160
Poly(vinylbenzyltrimethylammonium fluoride)-CsF (Quinn et al., 1997)	23	5.88	33% CO <sub>2</sub> , 34% H <sub>2</sub> , 33% CH <sub>4</sub>	~510	127	N/A
Dimethylglycine-Li/PVA (Tee et al., 2005)	90	3.53	20% CO <sub>2</sub> , 40% H <sub>2</sub> , 40% N <sub>2</sub>	1700	50	N/A
AIBA-K/polyallylamine/PVA	110	3.53	20% CO <sub>2</sub> , 40% H <sub>2</sub> , 40% N <sub>2</sub>	6000	300	1800
in this work (Figs. 2.25, 2.26)	150			1800	100	280
AIBA-K/polyallylamine/PVA	100	3.68	20% CO <sub>2</sub> , 40% H <sub>2</sub> , 40% N <sub>2</sub>	6500	210	N/A
in this work (Fig. 2.28)	150			2500	80	N/A

Table 2.4: Comparison of membrane performance with literature results (Matsuyama et al., 1999; Quinn et al., 1997; Tee et al., 2006).

The results from this study were compared with the results reported in the literature (Quinn and Laciak, 1997; Quinn et al. 1997) and our previous results (Tee et al., 2006) as shown in Table 2.4. As we can see from the comparison, the results from this work are gratifying. The improvement in the working temperature can be mostly attributed to better crosslinking of PVA as the polymer matrix as confirmed previously by DSC and FTIR. The high permeability and selectivity are presumably attributable to better carriers, AIBA-K and  $\text{KHCO}_3\text{-K}_2\text{CO}_3$  as the mobile carriers and poly(allylamine) as the fixed carrier, as illustrated earlier.

Gas permeation results presented in this work, especially above  $150^\circ\text{C}$ , showed that the polymeric membranes that we prepared were capable of more applications, such as water gas shift membrane reactors, which incorporate both  $\text{CO}_2$  removal and the water gas shift reaction to produce high purity  $\text{H}_2$  (Huang et al., 2005), and synthesis gas purification at elevated temperature.

### 2.3.7 Membrane stability

For the facilitated transport membranes, especially supported liquid membranes, the stability is always an issue. Supported liquid membranes often suffered from two major problems: loss of solvent, and loss or degradation of carriers. The loss of solvent is caused by the evaporation of solvent especially at a high temperature and / or caused by its permeation through a microporous support under a high trans-membrane pressure. The loss of carrier is the result of the carrier solution permeating through the support, and

the degradation of carriers is the result of the irreversible reaction of the carrier with impurities or the feed gas stream (LeBlanc et al., 1980; Way et al., 1987). Membranes with reactive carriers bonded in the membrane matrices were believed to have better stability than the supported liquid membranes. Our synthesized membranes contained both mobile carriers and fixed-site carriers. The stability of these membranes was studied at 130°C. Fig. 2.29 shows the CO<sub>2</sub> permeability and CO<sub>2</sub>/H<sub>2</sub> selectivity over time. The membrane was consisted of 55 wt% PVA (60 mol% crosslinked with formaldehyde), 20.0 wt% AIBA-K, 15.0 wt% KOH, and 10.0% polyallylamine on GE E500A support. The feed gas contained 20.0 % CO<sub>2</sub>, 40.0 % H<sub>2</sub>, and 40.0 % N<sub>2</sub>. The temperature was kept at 130°C and the water rate was 0.06 cm<sup>3</sup>/min for each side. As shown in this figure, both the CO<sub>2</sub> permeability and CO<sub>2</sub>/H<sub>2</sub> selectivity remained stable for an experiment period of 10 days.

## 2.4 Conclusions

Polymeric CO<sub>2</sub>-selective membranes consisting of both mobile and fixed-site carriers in crosslinked poly(vinyl alcohol) were synthesized. Both formaldehyde and glutaraldehyde were chosen as the crosslinking agents for poly(vinyl alcohol). With the obtained crosslinking conditions, the thermal stability of the membranes was improved significantly over the previous studies. The membranes showed good CO<sub>2</sub>/H<sub>2</sub>, CO<sub>2</sub>/N<sub>2</sub>, and CO<sub>2</sub>/CO selectivities, and high CO<sub>2</sub> permeability up to 170°C. The effects of membrane composition, feed pressure, water concentration, and temperature on transport properties were investigated:

(1) The CO<sub>2</sub> permeability and CO<sub>2</sub>/H<sub>2</sub> selectivity decreased with increasing feed pressure, which can be explained with the carrier saturation phenomenon, a characteristic of the facilitated transport membranes.

(2) The CO<sub>2</sub> permeability and CO<sub>2</sub>/H<sub>2</sub> selectivity significantly increased with increasing water content in both feed and sweep, which suggested that water played an important role in the facilitated transport.

(3) The overall gratifying results obtained were presumably attributed to the improvement in crosslinking and better CO<sub>2</sub> transport carriers.

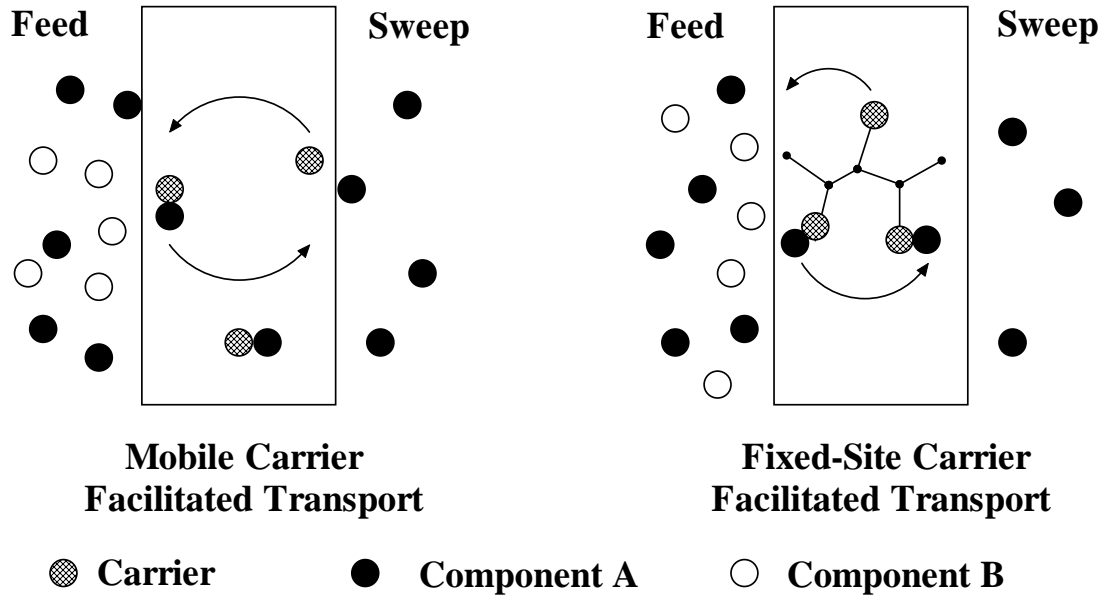


Figure 2.1: Schematic of facilitated transport membranes.

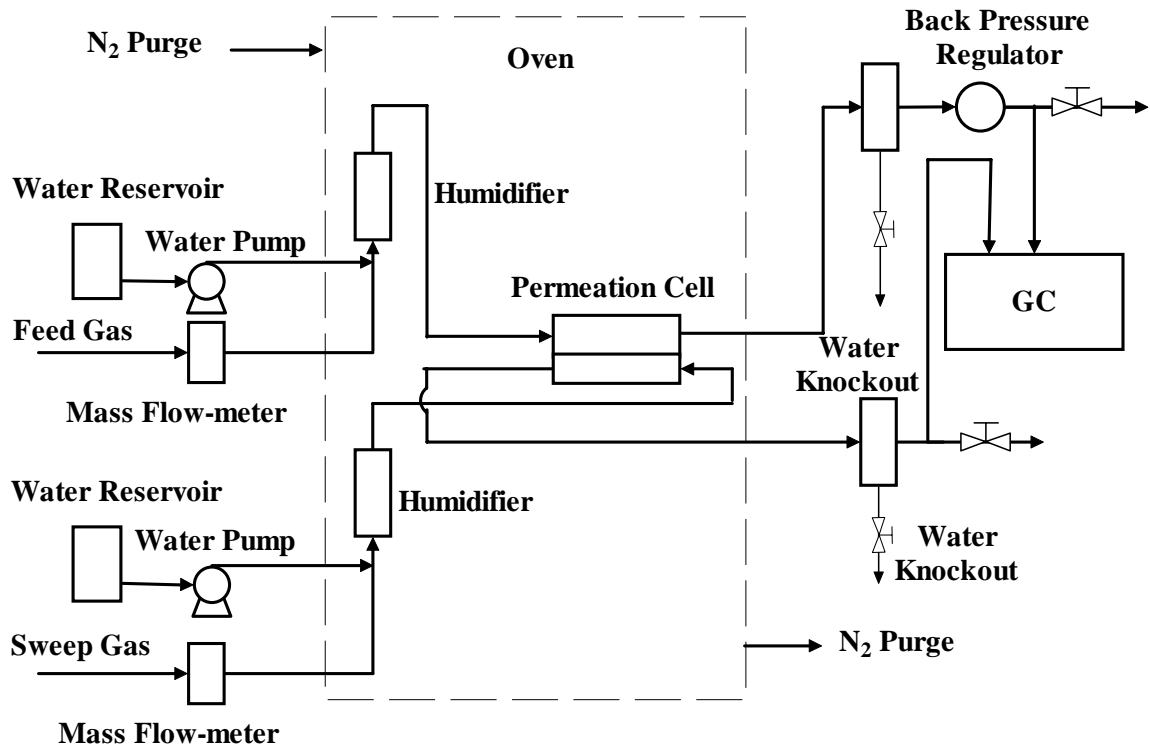


Figure 2.2: Schematic of gas permeation apparatus.

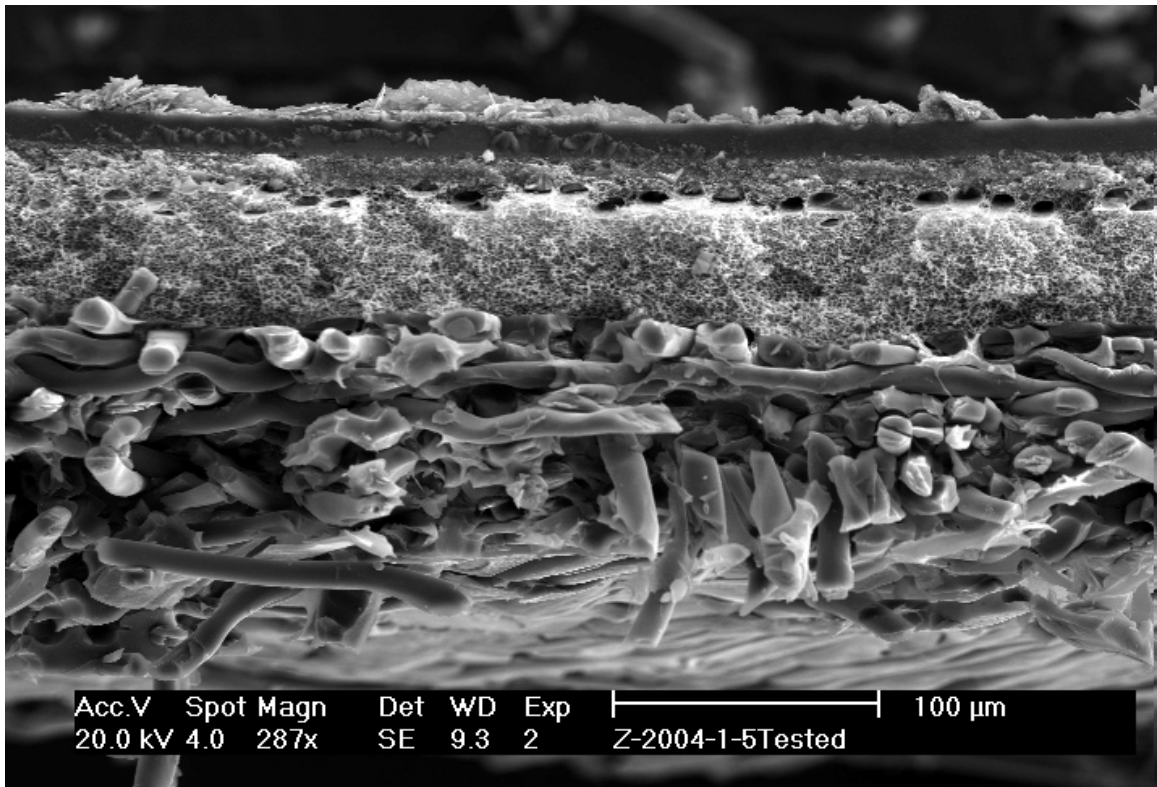


Figure 2.3: SEM image of the cross-section of the membrane synthesized (on GE E500A microporous polysulfone support, magnification: 287).

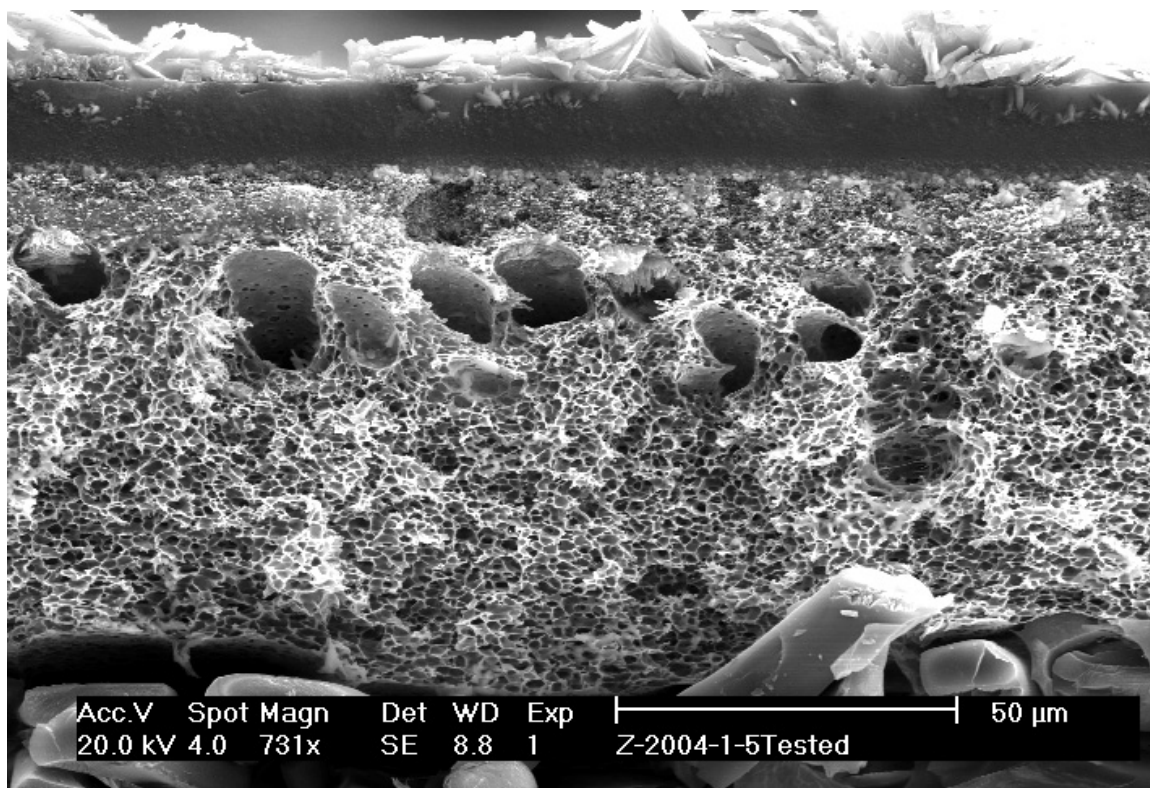
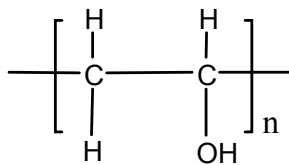
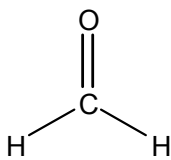


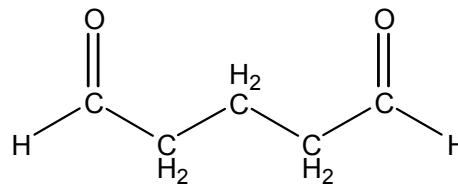
Figure 2.4: SEM image of the cross-section of the membrane synthesized (on GE E500A microporous polysulfone support, magnification: 731).



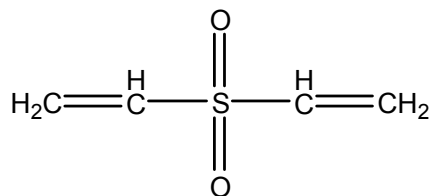
Poly(vinyl alcohol)



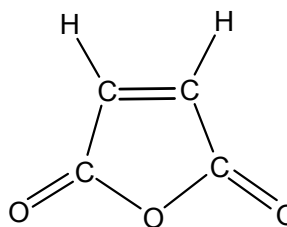
Formaldehyde



Glutaraldehyde



Divinyl sulfone



Maleic anhydride

Figure 2.5: Chemical structure of poly(vinyl alcohol) and crosslinking agents.

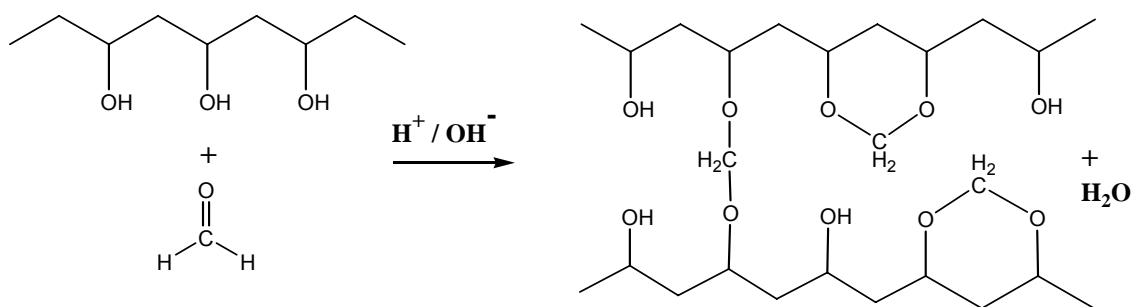


Figure 2.6: Diagram of the crosslinking reaction of poly(vinyl alcohol) with formaldehyde.

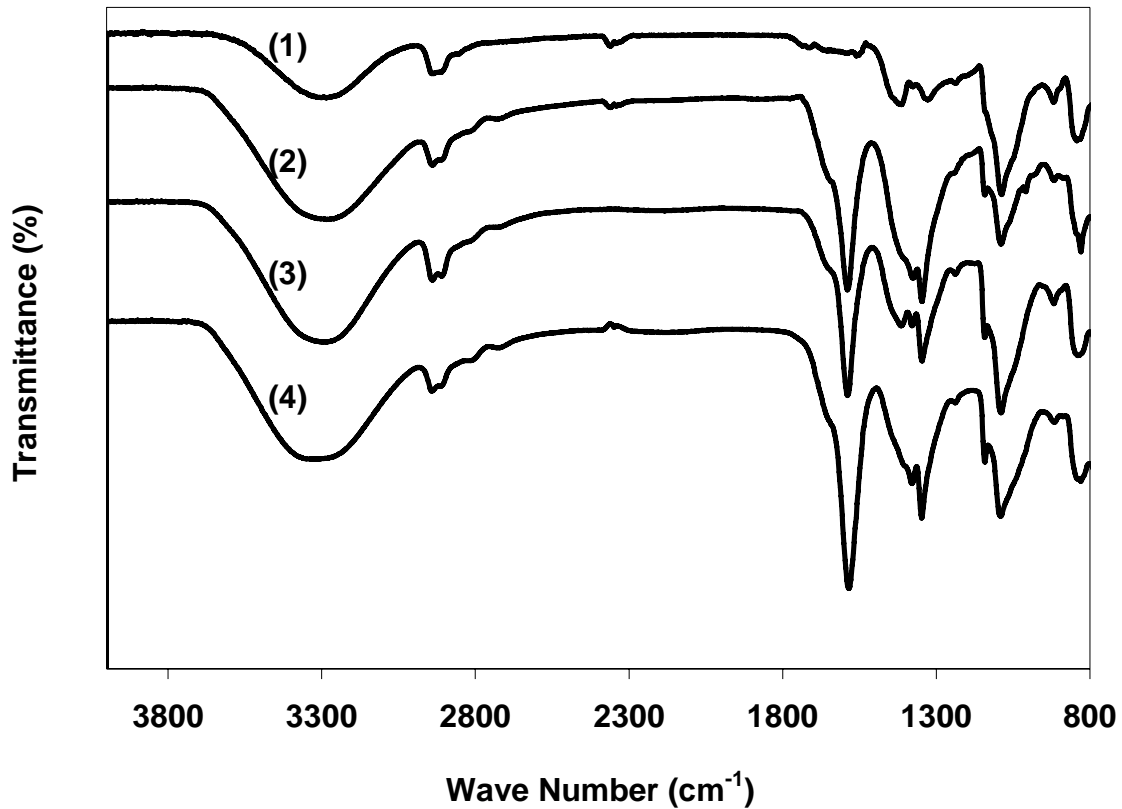


Figure 2.7: FTIR ATR spectra of PVA membranes (from top to bottom): (1) pure PVA, (2) PVA / formaldehyde crosslinked at 80°C for 5 minutes, (3) PVA / formaldehyde crosslinked at 80°C for 16 hours, (4) PVA / formaldehyde crosslinked at 80°C for 16 hours and heat-treated at 120°C for 6 hours.

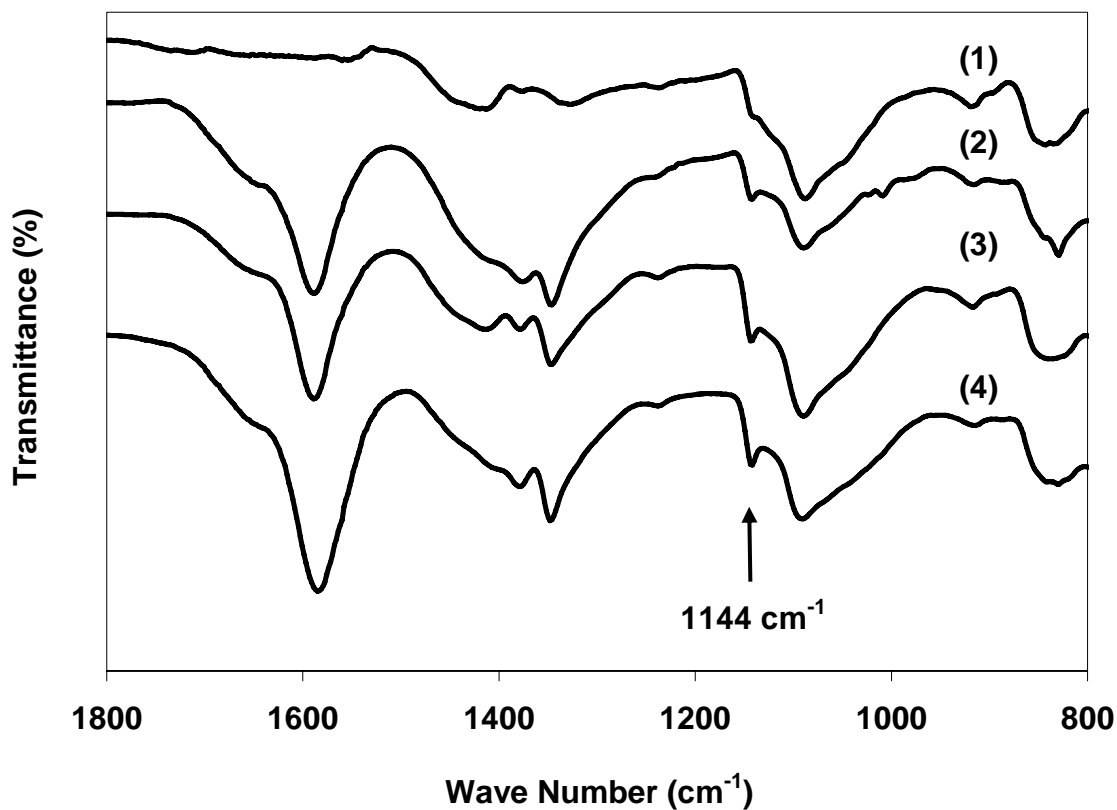


Figure 2.8: FTIR ATR spectra of PVA membranes (from top to bottom): (1) pure PVA, (2) PVA / formaldehyde crosslinked at 80°C for 5 minutes, (3) PVA / formaldehyde crosslinked at 80°C for 16 hours, (4) PVA / formaldehyde crosslinked at 80°C for 16 hours and heat-treated at 120°C for 6 hours.

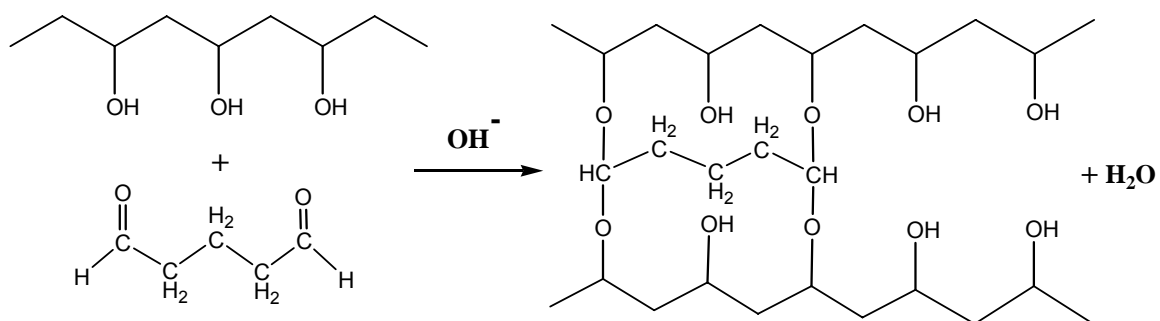


Figure 2.9: Diagram of the crosslinking reaction of poly(vinyl alcohol) with glutaraldehyde.

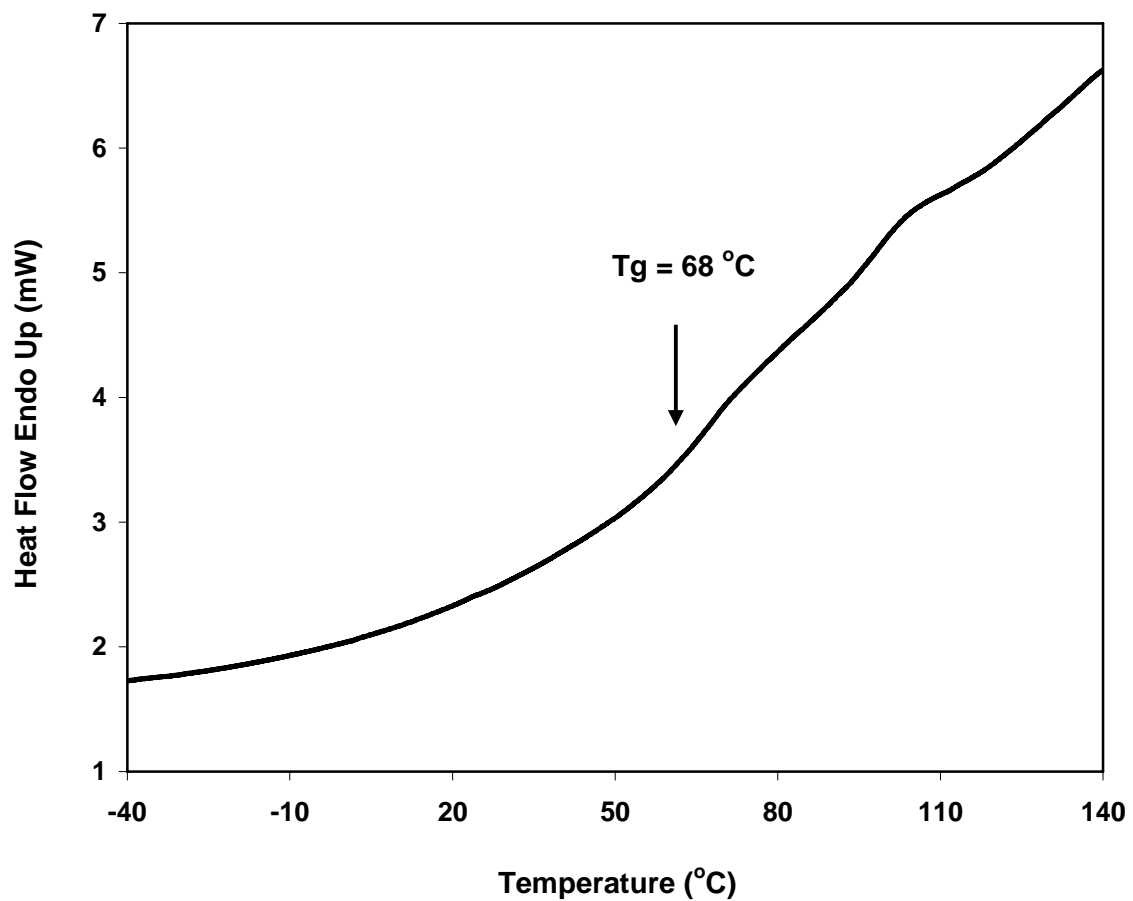


Figure 2.10: DSC curve of poly(vinyl alcohol) ( $M_w = 89,000 - 98,000$ , hydrolysis degree  $> 99\%$ ).

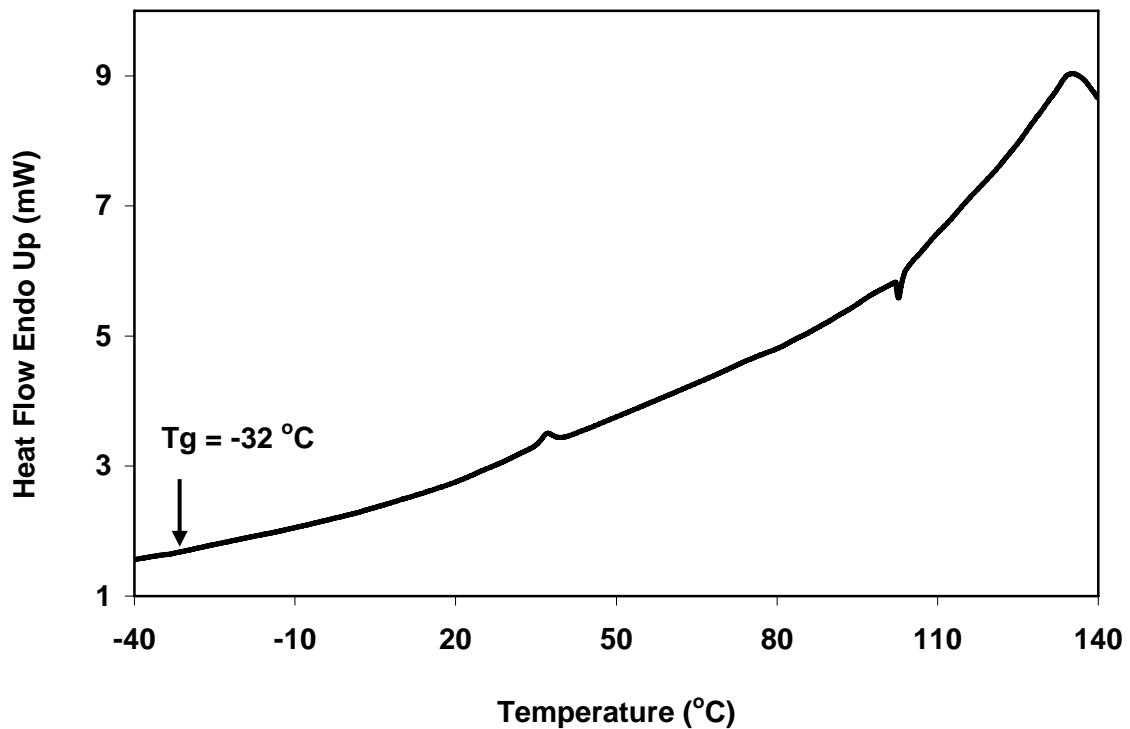


Figure 2.11: DSC curve of poly(allylamine) [prepared from poly(allylamine) hydrochloride, Mw = 68,000].

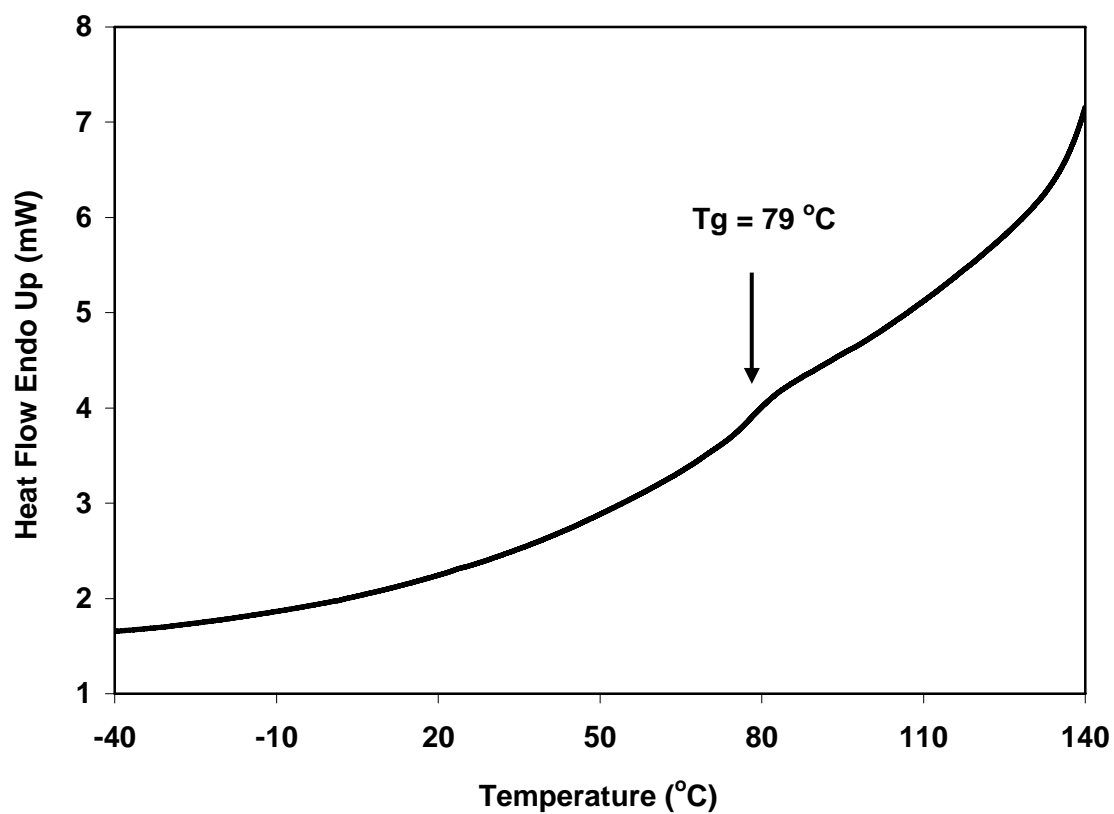


Figure 2.12: DSC curve of formaldehyde-crosslinked membrane [50% PVA/60mol% crosslinked with formaldehyde, 20.3% AIBA-K, 18.7% KOH, 11% poly(allylamine)].

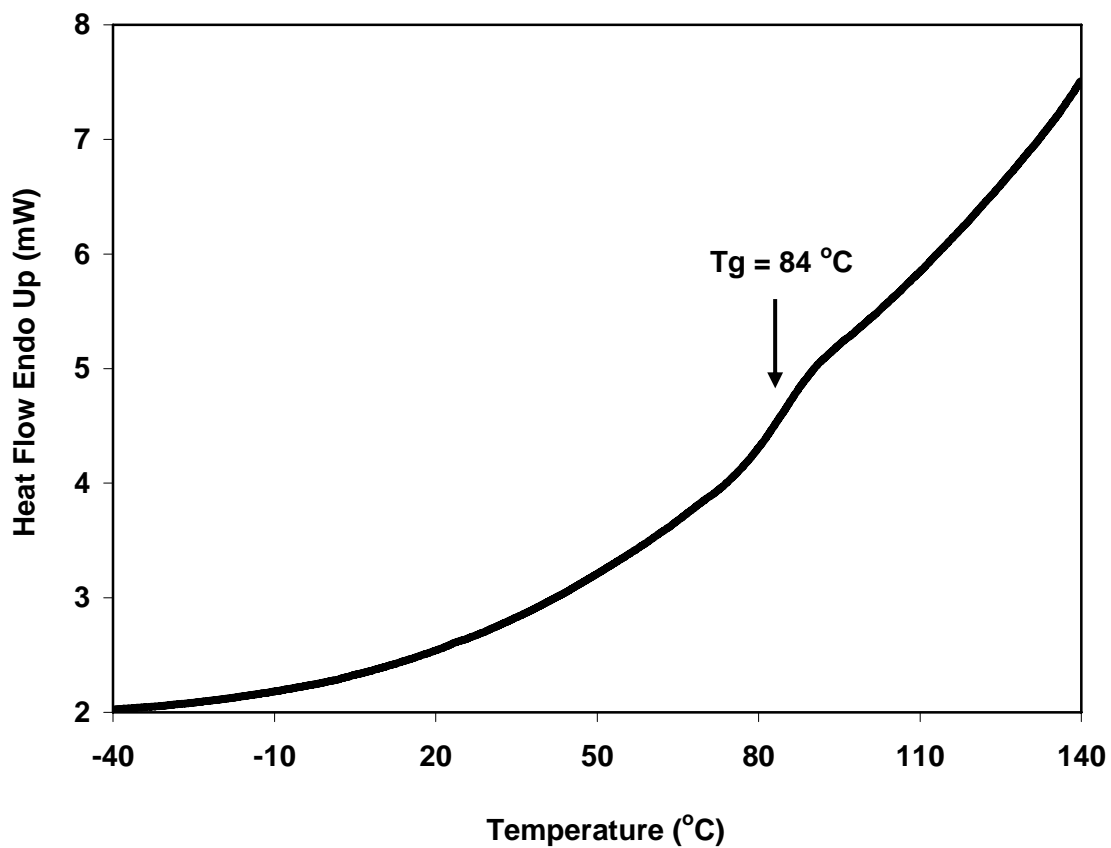


Figure 2.13: DSC curve of formaldehyde-crosslinked membrane [50% PVA/60mol% crosslinked with glutaraldehyde, 20.3% AIBA-K, 18.7% KOH, 11% poly(allylamine)].

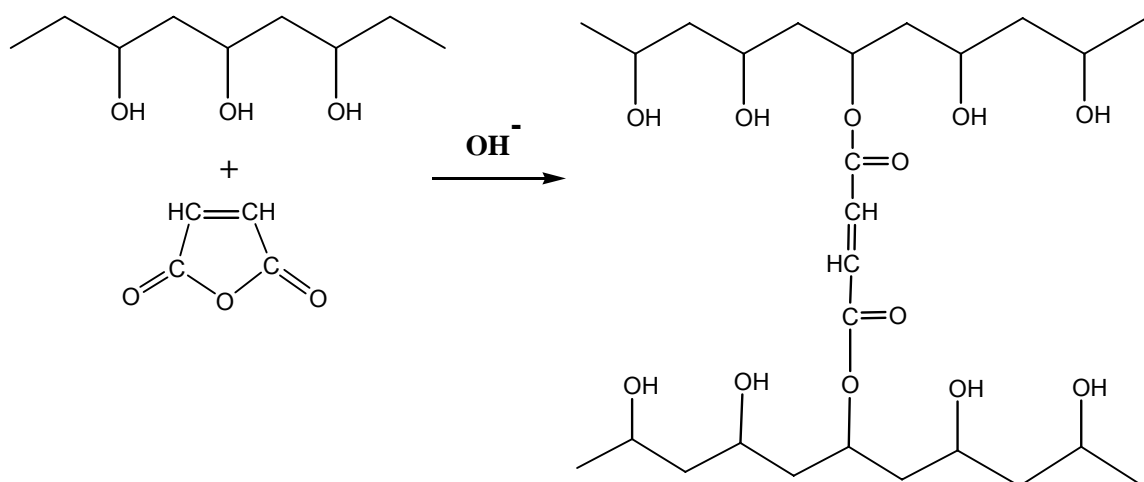


Figure 2.14: Diagram of the crosslinking reaction of poly(vinyl alcohol) with maleic anhydride.

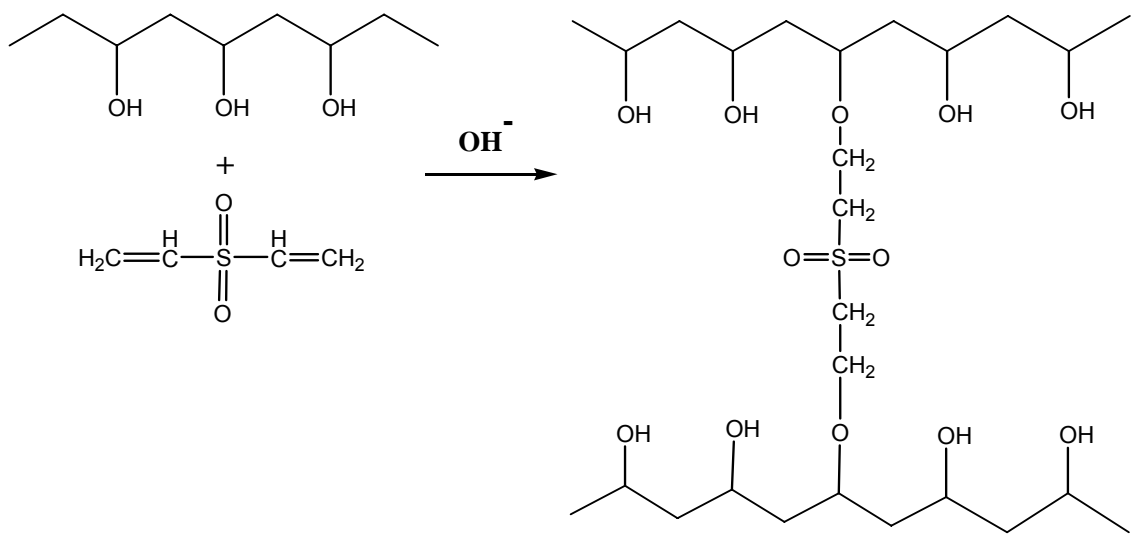


Figure 2.15: Diagram of the crosslinking reaction of poly(vinyl alcohol) with divinyl sulfone.

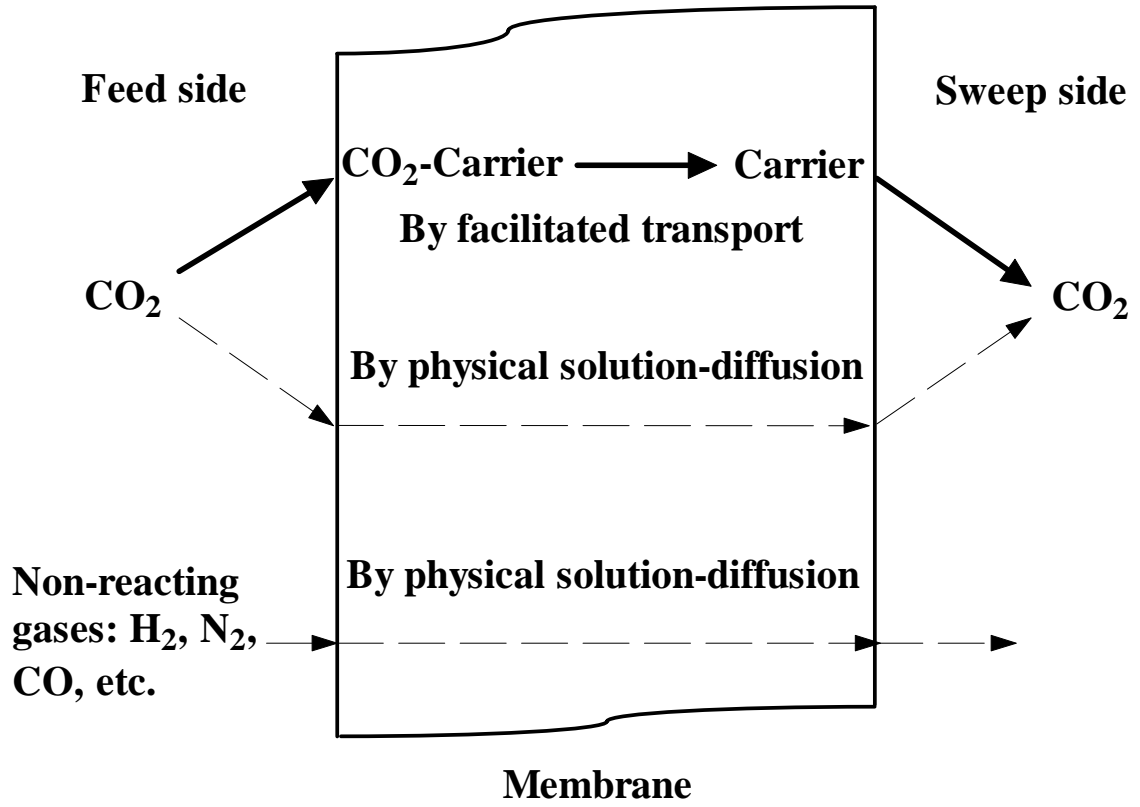
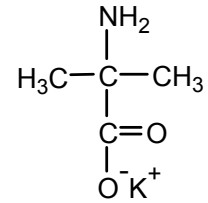


Figure 2.16: Schematic of  $\text{CO}_2$  transport mechanism in the membranes synthesized.

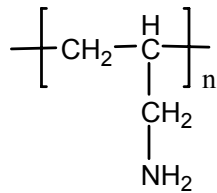
**Mobile carriers:**  $K_2CO_3$ - $KHCO_3$

Potassium carbonate-  
potassium bicarbonate

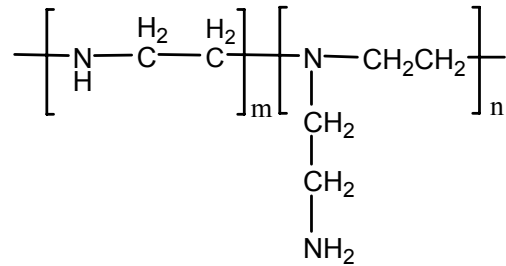


2-Aminoisobutyric acid-  
potassium salt

**Fixed carrier:**



Poly(allylamine)



Polyethylenimine

Figure 2.17: Chemical structure of carriers for  $CO_2$  transport.

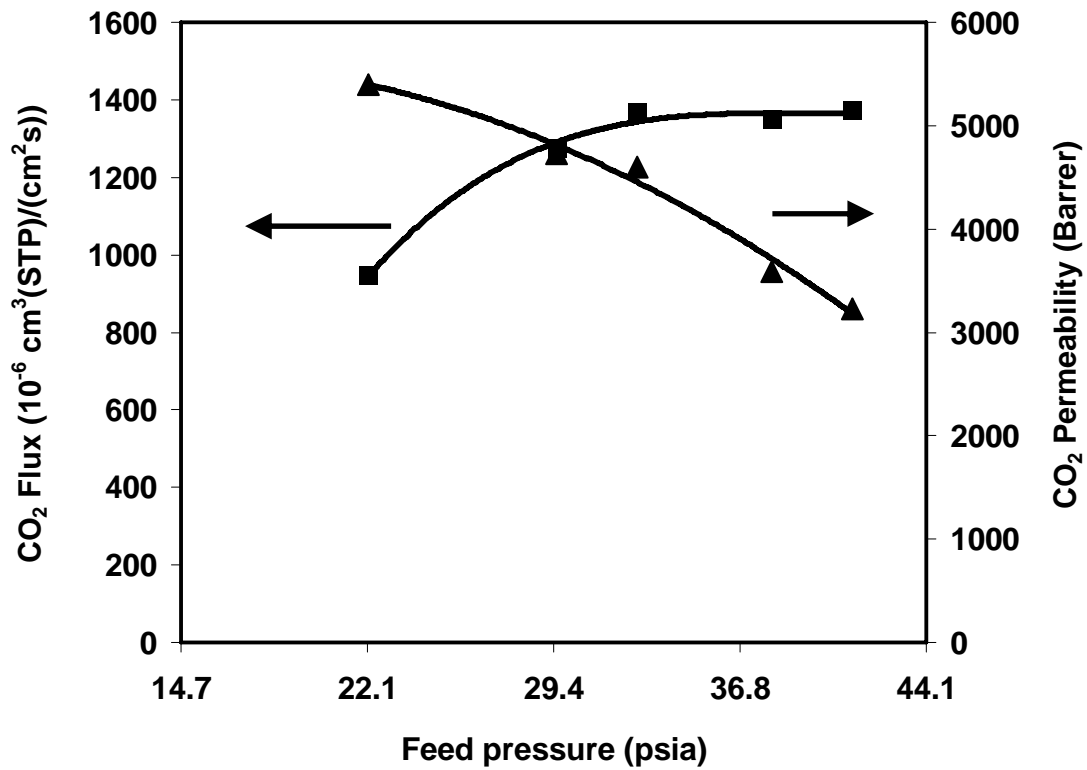


Figure 2.18: Effect of feed pressure on CO<sub>2</sub> flux and permeability.

(■) CO<sub>2</sub> flux; (▲) CO<sub>2</sub> permeability; at 110°C with water rates = 0.03 / 0.03 cm<sup>3</sup>/min (feed / sweep).

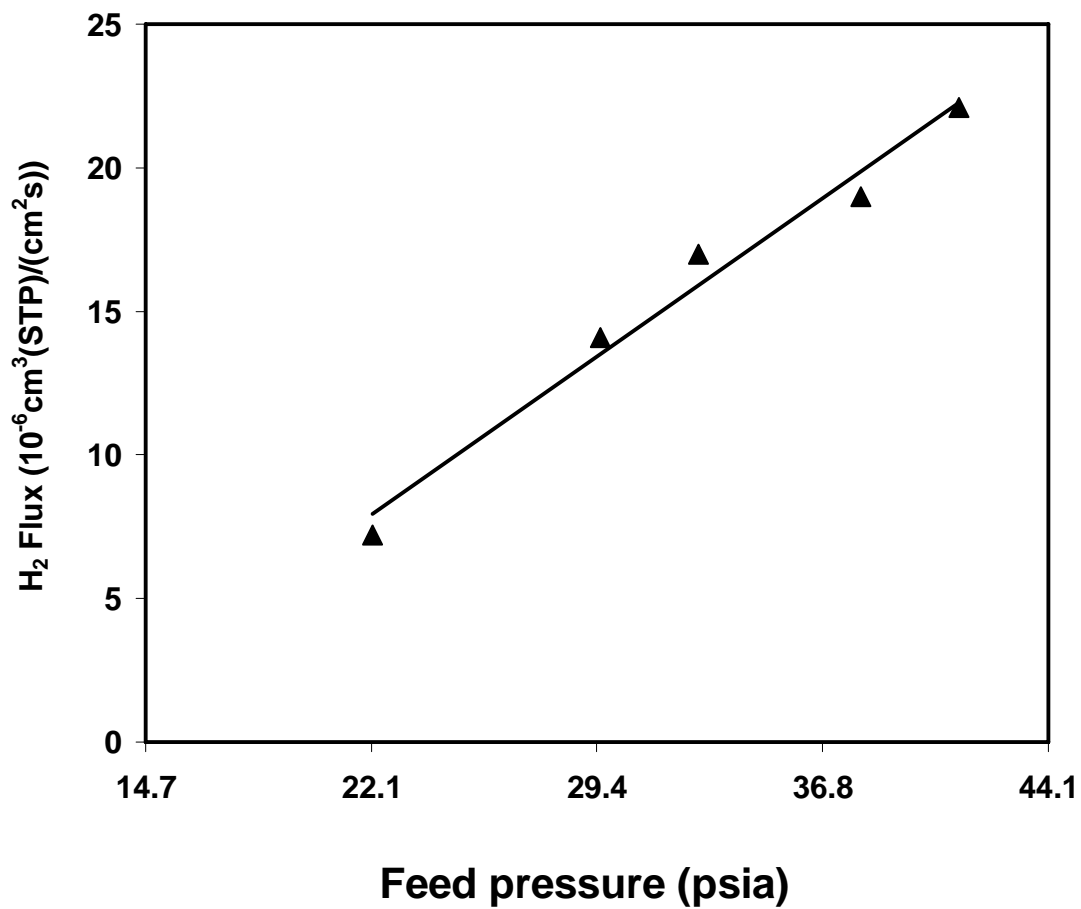


Figure 2.19: Effect of feed pressure on H<sub>2</sub> flux.  
At 110°C with water rates = 0.03 / 0.03 cm<sup>3</sup>/min (feed / sweep).

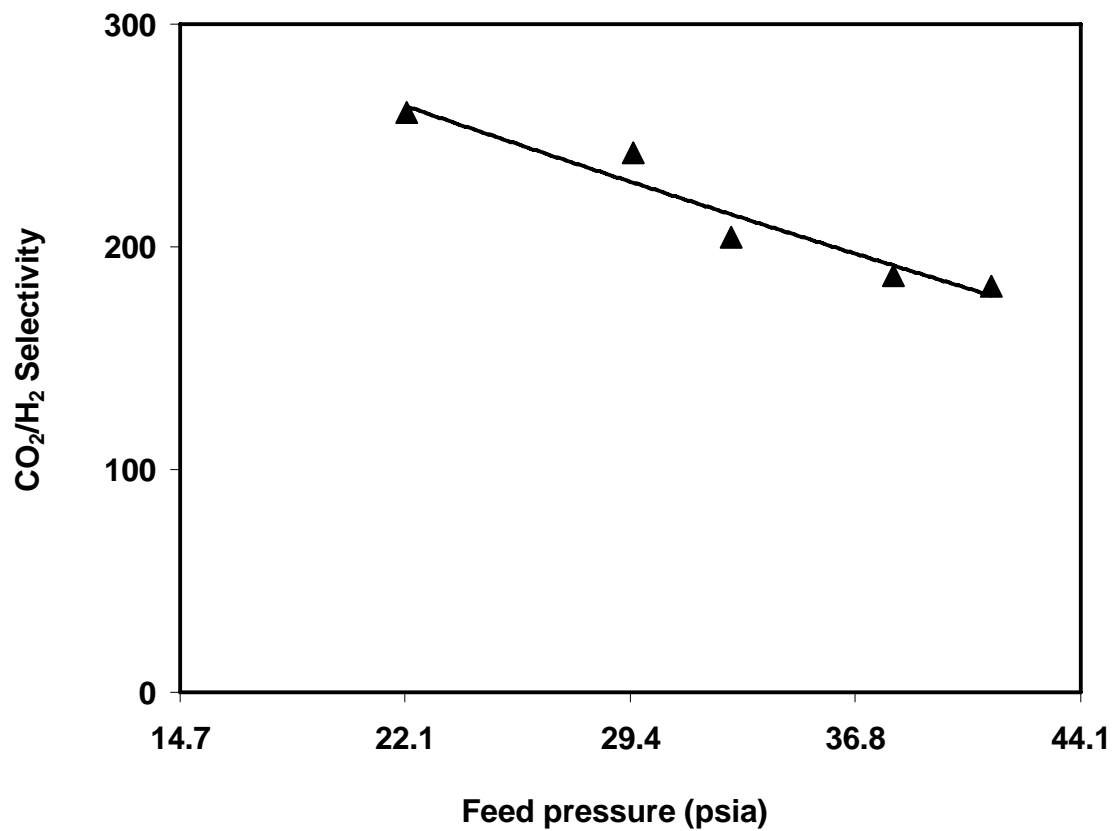


Figure 2.20: Effect of feed pressure on CO<sub>2</sub>/H<sub>2</sub> selectivity.

At 110°C with water rates = 0.03 / 0.03 cm<sup>3</sup>/min (feed / sweep).

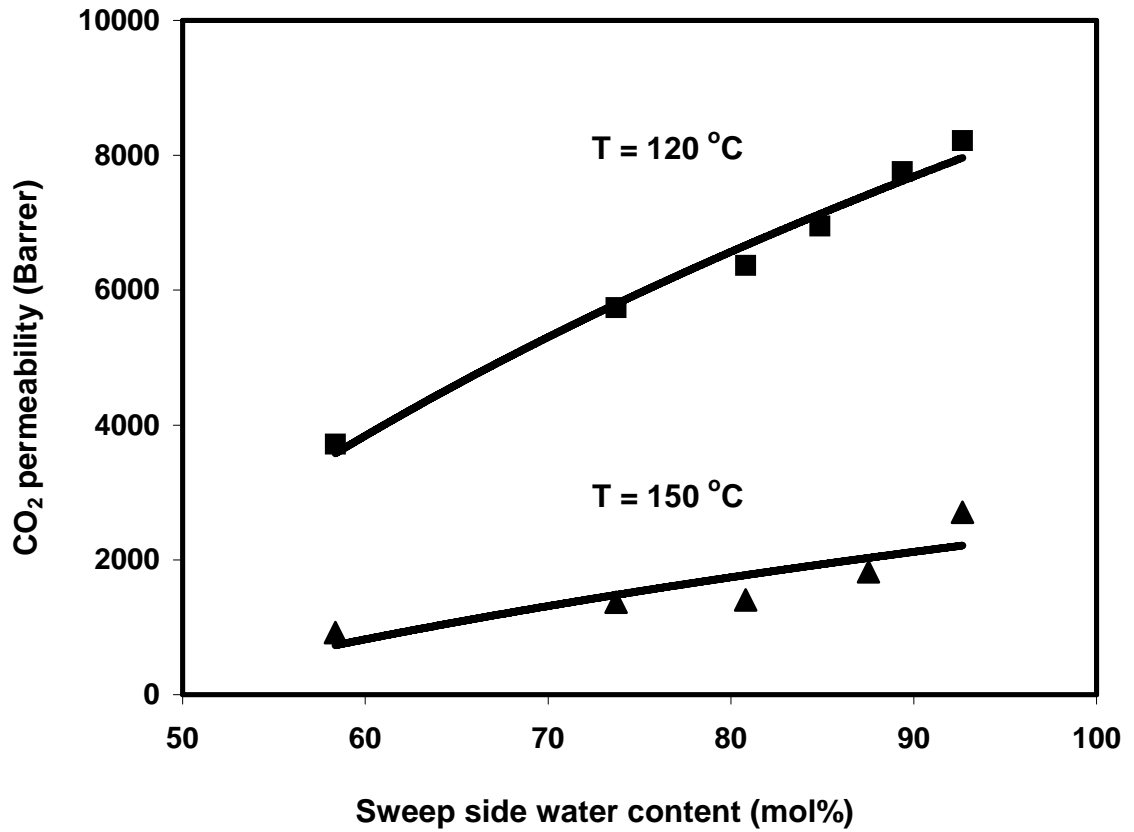


Figure 2.21: CO<sub>2</sub> permeability vs. water content on the sweep side.

(■) T = 120°C; (▲) T = 150°C; feed water content = 41 mol%; feed pressure = 29.1 psia.

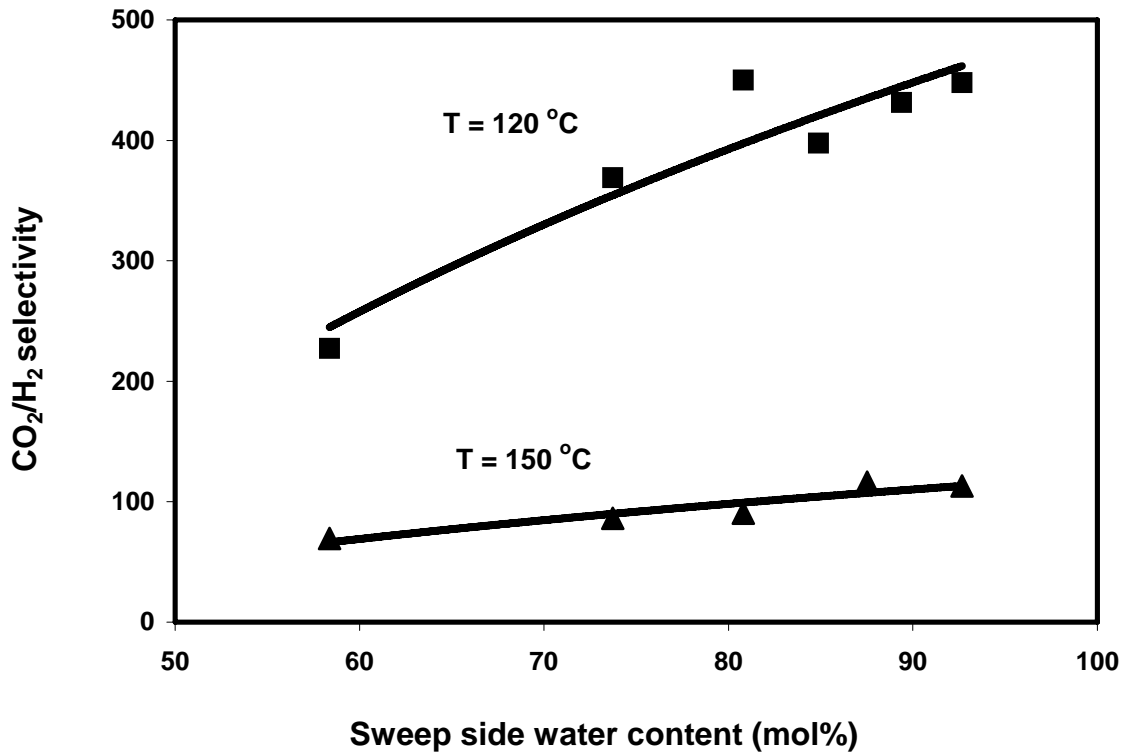


Figure 2.22: CO<sub>2</sub>/H<sub>2</sub> selectivity vs. water content on the sweep side.  
(■) T = 120°C; (▲) T = 150°C; feed water content = 41 mol%; feed pressure = 29.1 psia.

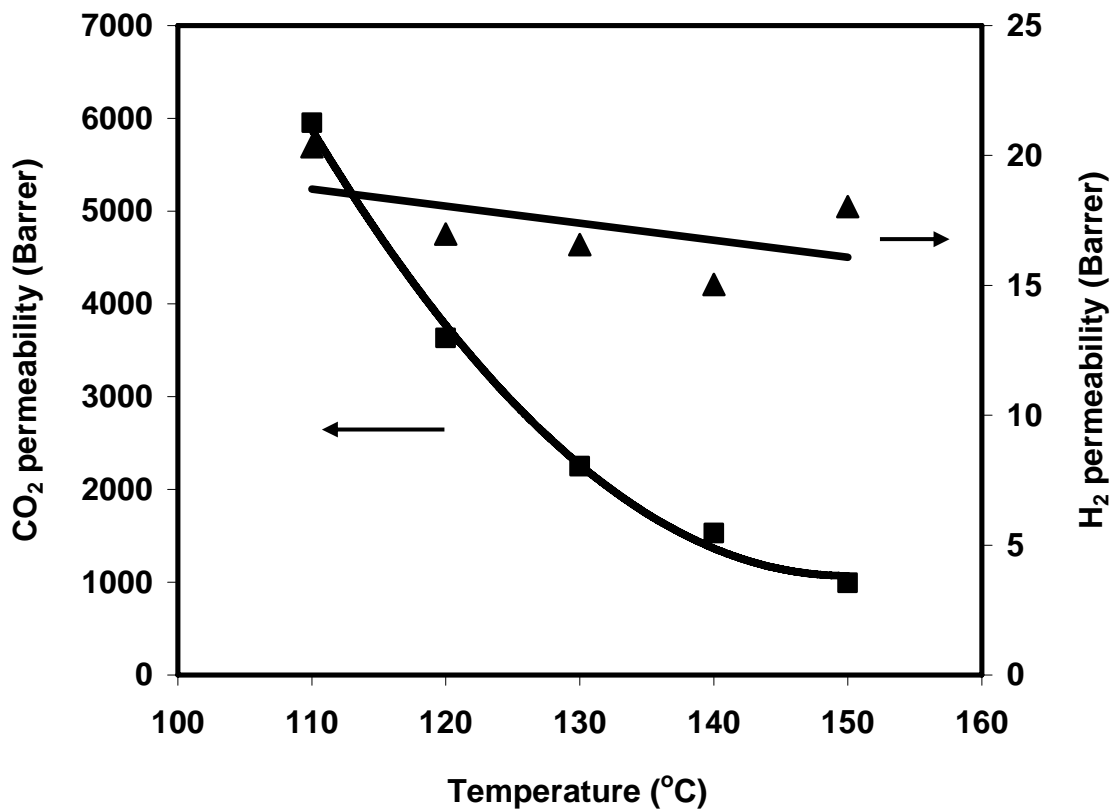


Figure 2.23: CO<sub>2</sub> and H<sub>2</sub> permeabilities vs. temperature.

(■) CO<sub>2</sub> permeability; (▲) H<sub>2</sub> permeability; feed pressure = 29.1 psia; water rates = 0.03 / 0.03 cm<sup>3</sup>/min (feed / sweep).

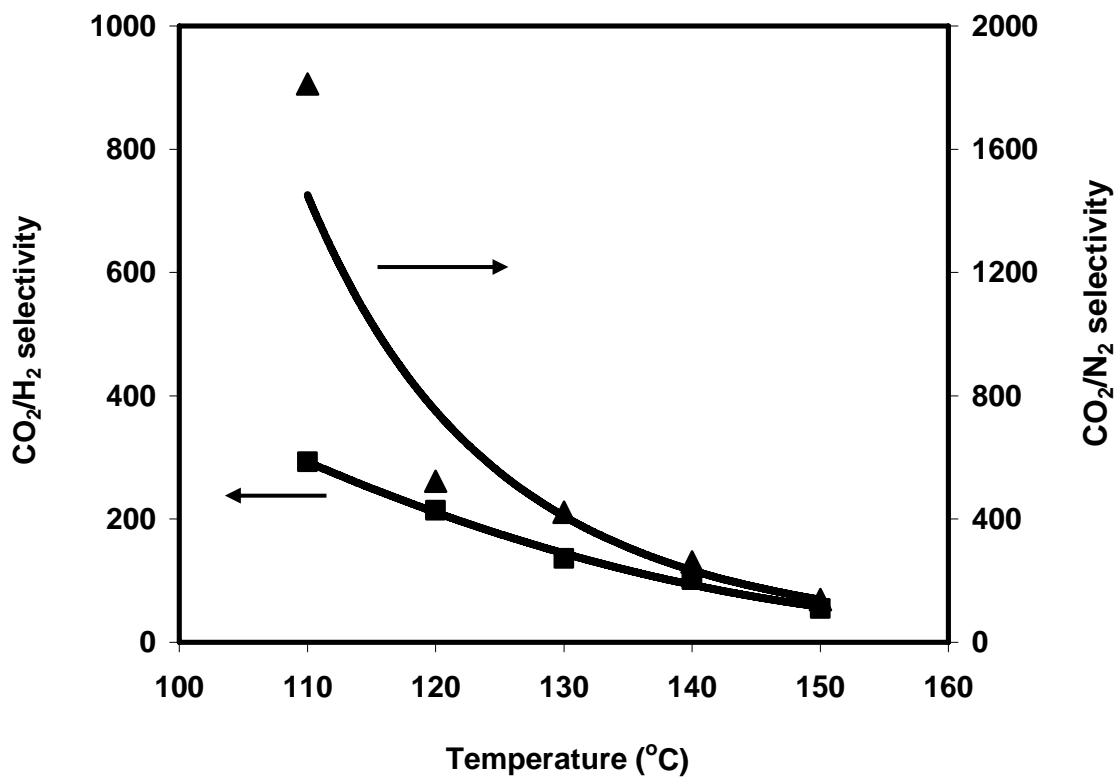


Figure 2.24: CO<sub>2</sub>/H<sub>2</sub> and CO<sub>2</sub>/N<sub>2</sub> selectivities vs. temperature.

(■) CO<sub>2</sub>/H<sub>2</sub> selectivity; (▲) CO<sub>2</sub>/N<sub>2</sub> selectivity; feed pressure = 29.1 psia; water rates = 0.03 / 0.03 cm<sup>3</sup>/min (feed / sweep).

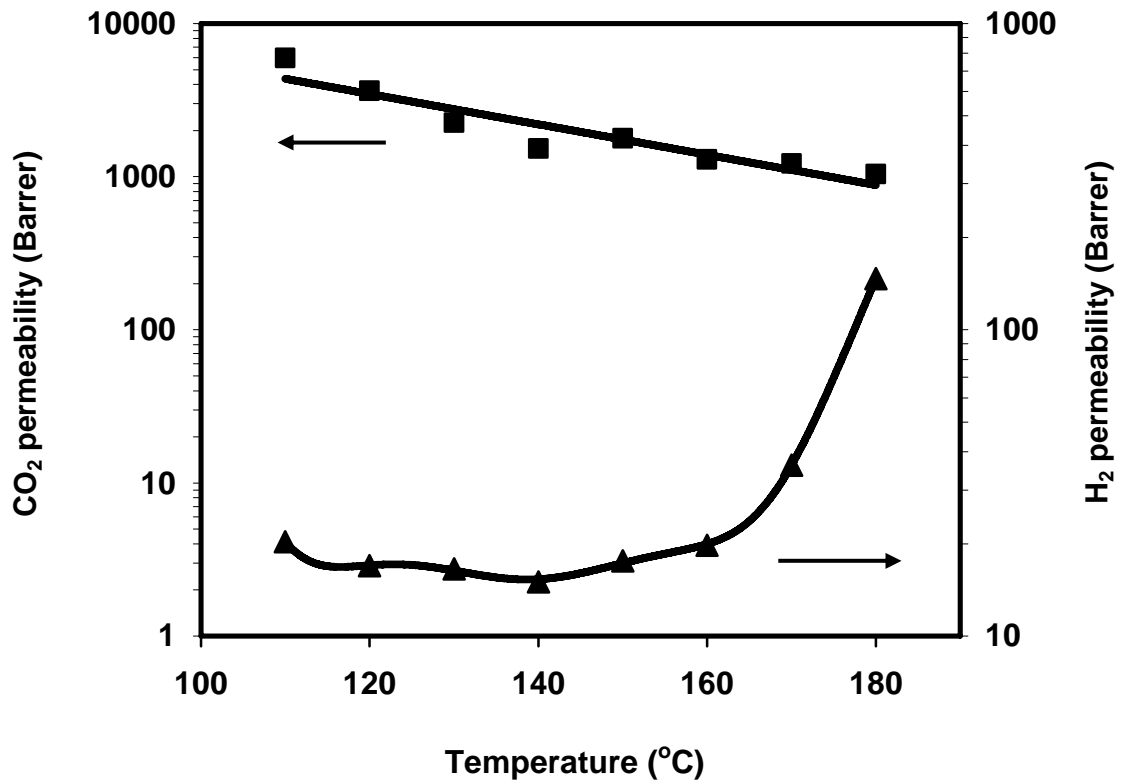


Figure 2.25: CO<sub>2</sub> and H<sub>2</sub> permeabilities vs. temperature.

(■) CO<sub>2</sub> permeability; (▲) H<sub>2</sub> permeability; feed pressure = 29.1 psia; with increasing water rates on the sweep side at elevated temperatures.

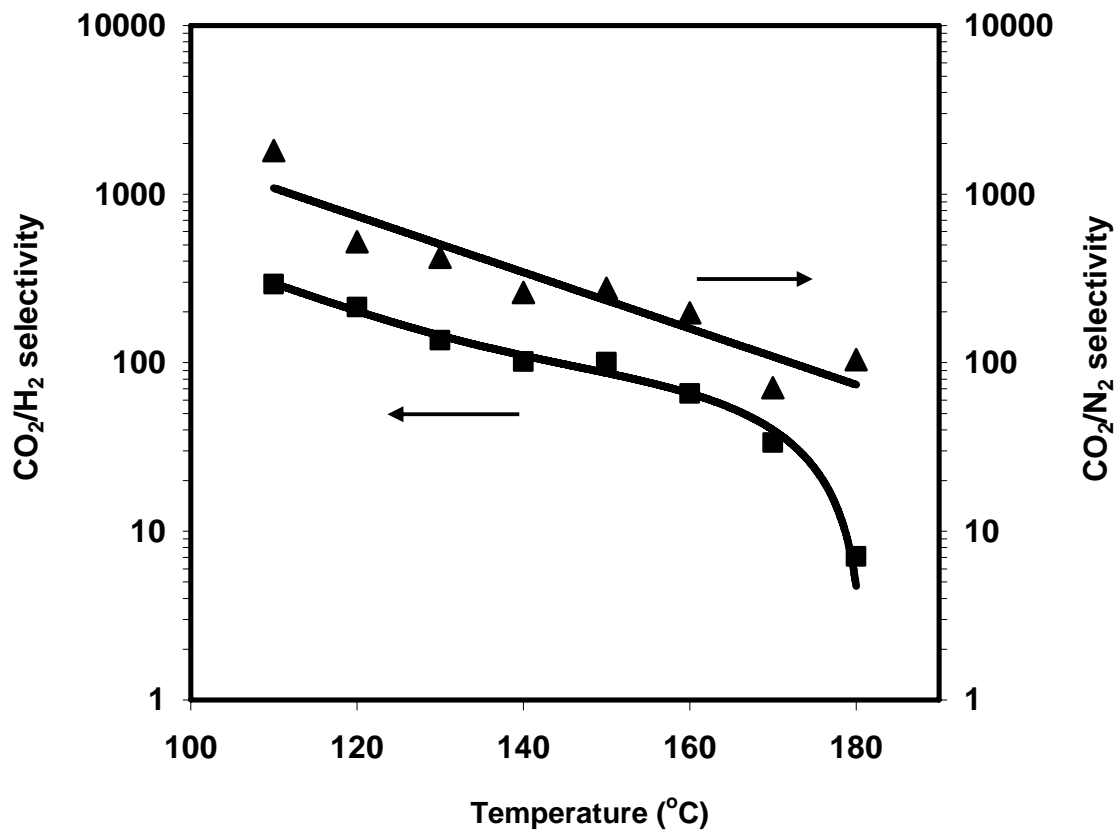


Figure 2.26: CO<sub>2</sub>/H<sub>2</sub> and CO<sub>2</sub>/N<sub>2</sub> selectivities vs. temperature.

(■) CO<sub>2</sub>/H<sub>2</sub> selectivity; (▲) CO<sub>2</sub>/N<sub>2</sub> selectivity; feed pressure = 29.1 psia; with increasing water rates on the sweep side at elevated temperatures.

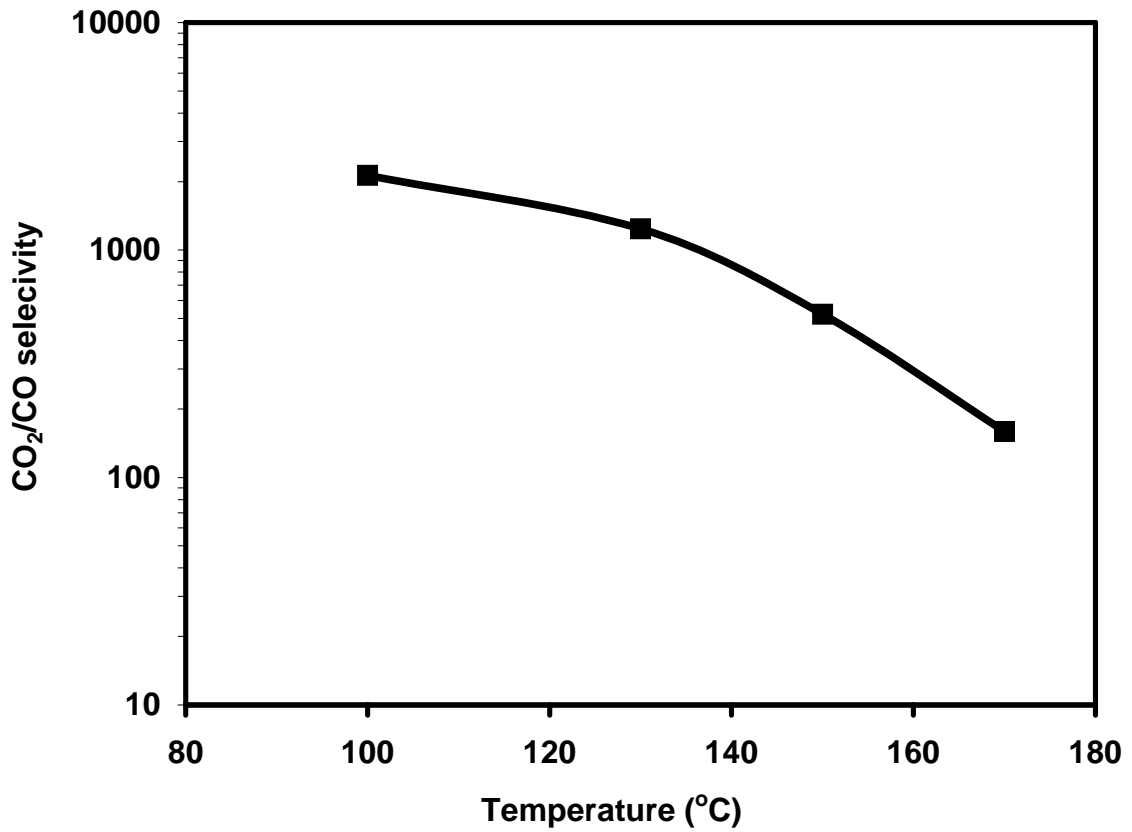


Figure 2.27: CO<sub>2</sub>/CO selectivity vs. temperature.

Feed pressure = 29.1 psia; with increasing water rates on the sweep side at elevated temperatures.

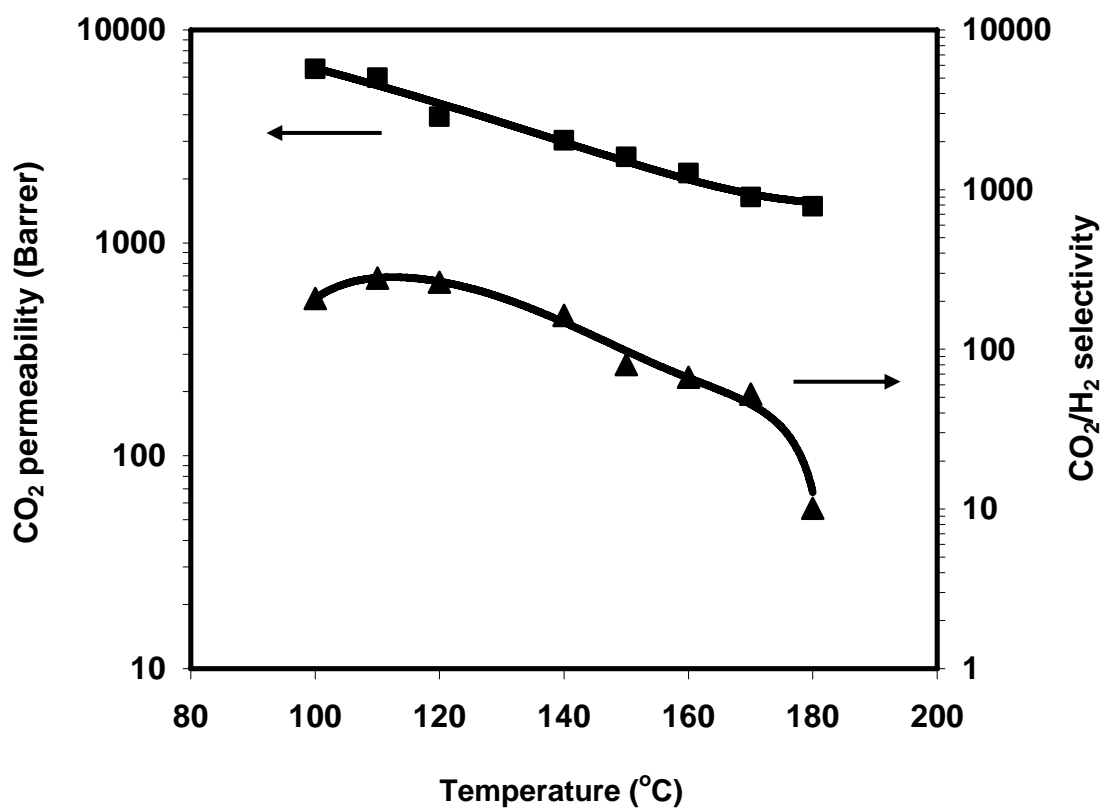


Figure 2.28: CO<sub>2</sub> permeability and CO<sub>2</sub>/H<sub>2</sub> selectivity vs. temperature.

(■) CO<sub>2</sub> permeability; (▲) CO<sub>2</sub>/H<sub>2</sub> selectivity; feed pressure = 31.7 psia; with increasing water rates at elevated temperatures.

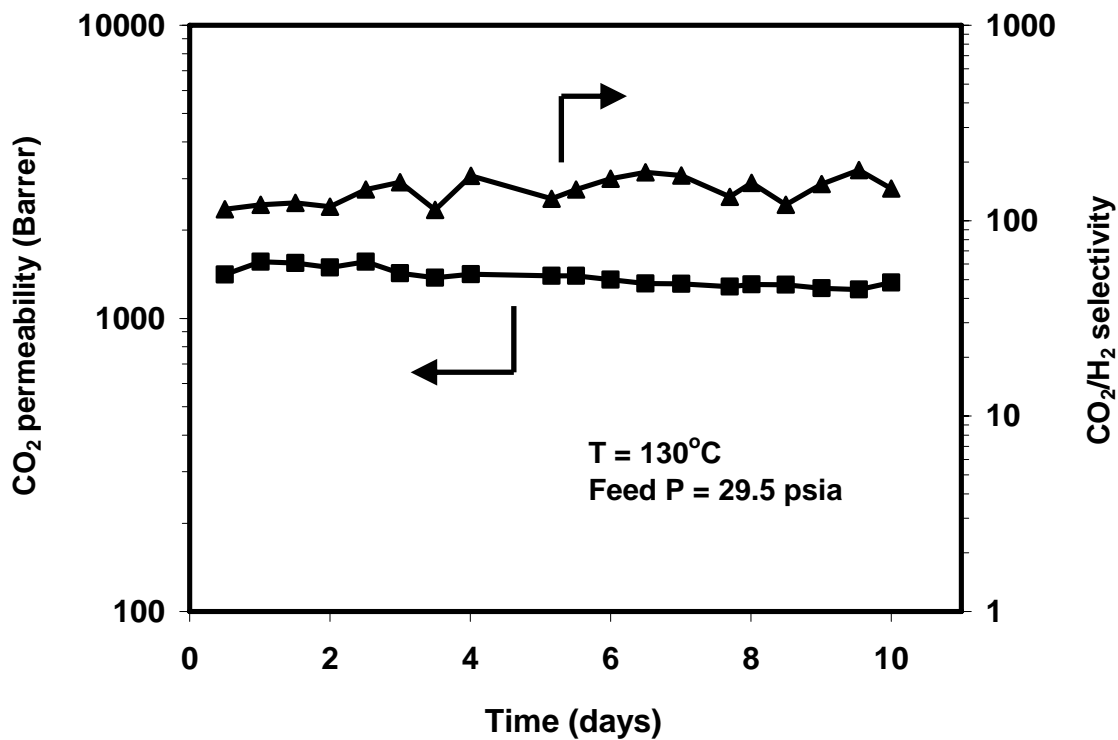


Figure 2.29: CO<sub>2</sub> permeability and CO<sub>2</sub>/H<sub>2</sub> selectivity vs. time.

(■) CO<sub>2</sub> permeability; (▲) CO<sub>2</sub>/H<sub>2</sub> selectivity; water rates = 0.06 / 0.06 cm<sup>3</sup>/min.

## CHAPTER 3

### CARBON DIOXIDE-SELECTIVE WATER GAS SHIFT MEMBRANE REACTOR

#### 3.1 Introduction

For current fuel cells, hydrogen is the preferred fuel in most cases, especially for the proton-exchange membrane fuel cells (PEMFCs), because of its high reactivity and clean emission (Dicks, 1996; Song, 2002). The generation of hydrogen on a commercial scale usually consists of reforming of hydrocarbon fuels followed by the water gas shift (WGS) reaction. Since the resulting synthesis gas consists of a significant amount of CO, usually about 0.5 – 1%, a further CO clean-up step is needed to reduce the CO concentration to less than 10 ppm to meet the requirement of PEMFCs. Several methods are currently used or being under development for the CO clean-up, including methanation, preferential oxidation, pressure swing adsorption, sorption-enhanced reaction, and membrane separation.

Methanation (Eqs. 1.2 and 1.3) is one of the most widely used processes for the CO clean-up step (Twigg, 1989). In this process, H<sub>2</sub> reacts with CO to form methane. For PEMFCs, methane can be regarded as inert gas and does not affect the fuel cell

performance. Since the equilibrium constant of this reaction is much higher than the equilibrium constant of WGS, CO can be decreased to a very low level, usually below 10 ppm, with methanation. However, as we can see from Eqs 1.2 and 1.3, CO consumes H<sub>2</sub> at a molar ratio of 1:3, while CO<sub>2</sub> consumes H<sub>2</sub> at a molar ratio of 1:4. Therefore, CO<sub>2</sub> needs to be removed before the methanation step in order to minimize H<sub>2</sub> consumption (Twigg, 1989; Ledjeff-Hey et al., 2000). Amine scrubbing is usually used to reduce the CO<sub>2</sub> level (Twigg, 1989) before the methanation step. Table 3.1 shows typical process compositions for the hydrogen production in an industrial ammonia plant.

	High temperature WGS		Low temperature WGS		Methanation	
	Inlet	Exit	Inlet	Exit	Inlet	Exit
CO/%	12.76	3.33	3.33	0.40	0.49	< 5 ppm
CO <sub>2</sub> /%	8.18	15.85	15.85	18.24	0.20	
H <sub>2</sub> /%	56.34	60.02	60.02	61.15	74.68	74.06
CH <sub>4</sub> /%	0.22	0.21	0.21	0.20	0.24	0.95
N <sub>2</sub> /%	22.20	20.16	20.16	19.77	24.10	24.69
A/%	0.30	0.25	0.25	0.24	0.29	0.30
T/°C	370	432	220	242	318	365
Steam ratio	0.51	0.48	0.48	0.44	0.011	0.020
Wet gas space velocity/h <sup>-1</sup>	4100		4475		6409	

Table 3.1: Process gas composition (dry basis) and conditions for WGS/methanation in an ammonia plant (Twigg, 1989)

T (°C)	$K_{P(CO)} = P_{CH_4} P_{H_2O} / P_{CO} P_{H_2}^3$	$K_{P(CO_2)} = P_{CH_4} P_{H_2O}^2 / P_{CO_2} P_{H_2}^4$
	(bar <sup>-2</sup> )	(bar <sup>-2</sup> )
200	0.215 X 10 <sup>12</sup>	0.947 X 10 <sup>9</sup>
240	0.304 X 10 <sup>10</sup>	0.294 X 10 <sup>8</sup>
280	0.784 X 10 <sup>8</sup>	0.149 X 10 <sup>7</sup>
320	0.326 X 10 <sup>7</sup>	0.110 X 10 <sup>6</sup>
360	0.200 X 10 <sup>6</sup>	0.111 X 10 <sup>5</sup>
400	0.169 X 10 <sup>5</sup>	0.144 X 10 <sup>4</sup>

Table 3.2: Equilibrium constants for methanation (Twigg, 1989)

Table 3.2 shows the equilibrium constants of the methanation at various temperatures. As we can see from this table, the equilibrium constants of both reactions are very high; therefore, both reactions can almost go to completion at these temperatures. Commercial methanation catalysts are usually nickel metal dispersed on a support, such as alumina, silica, lime, and magnesia, together with compounds such as calcium aluminate cements. Ruthenium dispersed on Al<sub>2</sub>O<sub>3</sub> is also used for methanation. Ruthenium catalysts can operate at low temperatures, but are not more effective than conventional nickel catalysts under normal plant conditions (Twigg, 1989). The advantage of the methanation is the final CO concentration can be as low as several ppms. However, its disadvantage is the consumption of H<sub>2</sub>, which decreases the overall efficiency (Larminie and Dicks, 2003).

Preferential oxidation (PROX, Eq. 1.4) is another process being developed for the CO clean-up step. In the PROX process, a small amount of O<sub>2</sub> is introduced to react preferentially with CO over a precious metal catalyst. In order to reduce CO to less than 10 ppm, an excess amount of O<sub>2</sub> is needed because the catalyst is not selective enough. The excess amount of O<sub>2</sub> consumes H<sub>2</sub> by combustion and increases the risk of an accidental explosion; therefore, more selective catalysts are desired but unavailable at this time. Platinum supported on alumina (Pt/Al<sub>2</sub>O<sub>3</sub>) is often used as the catalyst for PROX (Oh and Sinkevitch, 1993; Manasilp and Gulari; 2002). Other major classes of catalysts being studied for PROX include base metals (Sedmak et al., 2003) and Au (Kung et al., 2003). In addition to the research on more selective catalysts, multi-stage PROX reactors have been proposed to reduce the amount of O<sub>2</sub> added (Igarashi et al., 1997; Echigo and Tabata, 2004; Lee et al., 2002). Igarashi et al. (1997) found that 1% CO in the gas feed was not completely oxidized on a Pt/Al<sub>2</sub>O<sub>3</sub> catalyst even 3% of O<sub>2</sub> was added into the feed gas. By using a two-stage PROX reactor with the platinum catalyst supported on mordenite zeolite, they oxidized 1% CO completely with 0.7% O<sub>2</sub> at 200°C. However, temperatures and O<sub>2</sub> injections along the multi-stages still need to be controlled with great caution (Larminie and Dicks, 2003).

Pressure swing adsorption uses adsorbents, like activated carbon and zeolite, to remove impurities and can obtain high-purity hydrogen (purity of hydrogen > 99.99%) from a synthesis gas feed containing 75% of H<sub>2</sub>. However, the hydrogen recovery is only 85 – 90% even with a multi-bed process (Ruthven et al., 1994; Thomas and Barry, 1998).

Methanation, preferential oxidation, and pressure swing adsorption all consume valuable hydrogen at various degrees and add additional steps and costs.

Sorption-enhanced hydrogen production involves the use of a sorbent for selective removal of one of the reaction products, usually CO<sub>2</sub>, thus shifting the equilibrium of the reversible WGS reaction and increasing the CO conversion and H<sub>2</sub> production (Ortiz and Harrison, 2001; Yi and Harrison, 2005; Lin et al., 2002). Harrison and his coworkers combined steam-methane reforming, water gas shift, and CO<sub>2</sub> removal in the same unit with a reforming catalyst and a CO<sub>2</sub> sorbent, and they obtained a H<sub>2</sub> concentration of 96 mol% and a CO concentration as low as 7 ppm (dry basis) (Ortiz and Harrison, 2001; Yi and Harrison, 2005). However, the sorbent had to be regenerated every time before use, thereby requiring additional equipment and cost.

The development of membrane reactor provides one promising approach to overcoming the thermodynamic constraint of WGS and to meeting the requirement of PEMFCs. A membrane reactor combines a reactor with a semi-permeable membrane that extracts product(s). In the water gas shift membrane reactor, the membrane extracts either CO<sub>2</sub> or H<sub>2</sub> to shift the reaction towards the products to improve the conversion. WGS membrane reactors have been studied in recent years (Basile et al., 1996a, 1996b; Huang et al., 2005; Tosti et al., 2003, Giessler et al., 2003). Most of studies were on the membrane reactors using H<sub>2</sub>-selective membranes, usually palladium or other inorganic membranes. Basile et al. (1996a, 1996b) deposited an ultra-thin double-layer palladium film on a tubular ceramic membrane using a co-condensation technique. With such a membrane, they obtained a CO conversion as high as 99.89%. Tosti et al. (2003) added

silver to palladium to decrease membrane embrittlement and to increase the hydrogen permeability. They developed a WGS membrane reactor with a thin Pd-Ag film (50 $\mu$ m thick) coated on the inside wall of a ceramic porous tube and achieved reaction conversions close to 100% (well above the equilibrium value of 80%) at 325 – 330°C. Giessler et al. (2003) packed Cu/Zn/Al<sub>2</sub>O<sub>3</sub> catalyst on the top of a molecular sieve silica membrane, which removed H<sub>2</sub>, and they obtained a conversion of 99% at 280°C. However, for palladium and palladium alloy membranes, the cost and stability of precious metals are still a concern. According to the economic study by Criscuoli et al. (2000), both the capital and operating costs of palladium membrane reactors were higher than those of conventional ones. Their analysis indicated that for the palladium membranes with a thickness equal or less than 20  $\mu$ m, the membrane reactors could be a potential alternative to the conventional reactors. However, preparing such thin, flawless, and durable membranes still remains a challenge for the commercial application of this type of membrane reactor (Armor, 1998).

It appears that no report on the membrane reactors using CO<sub>2</sub>-selective membranes before our previous modeling work (Huang et al., 2005). Our modeling showed that using CO<sub>2</sub>-selective membranes in the hollow fiber configuration with the commercial Cu/ZnO/Al<sub>2</sub>O<sub>3</sub> catalyst particles packed inside the fibers, a CO concentration less than 10 ppm and a H<sub>2</sub> recovery greater than 97% (on the dry basis) are achievable from autothermal reforming syngas. If steam reforming syngas is used as the feed gas, a H<sub>2</sub> concentration of greater than 99.6% and a CO concentration of less than 10 ppm (on the dry basis) can be obtained (Huang et al., 2005).

As we have discussed in Chapter 2, the CO<sub>2</sub>-selective polymeric membranes that we synthesized showed good CO<sub>2</sub>/H<sub>2</sub> and CO<sub>2</sub>/CO selectivities as well as high CO<sub>2</sub> permeability at 110 – 170°C. With these membranes, water gas shift membrane reactors containing both the synthesized flat-sheet CO<sub>2</sub>-selective membrane and the Cu/ZnO/Al<sub>2</sub>O<sub>3</sub> catalyst were developed. While CO<sub>2</sub> was continuously removed, the reversible WGS reaction was shifted forward to improve the CO conversion. In comparison with the H<sub>2</sub>-selective membrane reactor, the CO<sub>2</sub>-selective WGS membrane reactor is more advantageous because (1) a H<sub>2</sub>-rich product is recovered at high pressure (feed gas pressure) and ready to be fed into fuel cells; (2) air and/or steam can be used to sweep the permeated CO<sub>2</sub> on the low-pressure side of the membrane to obtain a high driving force for the separation; and (3) CO<sub>2</sub> at high concentration (>98%) is easily obtained on the permeate side for sequestration, when using low-pressure steam as the sweep gas.

## 3.2 Experiments

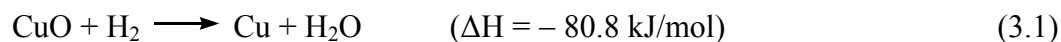
### 3.2.1 Membrane preparation

Flat-sheet CO<sub>2</sub>-selective membranes were prepared by coating an aqueous solution containing poly(vinyl alcohol) (PVA), formaldehyde (crosslinking agent), potassium hydroxide, 2-aminoisobutyric acid potassium (AIBA-K) salt, and poly(allylamine) onto Teflon microporous supports as described in Chapter 2. Most of

the membranes used in the present study contained 40 wt% PVA, 20 wt% KOH, 20 wt% AIBA-K, and 20 wt% poly(allylamine), unless otherwise indicated. The formaldehyde used was equivalent to a 60 mol% of crosslinking degree for PVA.

### 3.2.2 Catalyst preparation and characterization

The catalyst used in the membrane reactor experiments was Cu/ZnO/Al<sub>2</sub>O<sub>3</sub> low-temperature WGS catalyst (C18-AMT-2) obtained from Süd-Chemie Inc. (Louisville, KY). They were 3/16 by 3/32 inch tablets and were crushed to fractions of about 0.1 – 0.5 mm before loading. The commercial low-temperature WGS catalysts are supplied in the oxide form and need to be reduced to metallic copper before they are used (Eq. 3.1).



This reaction is highly exothermic and can easily raise the temperature of the catalyst bed to 500°C, which causes the catalyst to sinter and hence to lose activity (Twigg, 1989). In our case, the requirement to control the reduction temperature had to be followed strictly, since the catalyst was reduced *in situ* with the membrane adjacent to the catalyst bed in the membrane reactor. Temperature higher than 200°C would impose potential damage on the membrane. The usual practice is to conduct the reduction in the presence of an inert gas using a low concentration of hydrogen and then to increase the concentration of hydrogen to complete the reduction. In the present study, two sets of gases used to reduce catalyst due to the availability of the gas cylinders. The first set of gases were (1) 1% H<sub>2</sub>, 3% CO<sub>2</sub>, 3% N<sub>2</sub>, and 93% He and (2) 40% H<sub>2</sub>, 20% CO<sub>2</sub>, and 40%

N<sub>2</sub>. Another set of gases were (1) 2.0% H<sub>2</sub> and 98.0% N<sub>2</sub> and (2) 20.13% H<sub>2</sub> and 79.97% N<sub>2</sub>. Argon was used as the sweep gas in the membrane reactor. All the gas cylinders were purchased from Praxair Inc. (Danbury, CT) or Airgas Inc. (Radnor, PA). During the catalyst reduction, no water was injected to the gas stream. Temperature was kept at 150°C, and gas flow rates were 60 cm<sup>3</sup>/min and 10 cm<sup>3</sup>/min for feed and sweep, respectively. The reduction time for the circular cell was 8 to 10 hours for both the step using a low concentration of hydrogen and the step using a high concentration of hydrogen. The reduction time for the rectangular cell was 12 to 24 hours for each step. The Brunauer-Emmett-Teller (BET) surface areas of the original tablets and the grounded powder of the catalyst were measured by nitrogen adsorption at 77 K using a Micromeritics ASAP 2010 sorptometer (Micromeritics, Norcross, GA).

### 3.2.3 Test unit for membrane reactor experiments

The schematic diagram of the test unit for membrane reactor experiments is shown in Fig. 3.1, and the detailed diagram of the membrane reactor is shown in Fig. 3.2. The test unit was the same unit used previously for the gas permeation as described in Chapter 2. Two stainless steel permeation cells, one circular and one rectangular, were used for both the gas permeation and membrane reactor experiments. The circular permeation cell had an active membrane area of 45.60 cm<sup>2</sup>, and the rectangular permeation cell had a width of 17.5 cm and an active membrane area of 342.7 cm<sup>2</sup>. In both cells, the feed gas flow and the sweep gas flow were counter-current. For the membrane reactor experiments, a specific amount of the catalyst was loaded onto the top

of the membrane for each experiment. One piece of filter paper (particle retention 5 – 10  $\mu\text{m}$ , from Fisher Scientific, Pittsburgh, PA), and one piece of either BHA Teflon support or GE E500A polysulfone support were used between the catalyst and the membrane to keep the catalyst from damaging the membrane. For the circular cell, about 22 to 25 grams of catalyst was loaded each time, while for the rectangular cell, about 40 to 45 grams of catalyst was loaded each time.

The feed gas consisted of 1.0% CO, 17% CO<sub>2</sub>, 45% H<sub>2</sub>, and 37% N<sub>2</sub>, simulating the composition of the synthesis gas from autothermal reforming with air (autothermal reformat). Argon was used as the sweep gas for the ease of gas chromatography analysis. Gas flow rates were controlled by two Brooks flow-meters, one for the feed gas and the other for the sweep gas. A proper amount of water was pumped into two vessels using two Varian Prostar 210 pumps to control the water contents of the feed gas and the sweep gas, respectively, before they entered the permeation cell. During the catalyst reduction for the membrane reactor experiments, no water was pumped. The pressure on the permeate side was set close to atmospheric pressure via a pressure regulator and measured with a pressure gauge. The compositions for both the retentate and permeate gases were analyzed using an Agilent 6890N gas chromatograph with two thermal conductivity detectors (TCDs).

### 3.3 Thermodynamic Analysis

The CO concentration of the synthesis gas from the WGS reaction is usually controlled by the equilibrium of the reaction. Since CO<sub>2</sub> is a product of the WGS reaction, a lower CO concentration is expected if CO<sub>2</sub> is removed from the feed stream of the reaction. A thermodynamic analysis was conducted to estimate the exit CO concentration from this reaction if there is no CO<sub>2</sub> removal. The WGS equilibrium constant,  $K$ , shown in Eq. 3.2 is given by Twigg (1989):

$$K = \exp\left[-13.148 + \left(\frac{5639.5}{T}\right) + 1.077 \ln T + (5.44 \times 10^{-4})T - (1.125 \times 10^{-7})T^2 - \left(\frac{49170}{T^2}\right)\right] \quad (3.2)$$

Another simplified equation (Eq. 3.3) was used by many researchers to calculate the WGS equilibrium constant (Keiski et al., 1993). However, our calculations indicated that the simplified equation (Eq. 3.3) gave significant different results at temperatures ranging from 130 to 200°C compared with the results from Eq. 3.2 as listed in Table 3.3. Therefore, the un-simplified equation Eq. 3.2 was used for the thermodynamic analysis.

$$K = \exp\left(-4.33 + \frac{4577.8}{T}\right) \quad (3.3)$$

T (°C )	<i>K</i> calculated from Eq. 3.3	<i>K</i> calculated from Eq. 3.2
130	1124.5	1531.9
140	854.3	1138.9
150	657.5	859.1
160	512.2	656.82
170	403.5	508.54
180	321.2	398.38
190	258.3	315.54
200	209.6	252.51

Table 3.3: WGS reaction constant from different equations.

### 3.4 Results and discussion

The application in a WGS membrane reactor is quite demanding for polymeric membranes, given the fact that the current commercial WGS catalysts have to be used above 150°C to have enough activity. As shown in Fig. 2.28, the CO<sub>2</sub> permeability was about 4,000 Barrers for the temperatures at 140 – 150°C. Also shown in Fig.2.28, the CO<sub>2</sub>/H<sub>2</sub> selectivity was about 80 or higher for the temperatures at 140 – 150°C. In addition, Fig. 2.26 showed that this type of membrane had a higher CO<sub>2</sub>/N<sub>2</sub> selectivity than CO<sub>2</sub>/H<sub>2</sub> selectivity in this temperature range. Fig. 2.27 shows that the CO<sub>2</sub>/CO selectivity results for this temperature range were greater than 265. Gas permeation results presented above showed that the polymeric membranes that we prepared were capable for the WGS membrane reactor application.

As discussed previously in Section 2.3.5, CO<sub>2</sub> permeability and CO<sub>2</sub>/H<sub>2</sub> selectivity increased significantly as the water concentration on the sweep side or the feed side increased. The performance behavior provides us with a good approach for increasing CO<sub>2</sub> permeability without injecting too much water into the feed stream, since lower water content in the feed stream presents a lower possibility of membrane damage due to water condensation on the feed side. On the other hand, high water concentration in the sweep stream is generally not a threat to the membrane, since liquid water is difficult to permeate through the microporous Teflon support to the high-pressure feed side. So using a high water content in the sweep stream, for example 90 to 95%, while maintaining a relatively low water content in the feed stream, for example 30 to 50%, is a good approach to obtaining high permeability without damaging the membrane. Thus, in the WGS membrane reactor experiments, the water contents in the feed and the sweep streams were kept at 30 – 50% and 93%, respectively, unless stated otherwise.

In the present study, argon was used as the sweep gas for the ease of gas chromatography analysis. Steam can be used to sweep CO<sub>2</sub> on the low-pressure side of the membrane to obtain a high driving force for the separation. It is feasible to use steam alone as the sweep gas, therefore the permeated CO<sub>2</sub> can easily be separated from steam to obtain a high concentration (>98%) for sequestration.

A previous modeling study on the WGS membranes have indicated that H<sub>2</sub> recovery increases from about 90% to more than 97% as the CO<sub>2</sub>/H<sub>2</sub> selectivity increases from 10 to 40 (Huang et al., 2005). A higher CO<sub>2</sub>/H<sub>2</sub> selectivity further increases H<sub>2</sub> recovery and decreases the H<sub>2</sub> loss because of the reduction in H<sub>2</sub> permeation through the

membrane. The modeling work has also shown that the required membrane area drops significantly as CO<sub>2</sub> permeability increases from 1000 to 4000 Barrers; but there is no significant effect for a further CO<sub>2</sub> permeability increase due to the reaction-controlled regime.

### 3.4.1 Catalyst characterization and reduction

The catalyst used in this study was CuZnO/Al<sub>2</sub>O<sub>3</sub> WGS catalyst (C18-AMT-2) from Süd-Chemie Inc. The BET surface areas of the original catalyst tablets and the grounded powder were 121 m<sup>2</sup>/g and 116 m<sup>2</sup>/g, respectively. Both values were higher than the values of 70 to 80 m<sup>2</sup>/g for earlier catalyst samples cited in the literature (Keiski et al., 1993; Twigg, 1989). The catalyst was reduced *in situ* with the membrane in the membrane reactor as described earlier.

In the present study, two sets of gases used to reduce catalyst due to the availability of gas cylinders. First set of gases were (1) 1% H<sub>2</sub>, 3 % CO<sub>2</sub>, 3 % N<sub>2</sub>, and 93 % He, and (2) 40 % H<sub>2</sub>, 20 % CO<sub>2</sub>, and 40 % N<sub>2</sub>. Another set of gases were (1) 2% H<sub>2</sub> and 98% N<sub>2</sub>, and (2) 20.13 % H<sub>2</sub> and 79.97 % N<sub>2</sub>. During the reduction, no water was injected to the gas streams. Temperature was kept at 150°C and gas flow rates were 60 cm<sup>3</sup>/min and 10 cm<sup>3</sup>/min for feed and sweep, respectively. The reduction time for the circular cell was 8 to 10 hours for both the first step using low concentration H<sub>2</sub> and the second step using high concentration of H<sub>2</sub>. While the reduction time for the rectangular cell was 12 to 24 hours for each step.

Figs. 3.3 and 3.4 present typical retentate composition changes during the catalyst reduction using the rectangular cell with a low concentration  $H_2$  and a high concentration  $H_2$  gas mixtures, respectively. These kinds of composition changes were observed for both cells. As we can see,  $H_2$  was consumed significantly during the reduction steps with both low concentration the  $H_2$  and high concentration  $H_2$  gas mixtures. The  $H_2$  concentration increased to the original composition when the catalyst reduction was complete. As high as 4 % of  $CO_2$  was released during reduction, which could be attributed to some carbonate residues from the preparation of the catalyst. When the catalyst reduction reached completion, the  $CO_2$  concentration dropped to zero. Thus,  $H_2$  and  $CO_2$  concentrations were actually used as indicators for the extent of reduction. The catalyst reduction was stopped after the  $H_2$  concentration increased to the original composition and  $CO_2$  disappeared.

Although  $CO_2$  was usually regarded as an inert gas in the catalyst reduction, our results did show some difference between using the first set gases containing  $CO_2$  and using the second set of gases without  $CO_2$ . Fig. 3.5 shows a significant amount of CO was produced near the end of reduction, while no CO was found during reduction with the second set of gases without  $CO_2$ . Such difference can be explained by the presence of the reverse reaction of WGS, in which  $CO_2$  reacts with  $H_2$  to produce CO and  $H_2O$ . This reaction only shows its significant effect after the catalyst has been reduced to a certain extent, thereby having certain activity.

### 3.4.2 Membrane reactor results

After the catalyst activation, the synthesis gas feed containing 1% CO, 17% CO<sub>2</sub>, 45% H<sub>2</sub>, and 37% N<sub>2</sub> (on the dry basis) was admitted into the membrane reactor. Water was pumped into both sides. Fig. 3.6 presents data obtained from this laboratory WGS membrane reactor using the circular cell. The equilibrium CO concentration data from the WGS reaction without CO<sub>2</sub> removal are also plotted in the figure for comparison. The operating temperature was 150°C, and the feed pressure of the synthesis gas was about 32.3 psia. As shown in this figure, the CO concentration in the exit stream, i.e., the H<sub>2</sub> product, was less than 30 ppm (on the dry basis) for various feed water concentrations ranging from 18% to 48%. The water concentration of the sweep steam was kept at 93%. The flow rates of the feed and sweep streams were kept at 1/1 ratio on the dry basis. Since the sweep stream had much more steam, the actual flow rate ratio of the sweep to the feed was about 4/1 to 12/1, mostly 8/1, which gave more driving force for CO<sub>2</sub> transport. As also shown in this figure, higher H<sub>2</sub>O contents decreased the dry CO concentration on the retentate side since higher H<sub>2</sub>O contents not only shifted the WGS reaction equilibrium forward, but also increased the WGS reaction rate and the CO<sub>2</sub> transfer rate. The experimental retentate CO concentrations were much lower than the equilibrium CO concentrations without CO<sub>2</sub> removal. This clearly showed the advantage of *in situ* CO<sub>2</sub> removal.

Since the circular cell had a relatively small membrane area and more chance of having a channeling effect, we set up a rectangular membrane reactor for the scale-up of WGS membrane reactor. This membrane reactor was a rectangular cell with a well-

defined gas flow and velocity profile both for the feed and sweep sides. Thus, it was suitable for modeling and scale-up work. This membrane reactor had 7.5 times the membrane area and two times the catalyst loading of the circular cell membrane reactor, which made both CO<sub>2</sub> removal and catalyst usage more efficient.

For the rectangular membrane reactor experiments, the water concentration of the feed stream was between 40 to 50%, while the water concentration of the sweep steam was kept at 93%. The flow rates of the feed and sweep streams were kept at 1/1 ratio on the dry basis. The actual flow rate ratio of the sweep to the feed was about 8/1, if steam was taken into account. The operating temperature was 150°C, and the feed pressure of the synthesis gas was 29.4 psia.

Fig. 3.7 shows the results obtained from this rectangular WGS membrane reactor. As shown in this figure, the CO concentration in the retentate was less than 10 ppm (on the dry basis), which was equivalent to almost 100% of CO conversion, for the various feed flow rates of the synthesis gas from 20 to 70 cm<sup>3</sup>/min. As the feed flow rate increased, the retentate CO concentration slightly increased owing to the reduced residence time. If the feed pressure of the synthesis gas was higher than 29.4 psia, a higher feed gas rate could be processed to obtain <10 ppm CO in the H<sub>2</sub> product for the given membrane area of the rectangular reactor, as a result of a higher driving force for the CO<sub>2</sub> transport.

Fig. 3.8 shows the equilibrium CO concentrations (on the dry basis) without CO<sub>2</sub> removal at various feed to steam ratios of 7/3, 6/4, and 5/5 (corresponding to the water concentrations of 30, 40, and 50 mol%) from 130 to 190°C. The equilibrium CO concentration was about 190 ppm at 150°C and 40% of steam. Comparison between this CO value and the results shown in Fig. 3.7 clearly demonstrates the effectiveness of the membrane reactor.

Fig. 3.9 gives the plot of the retentate H<sub>2</sub> concentrations vs. the feed flow rates in the rectangular membrane reactor. The percentage of H<sub>2</sub> lost due to its permeation through the membrane was very small. A H<sub>2</sub> concentration of greater than about 50% was achieved.

Temperature (°C)	Retentate CO concentration (ppm, dry)
120*	1279.3
130	29.4
150	5.1

\* Circular cell, others were from the rectangular cell.

Table 3.4: Retentate CO concentration vs. temperature for membrane reactor experiments.

The WGS reaction is moderately exothermic, and hence a low reaction temperature favors a high CO conversion. However, as temperature reduces, the reaction rate decreases. The effect of temperature on the retentate CO concentration obtained from the membrane reactor experiments is shown in Table 3.4. The results suggested that the catalyst that we used did not have much activity below 150°C.

### 3.5 Conclusions

In this study, the water gas shift membrane reactor incorporating both CO<sub>2</sub> removal and the WGS reaction was developed for the hydrogen processing for fuel cells. By removing CO<sub>2</sub> with our synthesized polymeric membranes, the reversible WGS was shifted forward so that the CO concentration was significantly decreased to less than 10 ppm, which was equivalent to almost 100% of CO conversion. A H<sub>2</sub> concentration of greater than 50% (on the dry basis) was achieved. In comparison with methanation, preferential oxidation, and pressure swing adsorption, this process increased the yield of H<sub>2</sub> instead of losing H<sub>2</sub>. Compared with H<sub>2</sub>-selective membrane reactors, this process has some advantages: (1) a H<sub>2</sub>-rich product is recovered at high pressure and ready to be fed into fuel cells; (2) CO<sub>2</sub> at high concentration (>98%) is easily obtained on the permeate side for sequestration, when using low-pressure steam as the sweep gas; (3) the cost of the synthesized polymeric membranes is relatively low (vs. the cost of the H<sub>2</sub>-selective membranes based on precious metals, such as palladium and palladium alloy membranes).

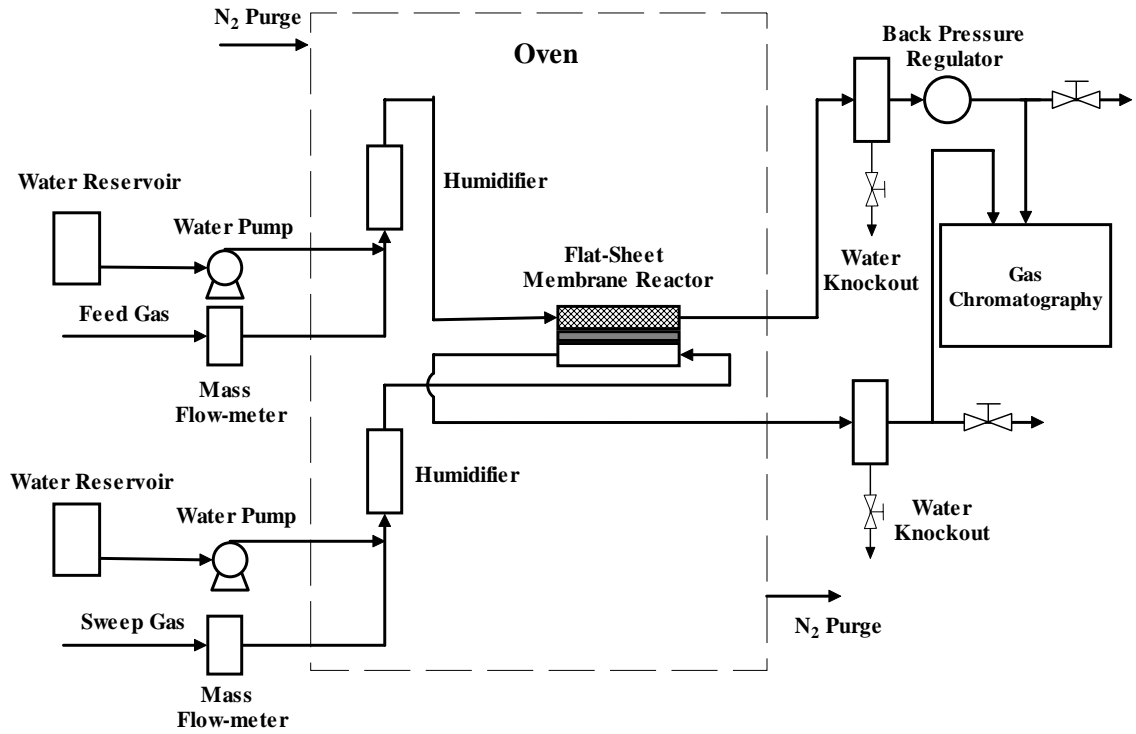


Figure 3.1: Schematic of the test unit for membrane reactors.

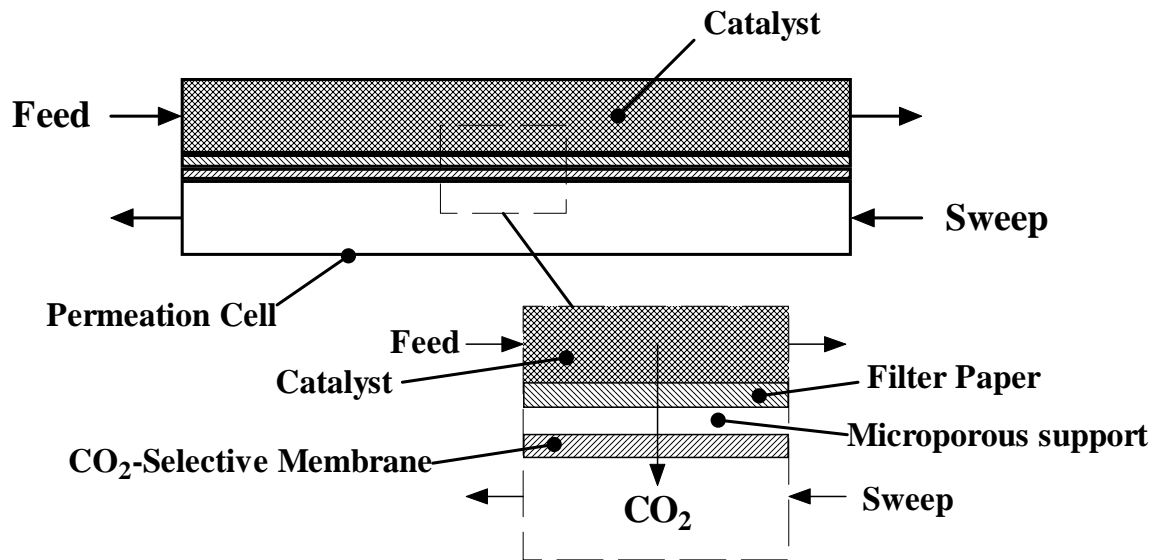


Figure 3.2: Schematic of the water gas shift membrane reactor.

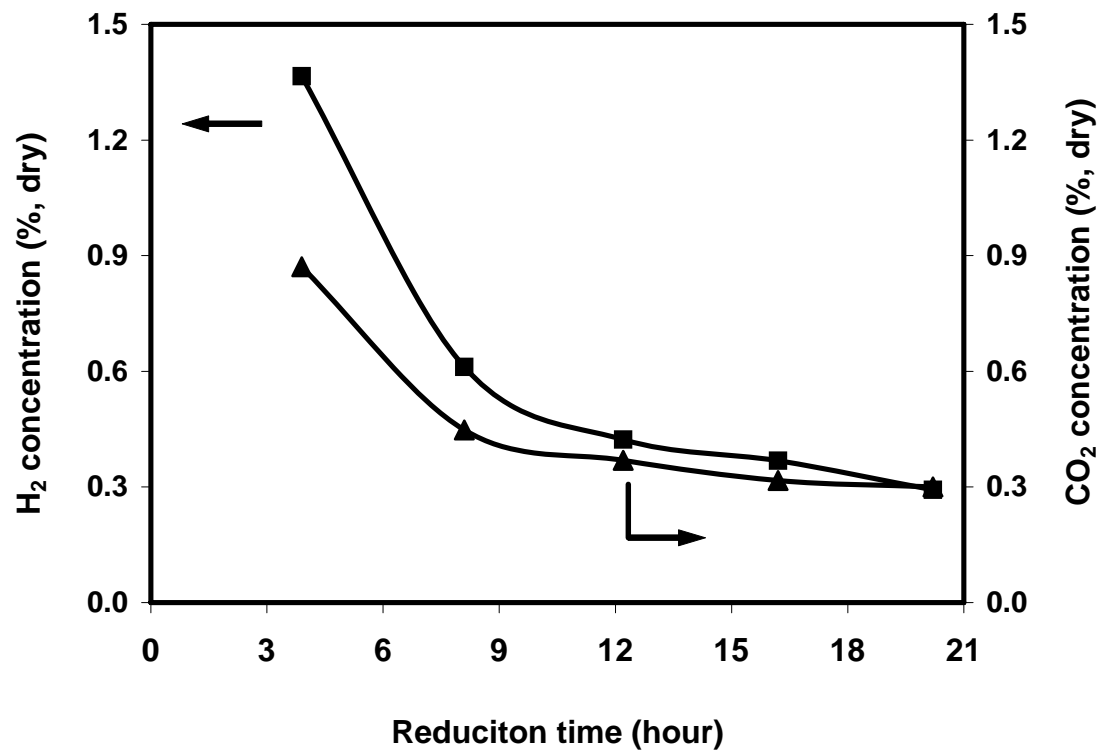


Figure 3.3: Retentate gas composition during catalyst reduction.

(Rectangular cell, feed: 2 % H<sub>2</sub>, and 98 % N<sub>2</sub>, feed pressure: 29.4 psia)

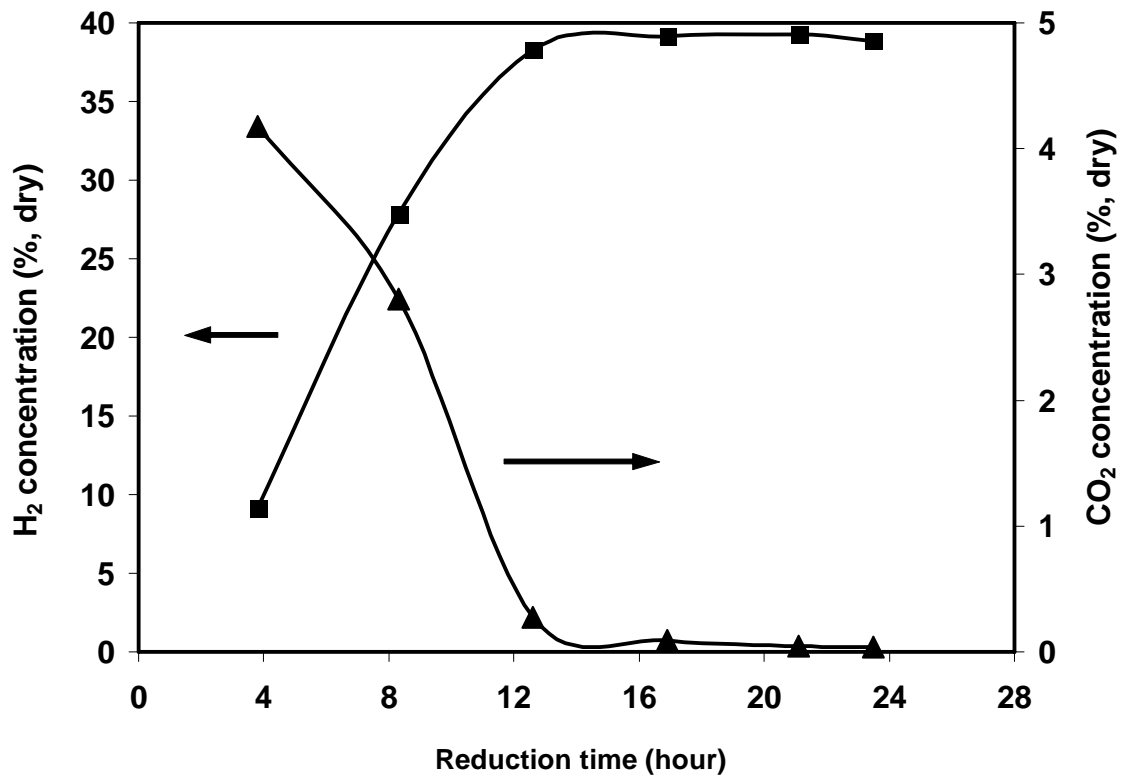


Figure 3.4: Retentate gas composition during catalyst reduction.  
 (Rectangular cell, feed: 39.03 % H<sub>2</sub>, and 60.97 % N<sub>2</sub>, feed pressure: 29.4 psia)

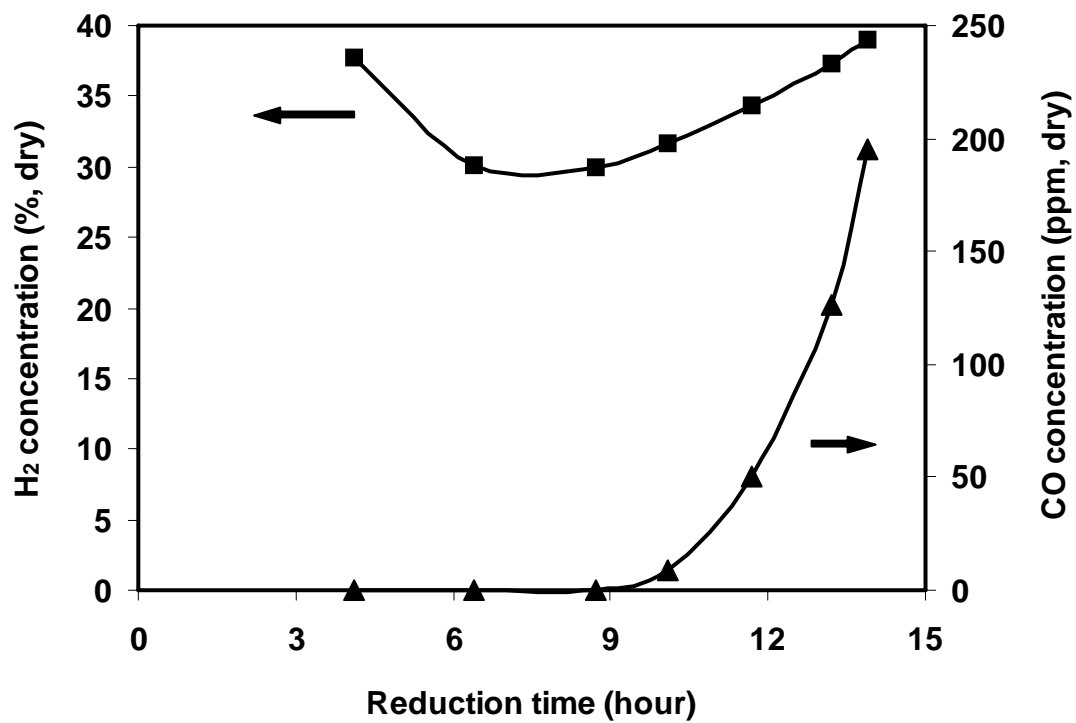


Figure 3.5: Retentate gas composition during catalyst reduction.

(Rectangular cell, feed: 40% H<sub>2</sub>, 40% N<sub>2</sub>, and 20% CO<sub>2</sub>, feed pressure: 29.4 psia, after 6 hours of reduction with 1% H<sub>2</sub>, 3 % CO<sub>2</sub>, 3 % N<sub>2</sub>, and 93 % He)

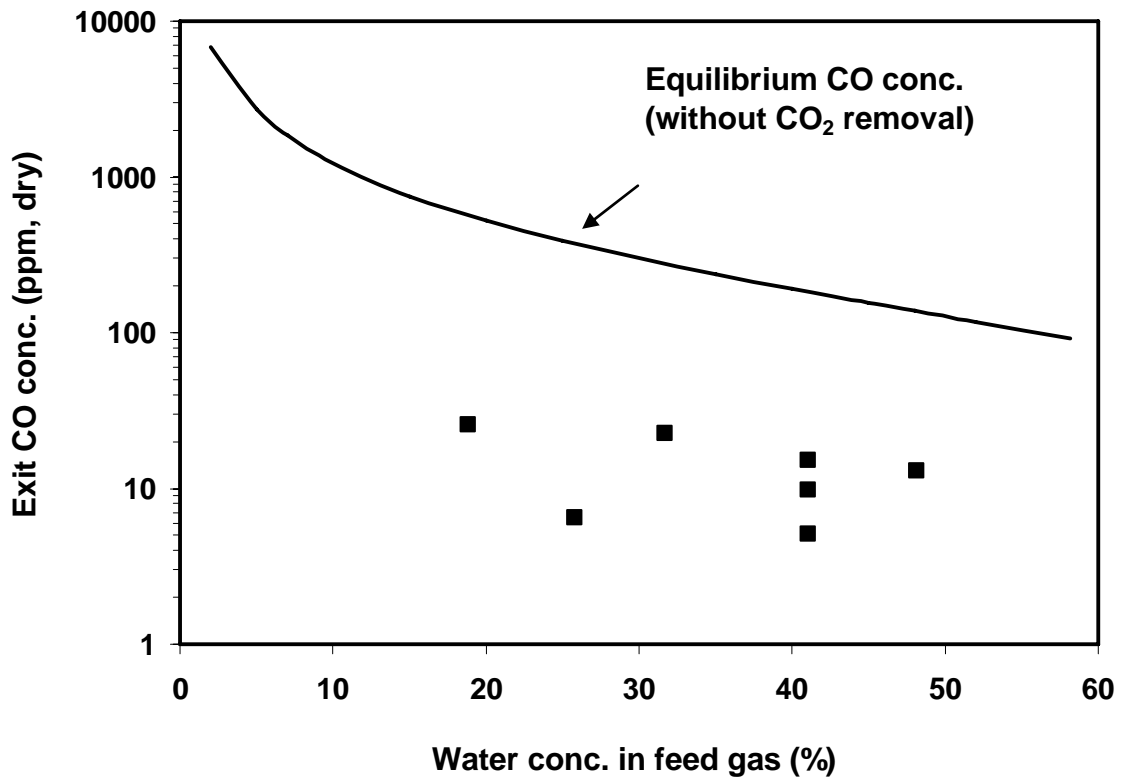


Figure 3.6: Retentate CO concentration vs. feed water concentration in the circular membrane reactor.

(Feed gas: 1% CO, 17% CO<sub>2</sub>, 45% H<sub>2</sub>, and 37% N<sub>2</sub>, T = 150°C, feed pressure = 32.3 psia, sweep pressure = 14.7 psia, feed/sweep flow rates = 1/1 (dry basis))

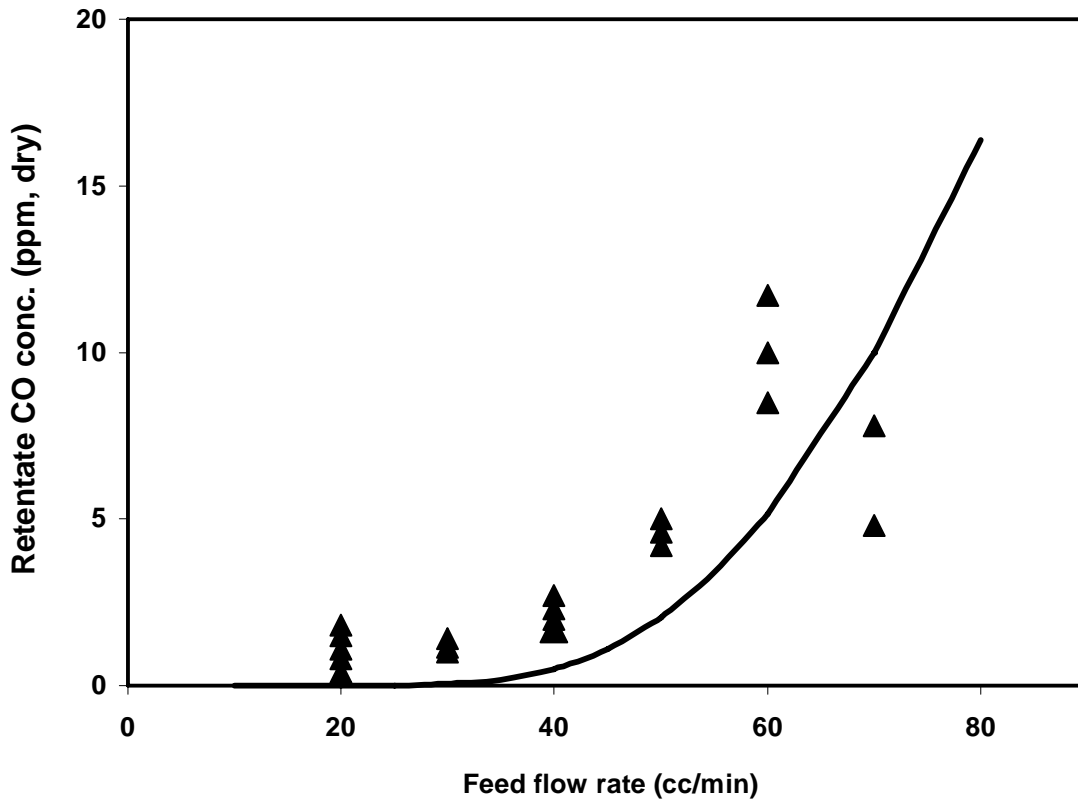


Figure 3.7: Retentate CO concentration vs. feed flow rate in the rectangular WGS membrane reactor.

(Feed gas: 1% CO, 17% CO<sub>2</sub>, 45% H<sub>2</sub>, and 37% N<sub>2</sub>, T = 150°C, feed pressure = 29.4 psia, sweep pressure = 14.7 psia, feed/sweep flow rates = 1/1 (dry basis))

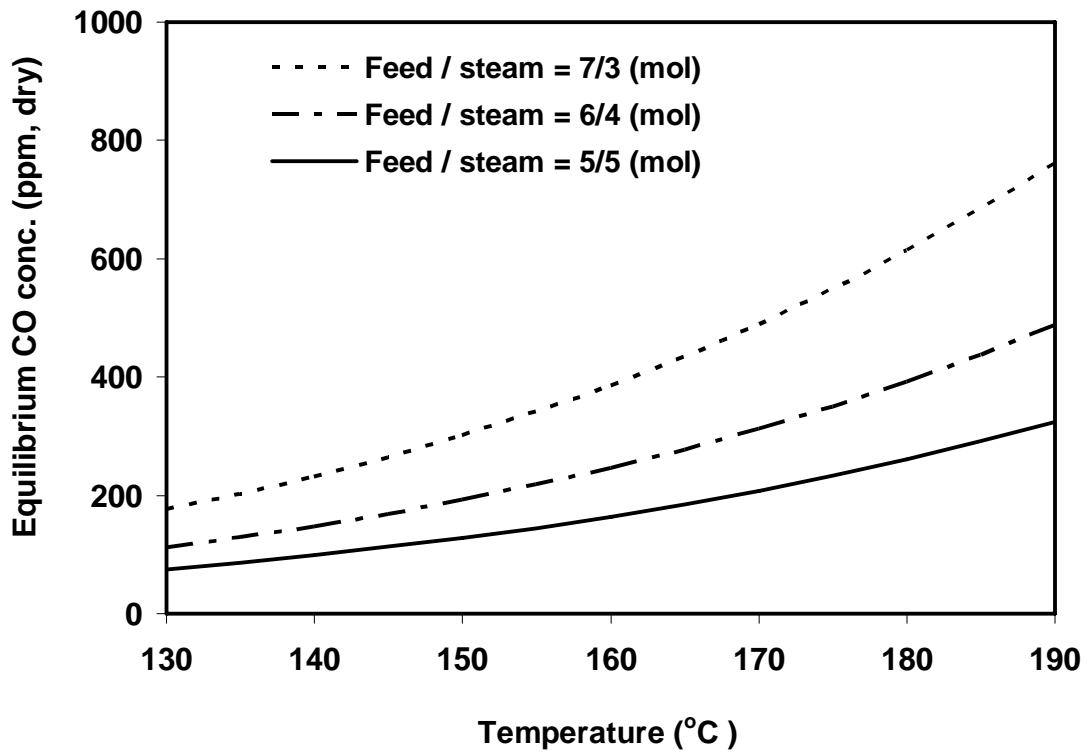


Figure 3.8: Equilibrium CO concentration without CO<sub>2</sub> removal vs. temperature.  
 (Feed gas: 1% CO, 17% CO<sub>2</sub>, 45% H<sub>2</sub>, and 37% N<sub>2</sub>.)

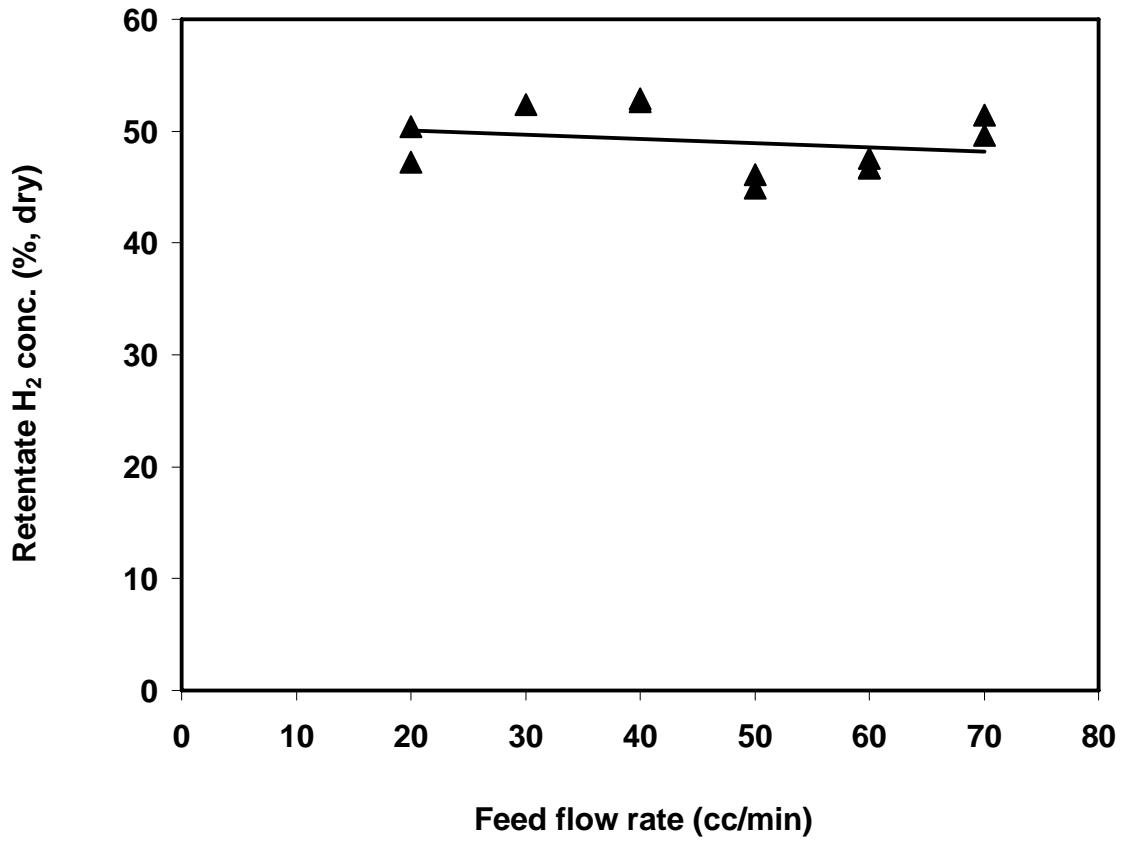


Figure 3.9: Retentate H<sub>2</sub> concentration vs. feed flow rate in the rectangular membrane reactor.

(Feed gas: 1% CO, 17% CO<sub>2</sub>, 45% H<sub>2</sub>, and 37% N<sub>2</sub>, T = 150°C, feed pressure = 29.4 psia, sweep pressure = 14.7 psia, feed/sweep flow rates = 1/1 (dry basis))

## CHAPTER 4

### HYDROGEN PURIFICATION BY CARBON DIOXIDE-REMOVAL MEMBRANE FOLLOWED BY WATER GAS SHIFT REACTION

#### 4.1 Introduction

In the commercial process to produce hydrogen for fuel cells, the synthesis gas after the conventional water gas shift reaction still consists of a significant amount of CO, usually about 0.5 – 1%, which needs to be reduced to less than 10 parts per million (ppm) for proton exchange membrane fuel cells. Therefore, a further CO clean-up step is usually used to decrease CO concentration to meet this requirement. Several methods are currently used or under development for the CO clean-up, including methanation, preferential oxidation, pressure swing adsorption, sorption-enhanced reaction, and membrane separation. The advantages and disadvantages have been discussed in the previous chapters.

In the previous chapter, water gas shift membrane reactors containing both a CO<sub>2</sub>-selective polymeric membrane and the commercial Cu/ZnO/Al<sub>2</sub>O<sub>3</sub> catalyst were developed for the purification of synthesis gas to produce high purity hydrogen. By removing CO<sub>2</sub> simultaneously using the membrane, a CO concentration less than 10 ppm and a H<sub>2</sub> concentration greater than 50% (on the dry basis) were achieved at various flow rates of a simulated synthesis gas in the membrane reactor.

In this chapter, we reported a new process for H<sub>2</sub> purification for fuel cells. This process consisted of CO<sub>2</sub>-removal using a membrane module followed by a conventional low-temperature water gas shift reactor. The schematic diagram of this process is shown in Fig. 4.1. The membrane module can remove more than 99.5% of CO<sub>2</sub> from the feed stream; therefore, the reversible WGS reaction equilibrium can be shifted forward to reduce the CO concentration to less than 10 ppm. With both CO<sub>2</sub>-removal and WGS reaction running at their best operation temperatures, respectively, the best performances of these two processes were combined.

Since CO<sub>2</sub> removal by amine scrubbing followed by methanation is one of the most widely used processes for the CO clean-up, we also investigated a process consisting CO<sub>2</sub> removal followed by methanation. The results of these processes were compared.

## 4.2 Thermodynamic Analysis

The CO concentration of the synthesis gas from the WGS reaction is usually controlled by the equilibrium of the reaction. Since CO<sub>2</sub> is a product of the WGS reaction, a lower CO concentration is expected if CO<sub>2</sub> is removed from the feed stream before the reaction. A thermodynamic analysis was conducted to estimate the effect of CO<sub>2</sub> removal on the exit CO concentration from this reaction. The WGS equilibrium constant,  $K$ , was given in Eq. 3.2.

Fig. 4.2 shows the equilibrium CO concentrations (on the dry basis) of the WGS reaction with a feed gas consisting of 1% CO, 17% CO<sub>2</sub>, 45% H<sub>2</sub>, and 37% N<sub>2</sub>. This feed gas composition was used to simulate the composition of synthesis gas from the

autothermal reforming of gasoline with air. This figure shows the equilibrium CO concentrations at various feed-to-steam ratios of 7/3, 6/4, and 5/5 (corresponding to the steam concentrations of 30, 40, and 50 mol%) from 140 to 200°C. At a feed-to-steam ratio of 5/5 and 150°C, the equilibrium CO concentration was about 97 ppm, which was too high for PEMFCs.

Fig. 4.3 shows the equilibrium CO concentrations (dry basis) of the WGS reaction with a feed gas consisting of 0.10% CO<sub>2</sub>, 1.19% CO, 53.87% H<sub>2</sub>, and 44.84% N<sub>2</sub>. This feed gas composition was used to simulate the composition of the synthesis gas (1% CO, 17% CO<sub>2</sub>, 45% H<sub>2</sub>, and 37% N<sub>2</sub>) after 99.5% of its CO<sub>2</sub> was removed. As we can see from this figure, with 99.5% of the CO<sub>2</sub> removed from the feed gas, the equilibrium CO concentrations were much lower than the values shown in Fig. 4.2. At a feed-to-steam ratio of 5/5 and 150°C, the equilibrium CO concentration was about 8 ppm, which clearly indicates a significant effect of CO<sub>2</sub> removal on the equilibrium CO concentration of WGS reaction.

The thermodynamic analysis shows that if the CO<sub>2</sub>-removal membrane module can remove more than 99.5 % of CO<sub>2</sub> from the feed stream, the reversible WGS reaction equilibrium can be shifted forward to reduce the CO concentration to less than 10 ppm.

## 4.3 Experimental

### 4.3.1 Membrane preparation

The CO<sub>2</sub>-removal membrane module that we used contained one piece of flat-sheet CO<sub>2</sub>-selective membrane. This membrane was prepared by coating an aqueous solution containing poly(vinyl alcohol) (PVA), formaldehyde (crosslinking agent), 2-aminoisobutyric acid (AIBA), potassium hydroxide (KOH), and poly(allylamine) onto a BHA Teflon porous support as described in Chapter 2.

### 4.3.2 Catalyst preparation

The WGS catalyst used in this study was Cu/ZnO/Al<sub>2</sub>O<sub>3</sub> low-temperature WGS catalyst (C18-AMT-2) obtained from Süd-Chemie Inc. They were 3/16-inch by 3/32-inch tablets and were crushed to fractions of about 0.1 – 0.5 mm before loading into a WGS reactor. The catalyst was supplied in the oxide form and was reduced to metallic copper before it was used. The reduction procedure was similar to that described in Chapter 3. In the present study, the catalyst was reduced by using a gas mixture consisting of 2% H<sub>2</sub> and 98% N<sub>2</sub> at 150°C for 8 – 12 hours. Then another gas mixture consisting of 39% H<sub>2</sub> and 61% N<sub>2</sub> was introduced to reduce the catalyst at 150°C for 12 hours. During the catalyst reduction, no water was injected to the gas stream.

The catalyst used for methanation was 0.3 wt% ruthenium on Al<sub>2</sub>O<sub>3</sub> catalyst (C13-LT), which was also from Süd-Chemie Inc. The catalyst was crushed to fractions of about 0.1 – 0.5 mm before loading. The catalyst was activated in the process gas, which consisted of 1.19% CO, 0.10% CO<sub>2</sub>, 53.87% H<sub>2</sub>, and 44.84% N<sub>2</sub>, before it was

used. The activation temperature was 240°C, and the activation duration was about 5 – 8 hours. Again, during the catalyst reduction step, no water was injected to the gas stream.

#### 4.3.3 Test unit for gas permeation, WGS or methanation

The complete test unit for gas permeation, WGS or methanation was the unit depicted in Figs. 2.2 and 3.1. The oven was used to house the membrane permeation cell, the WGS reactor, or the methanation reactor and to control the temperature of one of the devices in use. The stainless-steel rectangular membrane permeation cell was used for the CO<sub>2</sub>-removal experiments, and it had a membrane area of 342.7 cm<sup>2</sup>. A feed gas consisted of 1% CO, 17% CO<sub>2</sub>, 45% H<sub>2</sub>, and 37% N<sub>2</sub> was used for the CO<sub>2</sub>-removal experiments. Argon was used as the sweep gas for the CO<sub>2</sub>-removal experiments. For WGS reaction and methanation, only the feed gas was used, and there was no sweep gas.

For the WGS reaction, a 1/4-inch stainless-steel tubing was used as the reactor to house the Cu/ZnO/Al<sub>2</sub>O<sub>3</sub> catalyst, and about 0.7 – 0.8 gram of the ground catalyst was loaded each time. The direction of gas flow in this reactor was downward. Some quartz wool was placed on both sides of the packed catalyst to prevent the catalyst from moving. After the catalyst was activated as described earlier, a feed gas with steam was introduced into the reactor. Two feed gases with certified compositions were used for the WGS reactor experiments: one consisted of 1% CO, 17% CO<sub>2</sub>, 45% H<sub>2</sub>, and 37% N<sub>2</sub>, and the other was 1.19% CO, 0.10% CO<sub>2</sub>, 53.87% H<sub>2</sub>, and 44.84% N<sub>2</sub>. The first gas mixture was used to simulate the synthesis gas from autothermal reforming of gasoline with air, while the second gas mixture was used to simulate the exit gas after the removal of CO<sub>2</sub>

(approximately 99.5%) from the first gas mixture. The steam concentration in each of the feed gases (one gas used in each experiment) was controlled by using the Varian Prostar 210 pump.

For methanation, a 1/4-inch stainless steel tubing was used as the reactor to house the catalyst of 0.3 wt% ruthenium supported on  $\text{Al}_2\text{O}_3$ , and about 1.5 grams of the ground catalyst was loaded each time. The direction of gas flow in this reactor was downward, and some quartz wool was placed on both sides of the packed catalyst to prevent it from moving. The catalyst was activated as described earlier. The feed gas consisted of 1.19% CO, 0.10%  $\text{CO}_2$ , 53.87%  $\text{H}_2$ , and 44.84%  $\text{N}_2$ , which simulated the exit gas after the removal of  $\text{CO}_2$  (approximately 99.5%) from the first gas mixture used for the WGS reaction as mentioned earlier. No steam was injected into the reactor during methanation.

## 4.4 Results and discussion

### 4.4.1 $\text{CO}_2$ removal experiments

As we have discussed in Chapter 3, using a high water content in the sweep stream while maintaining a relatively low water content in the feed stream is a good approach to obtaining high permeability without damaging the membrane. Thus, in the  $\text{CO}_2$  removal experiments, the water contents in the feed and the sweep streams were kept at 30 – 50% and 93 – 96%, respectively.

As we can see from Figs 2.25 and 2.28, the membranes that we synthesized had gratifying performance at 110 – 120°C. But the performance decreased as temperature increased to 150°C or higher. We therefore chose 120°C as the temperature for the  $\text{CO}_2$

removal step, since steam condensation is not an issue at such a temperature. In addition, waste steam at about 120°C is readily available, especially in petrochemical plants and refineries.

Since the circular permeation cell had a relatively small membrane area (45.6 cm<sup>2</sup>) and more chance to have the channeling effect, we used a rectangular flat-sheet membrane permeation cell (342.7 cm<sup>2</sup>) for the CO<sub>2</sub> removal experiments. This cell had 7.5 times the membrane area of the circular cell permeation cell and a well-defined gas flow and velocity profile on both the feed and sweep sides. The feed gas consisted of 1% CO, 17% CO<sub>2</sub>, 45% H<sub>2</sub>, and 37% N<sub>2</sub> (dry basis). The temperature was 120°C, and the feed pressure was about 29.4 psia (2 atm). The water contents on the feed and sweep sides were approximately 35 – 45 % and 95%, respectively.

Fig. 4.4 shows the CO<sub>2</sub> concentration of the retentate vs. feed gas flow rate (dry basis) for this rectangular cell with water contents of about 35% in the feed stream. The membrane had a thickness of about 35 μm. As we can see in this figure, the membrane was able to remove CO<sub>2</sub> in the retentate from 17 mol% to about 55 ppm at a feed flow rate of 70 cm<sup>3</sup>/min. Fig. 4.5 shows the CO<sub>2</sub> concentration of the retentate vs. feed gas flow rate with water contents of about 45% in the feed stream. This membrane had a thickness of 31 μm. As we can see in Fig. 4.5, the CO<sub>2</sub>-removal was more effective than the results shown in Fig. 4.4. The membrane removed CO<sub>2</sub> in the retentate from 17 mol% to less than 10 ppm at a feed rate of 60 cm<sup>3</sup>/min and to 1,000 ppm at a feed rate of 120 cm<sup>3</sup>/min. The flow rates of the feed and sweep streams were kept at 1/1 ratio on dry basis for both Figs. 4.4 and 4.5. Since the sweep stream had much more steam, the actual flow rate ratio of the sweep to the feed was about 10/1 to 14/1, mostly 12/1, which gave

more driving force for CO<sub>2</sub> transport. The better CO<sub>2</sub>-removal results shown in Fig. 4.5 than those in Fig. 4.4 were mainly due to the higher feed water contents used in the experiment, which resulted in higher CO<sub>2</sub> transport rates due to the reasons described in Chapter 2.

Fig. 4.6 shows the corresponding H<sub>2</sub> concentration of the retentate vs. feed gas flow rate (dry basis) for this rectangular cell with feed water contents of 45%. As shown in this figure, the retentate H<sub>2</sub> concentrations were from 52.0% to 53.4 mol%, which indicated the H<sub>2</sub> loss due to the H<sub>2</sub> permeation across the membrane was negligible.

With the aforementioned membrane area and operating conditions, a feed gas consisting of 1% CO, 17% CO<sub>2</sub>, 45% H<sub>2</sub>, and 37% N<sub>2</sub> could be processed at a flow rate around 100 – 120 cm<sup>3</sup>/min to achieve about 99.5% CO<sub>2</sub> removal. With the above experimental data, we chose a feed gas composition of 1.19% CO, 0.10% CO<sub>2</sub>, 53.87% H<sub>2</sub>, and 44.84% N<sub>2</sub> to simulate the gas composition after the CO<sub>2</sub> removal step.

#### 4.4.2 Water gas shift reaction

After the catalyst activation, the feed gas containing 1.19% CO, 0.10% CO<sub>2</sub>, 53.87% H<sub>2</sub>, and 44.84% N<sub>2</sub> (dry basis) was admitted into the water gas shift reactor. The steam concentrations were 41 to 44 mol%. Table 4.1 summarizes the data at 140 and 150°C for a feed pressure of 29.4 psia. As shown in this table for both temperatures, the CO concentration in the exit stream, i.e., the H<sub>2</sub> product, was less than 10 ppm (dry basis), which met the requirement of PEMFCs. The results were close to the estimation from the thermodynamic analysis described earlier. The gas hourly space velocity (GHSV) was calculated using the following equation. The unit of GHSV is hour<sup>-1</sup>.

$$\text{Gas hourly space velocity} = \frac{\text{Gas flow rate (cm}^3 / \text{h)}}{\text{Reactor volume (cm}^3)} \quad (4.1)$$

Since the WGS reaction is moderately exothermic, lower reaction temperatures decrease the reaction rate but favor a higher CO conversion. As shown in the table, the gas hourly space velocity increased from 5100 to 7650 hour<sup>-1</sup> when the temperature increased from 140 to 150°C, indicating the effects of temperature. The resulting H<sub>2</sub> concentrations were increased to 55.10% and 54.37% at 140°C and 150°C, respectively, from the initial 53.87 mol%.

T (°C)	Steam conc. in feed (%)	CO conc. in exit (ppm, dry)	H <sub>2</sub> conc. in exit (% , dry)	Gas hourly space velocity (hour <sup>-1</sup> , dry)
140	40.97	5.5	55.10	5100
150	43.67	7.7	54.37	7650

Feed gas: 1.19% CO, 0.10% CO<sub>2</sub>, 53.87% H<sub>2</sub>, and 44.84% N<sub>2</sub> (dry basis); feed pressure = 29.4 psia.

Table 4.1: Results of CO<sub>2</sub> removal / water gas shift process.

#### 4.4.3 CO<sub>2</sub> removal / methanation process

Table 4.2 shows the results of the CO<sub>2</sub> removal / methanation process. Although the CO concentration was as low as 4.6 ppm, the H<sub>2</sub> concentration was significantly decreased from the initial 53.87 mol% to 46.84 mol%. Compared with the results from

the CO<sub>2</sub>-removal / water gas shift process shown in Tables 4.1, the advantage of the CO<sub>2</sub>-removal / water gas shift process was clearly demonstrated. The CO<sub>2</sub>-removal / water gas shift process showed higher H<sub>2</sub> concentration and recovery.

Concentration in exit (dry)				Gas hourly space velocity (hour <sup>-1</sup> )
CH <sub>4</sub> (%)	CO <sub>2</sub> (ppm)	CO (ppm)	H <sub>2</sub> (%)	
1.305	63.25	4.6	46.84	1154

Feed gas: 1.19% CO, 0.10% CO<sub>2</sub>, 53.87% H<sub>2</sub>, and 44.84% N<sub>2</sub> (dry basis); T = 240°C, feed pressure = 29.4 psia.

Table 4.2: Results of CO<sub>2</sub> removal / methanation process.

In this study, we chose a feed gas composition of 1% CO, 17% CO<sub>2</sub>, 37% N<sub>2</sub>, and 45% H<sub>2</sub> as the feed gas. In current hydrogen plants, the CO concentrations are mostly between 0.5 – 1 mol% (Twiggs, 1989). If we would choose a feed gas composition of 0.5% CO, 17.5% CO<sub>2</sub>, 37.0% N<sub>2</sub>, and 45.0% H<sub>2</sub> as the feed gas, the gas composition would become 0.6% CO, 0.1% CO<sub>2</sub>, 44.8% N<sub>2</sub>, and 45% H<sub>2</sub> after 99.5% removal of its CO<sub>2</sub> by membrane. A thermodynamic analysis was conducted to estimate the equilibrium CO concentration of the WGS reaction with this feed gas. For this WGS reaction, Figure 4.6 shows the equilibrium CO concentrations at various temperatures and steam concentrations. The thermodynamic analysis shows that lower CO concentrations are achievable compared with the results using the feed gas of 1.19% CO, 0.10% CO<sub>2</sub>,

53.87% H<sub>2</sub>, and 44.84% N<sub>2</sub>, which is shown in Fig. 4.7. This can give this CO<sub>2</sub>-removal / WGS process more flexibility in terms of operating conditions such as temperature and flow rates.

#### 4.5 Conclusions

In this study, a process combining the CO<sub>2</sub>-removal membrane with subsequent water gas shift reaction was developed to meet the requirement of hydrogen processing for fuel cells. With a rectangular membrane permeation cell running at 120°C, the CO<sub>2</sub> concentration in the gas mixture was reduced from 17% to 10 – 1000 ppm, depending on the feed flow rates. Then, a feed gas consisting of 1.19% CO, 0.10% CO<sub>2</sub>, 53.87% H<sub>2</sub>, and 44.84% N<sub>2</sub> was used to simulate the synthesis gas composition after the CO<sub>2</sub>-removal step. With this feed gas, a reactor packed with the low-temperature WGS catalyst of Cu/ZnO/Al<sub>2</sub>O<sub>3</sub> was operated at 140 – 150°C to convert CO to H<sub>2</sub>. With more than 99.5% of CO<sub>2</sub> removed from the synthesis gas in the CO<sub>2</sub> removal step, the reversible WGS reaction was shifted forward so that the CO concentration was decreased to less than 10 ppm (dry basis). The WGS reactor had a gas hourly space velocity of 7650 h<sup>-1</sup> at 150°C, and the H<sub>2</sub> concentration in the exit was more than 54 mol% (dry basis). Compared with the CO<sub>2</sub>-removal / methanation process, the CO<sub>2</sub>-removal / WGS process showed a significantly higher H<sub>2</sub> recovery.

In comparison with other CO clean-up approaches, this process has several advantages: (1) H<sub>2</sub> is not consumed but produced in the stream; (2) the best performance of the membrane separation and that of the conventional WGS reactor are fully utilized; (3) the H<sub>2</sub>-rich product is recovered at high pressure and ready to be fed into fuel cells;

(4) waste steam can be used to sweep the permeated CO<sub>2</sub> on the low-pressure side of the membrane to obtain a high driving force for the separation; (5) CO<sub>2</sub> is easily concentrated on the low-pressure side and thus ready for sequestration.

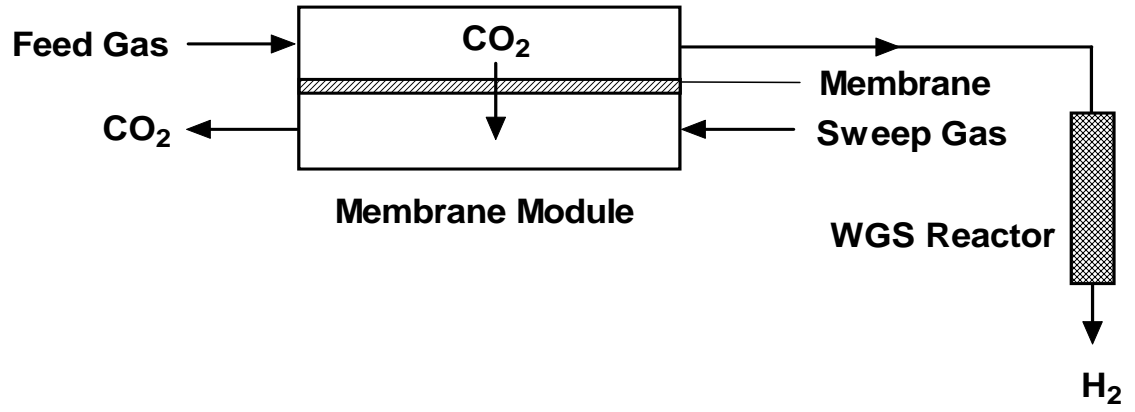


Figure 4.1: Schematic of the CO<sub>2</sub>-removal membrane / water gas shift process.

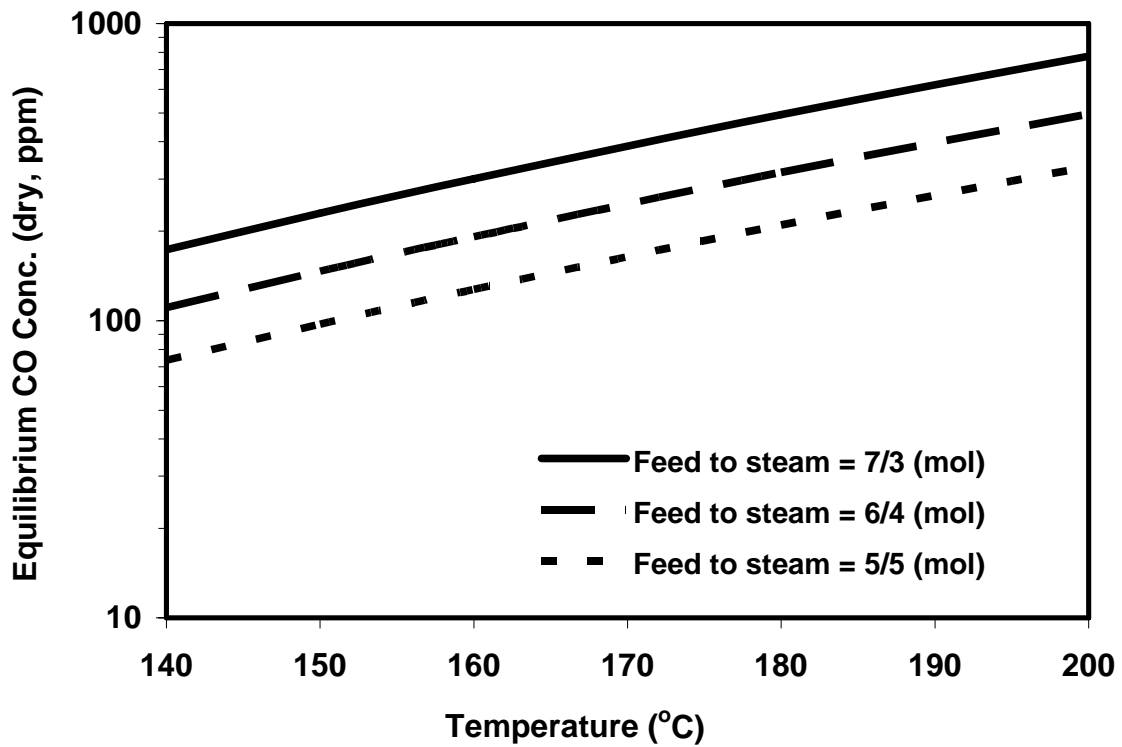


Figure 4.2: Equilibrium CO concentration of WGS reaction vs. temperature for the synthesis gas feed from autothermal reforming of gasoline with air.

Feed gas: 1% CO, 17% CO<sub>2</sub>, 45% H<sub>2</sub>, and 37% N<sub>2</sub>.

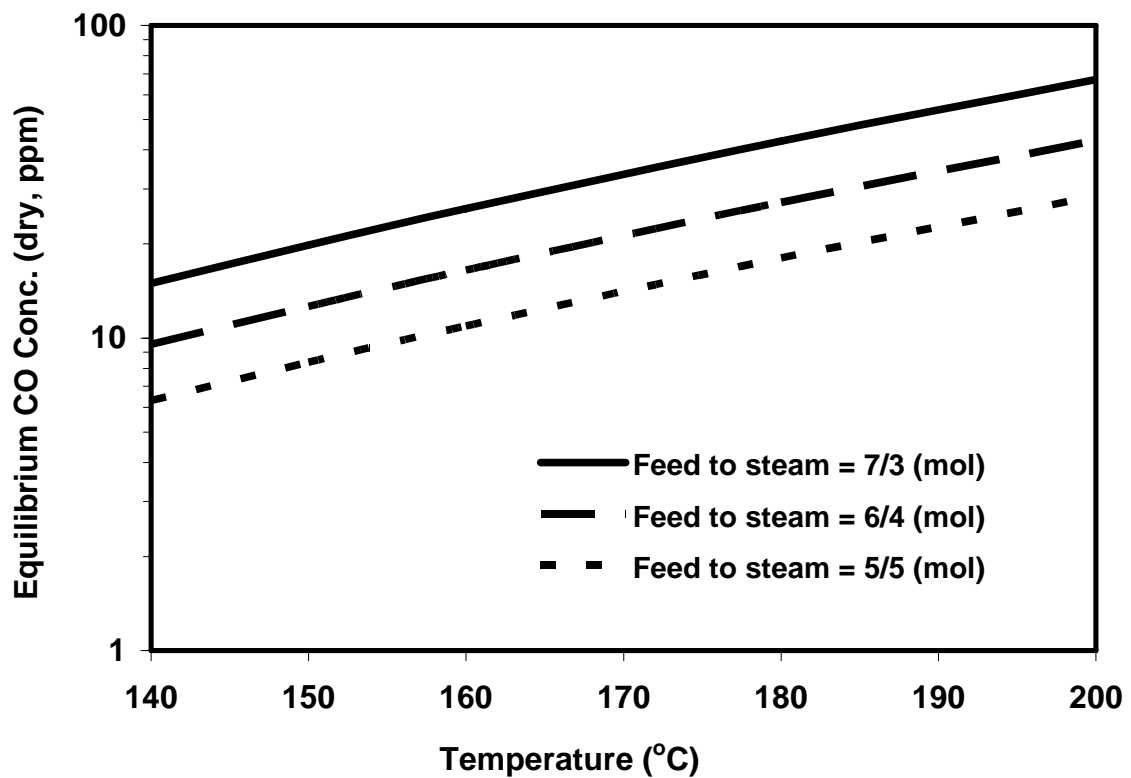


Figure 4.3: Equilibrium CO concentration of WGS reaction vs. temperature for the synthesis gas feed after CO<sub>2</sub> removal.

Feed gas: 1.19% CO, 0.10% CO<sub>2</sub>, 53.87% H<sub>2</sub>, and 44.84% N<sub>2</sub>.

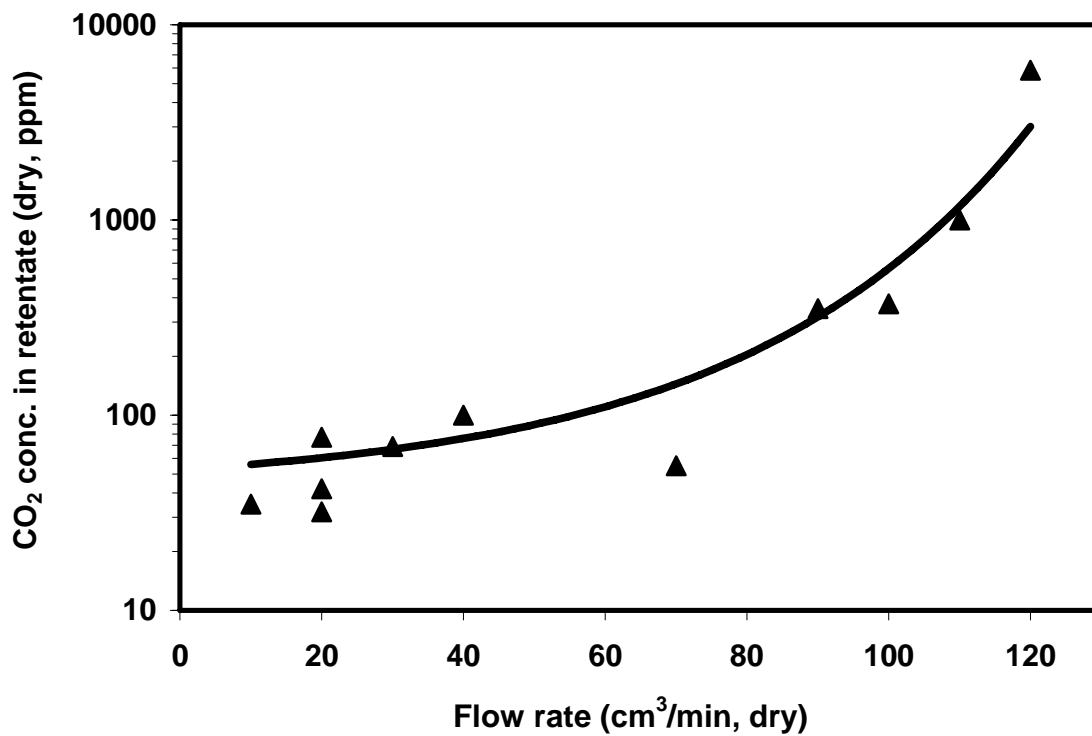


Figure 4.4: CO<sub>2</sub> concentration in retentate vs. feed flow rate in the rectangular cell.  
T = 120°C; feed gas: 1.0% CO, 17% CO<sub>2</sub>, 45% H<sub>2</sub>, and 37% N<sub>2</sub>; feed water content = 35%; feed pressure = 29.4 psia; feed / sweep ratio = 1/1 (dry basis).

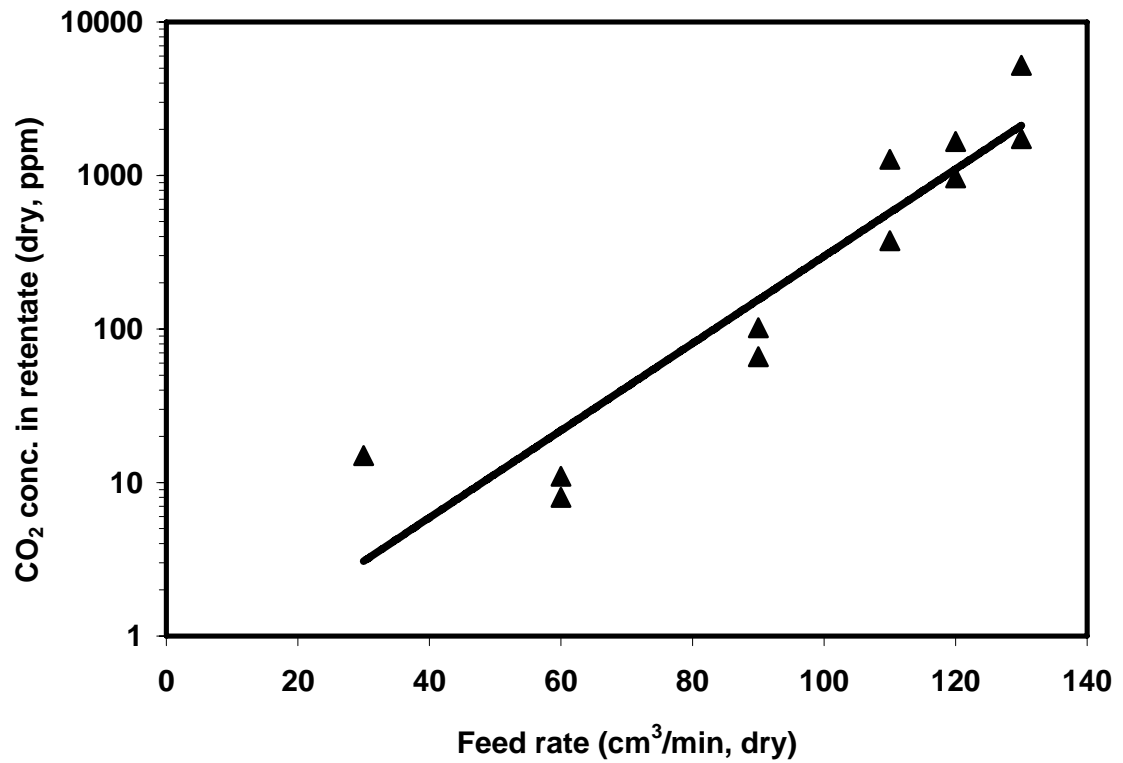


Figure 4.5: CO<sub>2</sub> concentration in retentate vs. feed flow rate in the rectangular cell.  
T = 120°C; feed gas: 1.0% CO, 17% CO<sub>2</sub>, 45% H<sub>2</sub>, and 37% N<sub>2</sub>; feed water content = 45%; feed pressure = 29.4 psia; feed / sweep ratio = 1/1 (dry basis).

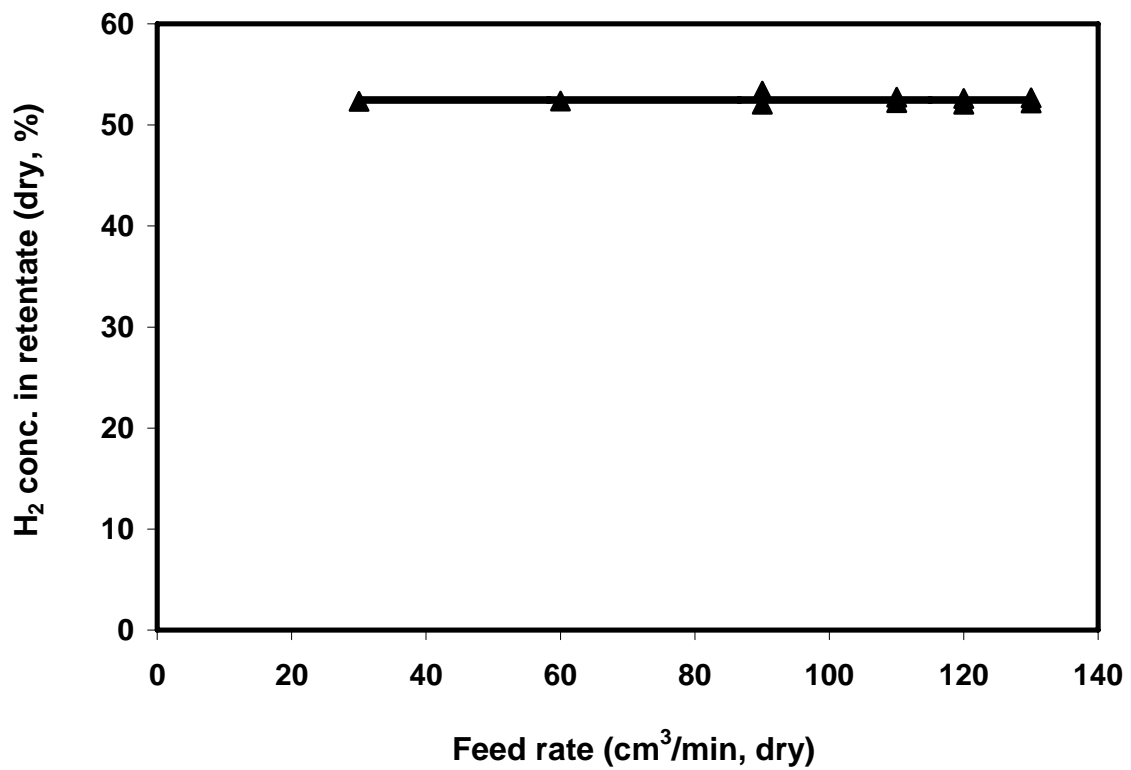


Figure 4.6: H<sub>2</sub> concentration in retentate vs. feed flow rate in the rectangular cell.  
T = 120°C; feed gas: 1.0% CO, 17% CO<sub>2</sub>, 45% H<sub>2</sub>, and 37% N<sub>2</sub>; feed water content = 45%; feed pressure = 29.4 psia; feed / sweep ratio = 1/1 (dry basis).

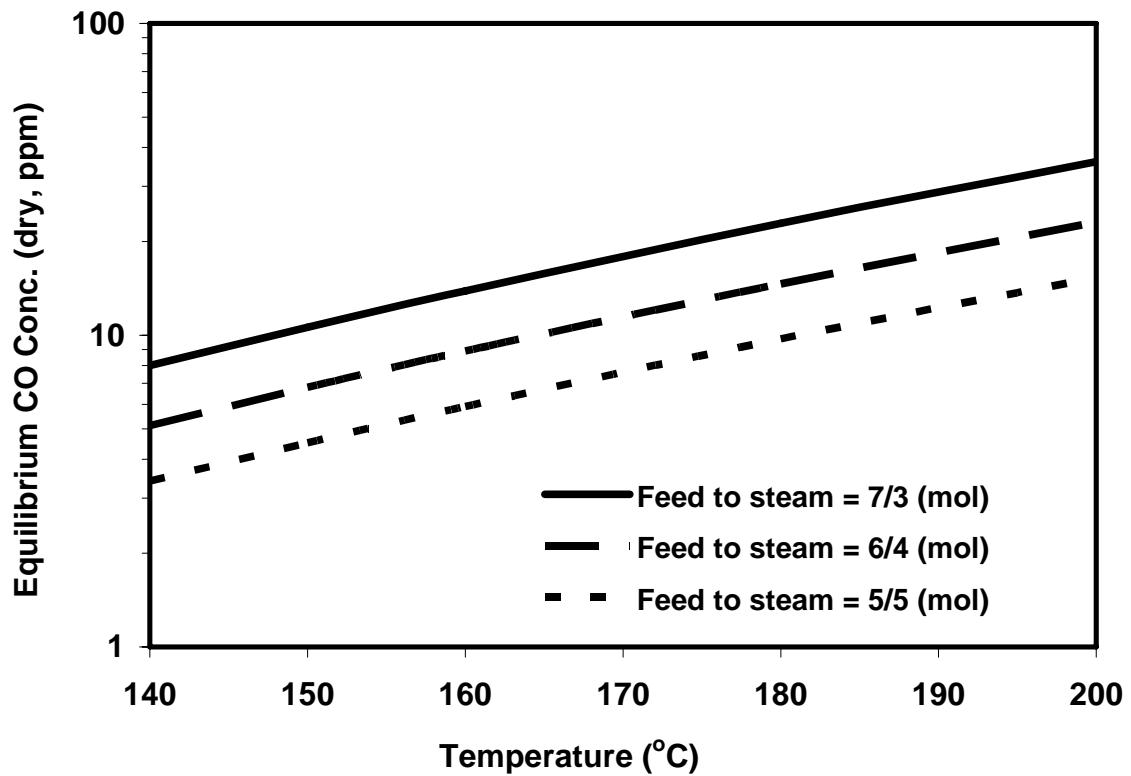


Figure 4.7: Equilibrium CO concentration of WGS reaction after CO<sub>2</sub> removal vs. temperature.

Feed gas: 0.60% CO, 0.10% CO<sub>2</sub>, 55.50% H<sub>2</sub>, and 44.80% N<sub>2</sub>.

## CHAPTER 5

### CO<sub>2</sub>-SELECTIVE MEMBRANES FOR HIGH PRESSURE APPLICATIONS

#### 5.1 Introduction

Synthesis gas is the primary source for hydrogen as well as an intermediate for a broad range of chemicals. In the United States, most hydrogen is produced by steam reforming of natural gas followed by the water gas shift reaction (Kroschwitz and Howe-Grant, 1995). The resulting synthesis gas contains hydrogen, carbon monoxide, and carbon dioxide. The separation of CO<sub>2</sub> from synthesis gas is a critical step to obtain high purity hydrogen, which is used as the fuel for fuel cells and an important raw material in many industrial processes. In comparison with removing H<sub>2</sub> from synthesis gas, removing CO<sub>2</sub> is more advantageous because a high-purity H<sub>2</sub> product is recovered at the feed gas pressure, thereby eliminating expensive recompression of H<sub>2</sub> for the subsequent process.

Using membrane for CO<sub>2</sub> separation is a relatively new approach to capturing and concentrating CO<sub>2</sub> with reduced energy consumption, enhanced weight and space efficiency, and operational simplicity. Current CO<sub>2</sub>-selective membranes are based on either the solution-diffusion mechanism or the facilitated transport mechanism. For

membranes based on the solution-diffusion mechanism, it was very challenging to achieve high CO<sub>2</sub>/H<sub>2</sub> selectivity since H<sub>2</sub> usually exhibits an unfavorably higher diffusion coefficient than CO<sub>2</sub> does. Although CO<sub>2</sub> usually has higher solubility than H<sub>2</sub> does, in most conventional polymeric membranes, diffusivity selectivity dominates the overall selectivity, thereby resulting in CO<sub>2</sub>/H<sub>2</sub> selectivity less than one (Lin and Freeman, 2005a). Lin, Freeman, and their coworkers synthesized highly branched crosslinked poly(ethylene glycol) membranes and achieved CO<sub>2</sub>/H<sub>2</sub> selectivity of 31 and a CO<sub>2</sub> permeability of 410 Barrers at -20°C (Lin and Freeman, 2005a; 2005b; Lin et al., 2005; 2006a; 2006b), which is not a common temperature for the practical operating conditions of synthesis gas. Their strategy was incorporating polar groups, such as ethylene oxide, to enhance the interactions between CO<sub>2</sub> and membranes, while maintaining membranes' size-sieving ability at a very weak level to bring  $D_{CO_2}/D_{H_2}$  as close to one as possible. Yet, with conventional solution-diffusion membranes, increasing selectivity for the gas of interest is often accompanied by a decrease in permeability, and vice versa (Gottschlich et al., 1988).

The requirements by the refinery industry for the applications of polymeric CO<sub>2</sub>-removal membranes for CO<sub>2</sub>/H<sub>2</sub> separation are challenging, since feed pressures higher than 200 psia and temperatures ranging from 100 to 200°C are preferred. High flux and CO<sub>2</sub>/H<sub>2</sub> selectivity higher than 30 are required for the membranes, since higher flux means less membrane area and less equipment investment and higher CO<sub>2</sub>/H<sub>2</sub> selectivity means less H<sub>2</sub> loss.

The present chapter reports on the experimental results using polymeric CO<sub>2</sub>-selective membranes for synthesis gas purification. The effects of feed pressure, microporous support, temperature, and permeate pressure were investigated using a simulated synthesis gas containing 20% of CO<sub>2</sub> and 80% of H<sub>2</sub> and a feed gas containing 20% of CO<sub>2</sub>, 40% of H<sub>2</sub>, and 40% of N<sub>2</sub>.

## 5.2 Experimental

### 5.2.1 Membrane preparation

Polymeric CO<sub>2</sub>-selective membranes with the thin-film-composite structure were prepared by casting an aqueous solution onto a microporous support as described in Chapter 2. The following microporous supports were evaluated in this study. The BHA Teflon® supports (thickness: 60 μm, average pore size: 0.2 μm) was given by BHA Technologies, Kansas City, MS. Microporous polysulfone supports, GE E500A (with a thickness of about 50 μm excluding a non-woven fabric support and an average pore size of about 0.05 μm) and GE A1 (with a thickness of about 50 μm excluding a non-woven fabric support and an average pore size of about 0.009 μm), were kindly given by GE Infrastructure (Vista, CA). The NL-2 microporous polysulfone supports (with a thickness of about 50 μm excluding a non-woven fabric support and an average pore size of about 0.05 μm) was kindly donated by NL Chemical Technology, Inc. (Mount Prospect, IL). GE E500A, GE A1, and NL-2 microporous polysulfone supports were mainly used for this study.

### 5.2.2 Gas permeation measurements

The gas permeation tests were conducted by using the same gas permeation apparatus shown in Fig. 2.2. The circular stainless steel cell with an active membrane area of 45.60 cm<sup>2</sup> was used for measuring the transport properties of the membranes. The bottom piece of the stainless steel cell was redesigned and tailor-made for this high-pressure application. As mentioned earlier, one feed gas consisted of 20% CO<sub>2</sub> and 80% H<sub>2</sub> (all on dry basis). This composition was used to simulate the composition of the synthesis gas from the methane-steam reforming and the subsequent water gas shift reaction. Another feed gas consisting of 20% CO<sub>2</sub>, 40% H<sub>2</sub>, and 40% N<sub>2</sub> was also used due to the availability of the gas cylinder. Argon was used as the sweep gas for the ease of gas chromatography (GC) analysis. Gas flow rates were controlled by two Brooks flow-meters. The feed and sweep gas rates were kept at 60 or 30 cm<sup>3</sup>/min. A proper amount of water was pumped into the two vessels housed in the oven using two Varian Prostar 210 pumps to control the water contents of the feed gas and the sweep gas, respectively.

## 5.3 Results and discussion

### 5.3.1 Effects of feed pressure on separation performance

The effects of feed pressure on CO<sub>2</sub> permeability and CO<sub>2</sub>/H<sub>2</sub> selectivity were investigated using the membranes with a thickness of 48 to 56 μm on the GE E500A microporous polysulfone support. The feed pressures ranged from 70 to 440 psia, while the permeate pressures were maintained at approximately 15 psia. The temperature was maintained at 110°C.

Fig. 5.1 illustrates the effect of feed pressure on CO<sub>2</sub> permeability. As illustrated in this figure, the CO<sub>2</sub> permeability decreased when the feed pressure increased. This can be explained with the carrier saturation phenomenon as described earlier in Chapter 2. When the partial pressure of CO<sub>2</sub> is equal to or higher than a critical CO<sub>2</sub> partial pressure,  $p_{1c}$ , the carrier saturation occurs, in which the concentration of CO<sub>2</sub>-carrier reaction product attains its maximum value and becomes a constant. In comparison with its facilitated transport, the transport of CO<sub>2</sub> via the solution-diffusion mechanism is negligible. Therefore, the total CO<sub>2</sub> flux remains constant as the feed pressure increases. In Eq. 2.2, in order to maintain the equality, increasing the CO<sub>2</sub> partial pressure,  $p_1$ , will not further increase the CO<sub>2</sub> flux. Thus, CO<sub>2</sub> permeability will decrease.

Fig. 5.2 depicts the effect of feed pressure on CO<sub>2</sub>/H<sub>2</sub> selectivity. As depicted in this figure, the CO<sub>2</sub>/H<sub>2</sub> selectivity reduced as the feed pressure increased. Again, this can be explained using the carrier saturation phenomenon described earlier that CO<sub>2</sub> permeability reduced as the pressure increased. Unlike CO<sub>2</sub>, H<sub>2</sub> has no chemical association with the carriers. Its sorption in the membrane can be described by the Henry's law, and its permeability does not subject to the carrier saturation phenomenon and usually does not change with pressure significantly. As a result, the CO<sub>2</sub>/H<sub>2</sub> selectivity reduced as the pressure increased. In addition to the carrier saturation phenomenon, we believe that the decrease of the water content in the membrane contributed to the decrease of CO<sub>2</sub> permeability at higher pressure shown in Fig. 5.2. The maximum water contents at various temperatures and pressures were plotted in Fig. 5.3. The saturated steam pressures used in the calculation were obtained from literature (Smith, Van Ness, and Abbott; 2005). As Fig. 5.3 shows, the maximum water content

drops as pressure is increased. At 29.4 psia, the maximum water contents are 50 to 98% in the temperature range of 100 – 120°C, the maximum water contents drop to 3.3 to 6.5% at 440 psia. As we have illustrated earlier in Chapter 2, the water content has a significant effect on the membrane performance. At low feed pressures, such as 29.4 psia, we can use a feed water content of 30 – 50 %, which is below the max water content but can still give the membrane excellent performance. However, at feed pressures, such as 220 and 440 psia, the maximum water contents are too low to provide the membranes the best performance.

### 5.3.2 Effects of microporous support on separation performance

The membranes that we synthesized had a composite structure. The dense active layer provided separation, and the microporous support provided mechanical strength. According to Ho and Dalrymple (1994), the total mass transfer resistance for the CO<sub>2</sub> transfer across the membrane can be expressed by Eq. 5.1.

$$\frac{p_1 - p_2}{N} = \frac{l}{k_f H_{AB|p1}} + \frac{l}{k_r H_{AB|p2}} + \frac{\ell}{D_A H_A + D_{AB} H_{AB|p1}} \quad (5.1)$$

The three terms on the right side of Eq. 5.1 are the mass transfer resistances due to the forward reactions between CO<sub>2</sub> and the carriers, the reverse reactions between CO<sub>2</sub> and the carriers, and the mass transfer resistances of CO<sub>2</sub> and CO<sub>2</sub>-carrier complexes in the membrane, respectively. Alternatively, Eq. 5.1 can be expressed as:

$$R_t = (R_f + R_r) + l/P \quad (5.2)$$

Thus,  $P$  in Eq. 5.2 represents the “true” permeability of CO<sub>2</sub> with both the mobile and fixed carriers, which is independent of membrane thickness and excluding the mass

transfer resistances due to the forward and reverse reactions. The mass transfer resistance due to the microporous support is usually neglected due to the open structure of the microporous support. But our experimental data suggested that this may be dependent on the type of microporous support and the feed pressure. Four microporous supports were investigated in the study as shown in Table 5.1.

Type	Microporous Teflon support	E500A polysulfone support	A1 polysulfone support	NL-2 polysulfone support
Source	BHA Technology	GE Infrastructure	GE Infrastructure	NL Chemicals, Inc.
Thickness ( $\mu\text{m}$ )	59.4	140 – 150	140 – 150	146
Thickness excluding fabric ( $\mu\text{m}$ )	59.4	~ 50	~ 50	~ 50
Average pore size ( $\mu\text{m}$ )	0.2	0.05	0.009	~ 0.05

Table 5.1: Microporous supports investigated.

At low feed pressures, such as 30 psia, the membranes coated on the four supports gave comparable results, and the mass transfer resistance due to the microporous support was negligible. When the feed pressures were increased to more than 65 psia, the  $\text{CO}_2$  flux and  $\text{H}_2$  flux showed different behaviors as the  $\text{CO}_2$  and  $\text{H}_2$  pressure differences were increased.

Feed P (psia)	CO <sub>2</sub> partial pressure difference, $\Delta p_{CO_2}$ (psia)	H <sub>2</sub> partial pressure difference, $\Delta p_{H_2}$ (psia)	$\alpha$ (CO <sub>2</sub> /H <sub>2</sub> )	CO <sub>2</sub> flux $10^{-6} \text{cm}^3$ (STP)/(cm <sup>2</sup> s)	H <sub>2</sub> flux $10^{-6} \text{cm}^3$ (STP)/(cm <sup>2</sup> s)
64.7	8.86	37.23	28.6	150.0	38.56
99.7	15.11	65.10	15.2	113.5	52.98
64.7	8.98	38.76	23.1	120.5	37.27

The data was summarized from Table A. 16 of Appendix A.

Table 5.2: Flux vs. partial pressure difference for a membrane on the microporous Teflon support.

As shown in Table 5.2, when the feed pressure was increased from 64.7 psia to 99.7 psia, the H<sub>2</sub> pressure difference across the membrane was increased by 74.8 % , but the H<sub>2</sub> flux of this membrane on the Teflon support only increased by 37.4 %. Since H<sub>2</sub> permeates through the membrane via the solution-diffusion mechanism, H<sub>2</sub> flux is usually linear with its driving force, the H<sub>2</sub> pressure difference, therefore; such a behavior is abnormal. On the other hand, the CO<sub>2</sub> flux even dropped by 24.3 %, when the CO<sub>2</sub> pressure difference across the membrane was increased by 70.5 %. It was believed that these behaviors were caused by the compaction of the BHA Teflon supports under the high pressures. The thickness of the support before testing was 59.4  $\mu\text{m}$  and the thickness of the support was reduced to less than 10  $\mu\text{m}$  after testing, which confirmed the compaction. These Teflon supports were highly porous and soft, which made them subject to compaction. As we can see from Table 5.2, the CO<sub>2</sub> flux and H<sub>2</sub> flux did not

reach the initial values when the feed pressure was decreased from 99.7 to 64.7 psia, which indicated that the compaction was not recovered when the feed pressure dropped.

Table 5.3 shows the CO<sub>2</sub> and H<sub>2</sub> fluxes of a membrane on an E500A microporous polysulfone support at different CO<sub>2</sub> and H<sub>2</sub> partial pressures. The H<sub>2</sub> flux increased by 21.3 %, while the H<sub>2</sub> pressure difference across the membrane was increased by 45.0 %. Although this might still suggest some minor compaction of the support, the effects were much less pronounced than in the case of the Teflon microporous support. As also shown in Table 5.3, the CO<sub>2</sub> flux increased by 9.1 % when the CO<sub>2</sub> pressure difference across the membrane was increased by 47.5 %, which can be explained by the carrier saturation phenomenon described earlier. Since pressures as high as 440 psia were required for some applications, the BHA Teflon microporous supports were not further used for such a high pressure application.

Feed P (psia)	CO <sub>2</sub> partial pressure difference, $\Delta p_{CO_2}$ (psia)	H <sub>2</sub> partial pressure difference, $\Delta p_{H_2}$ (psia)	$\alpha$ (CO <sub>2</sub> /H <sub>2</sub> )	CO <sub>2</sub> flux $10^{-6} \text{cm}^3$ (STP)/(cm <sup>2</sup> s)	H <sub>2</sub> flux $10^{-6} \text{cm}^3$ (STP)/(cm <sup>2</sup> s)
69.7	8.21	44.28	37.2	1053	333
94.7	12.11	64.20	32.2	1149	404

The data was summarized from Table A. 17 of Appendix A.

Table 5.3: Flux vs. partial pressure difference for a membrane on the E500A microporous polysulfone support.

### 5.3.3 Effects of temperature on separation performance

The effects of temperature on CO<sub>2</sub> permeability and CO<sub>2</sub>/H<sub>2</sub> selectivity were studied in the temperature range of 100°C to 180°C using the membranes with a thickness of 38 to 68 μm on the E500A support. The feed pressure was maintained at about 220 psia, while the permeate pressure was approximately 15 psia.

Fig. 5.4 illustrates the effect of temperature on CO<sub>2</sub> permeability from 100°C to 180°C. As illustrated in this figure, CO<sub>2</sub> permeability increased initially then decreased as temperature increased. The lower CO<sub>2</sub> permeability at 100°C than at 110°C was presumably due to the lower partial pressure of steam at 100°C, thus the lower water content inside the membrane. The CO<sub>2</sub> permeability decrease from 110°C to 180°C was presumably due to the reduction of water retention in the membrane as the temperature increased, since the mobility of mobile and fixed carriers and the reaction rates of CO<sub>2</sub> with the carriers were affected by the water content of the membrane. Lowering the water content inside the membrane decreased the mobility of both mobile and fixed carriers and the reaction rates of CO<sub>2</sub> with the carriers (Eqs. 2.4 – 2.6).

Fig. 5.5 shows the effect of temperature on CO<sub>2</sub>/H<sub>2</sub> selectivity from 100°C to 180°C. As shown in the figure, CO<sub>2</sub>/H<sub>2</sub> selectivity reduced as temperature increased. This is due to the fact that CO<sub>2</sub> permeability decreased as temperature increased, while the transport of H<sub>2</sub> was not affected by temperature significantly.

One membrane coated on NL-2 microporous polysulfone support was also investigated at temperatures ranging from 110 – 150°C and feed pressures of 219.7 and 429.7 psia. The feed gas consisted 19.7 % of CO<sub>2</sub>, 39.4 % of H<sub>2</sub>, and 40.9% of N<sub>2</sub>. Fig.

5.6 shows the CO<sub>2</sub> flux and H<sub>2</sub> flux as functions of temperature at a feed pressure of about 440 psia. At 110°C and 430 psia, the CO<sub>2</sub> flux was 2.81 X 10<sup>-3</sup> cm<sup>3</sup> (STP) / (cm<sup>2</sup>s), and the flux dropped to 1.48 X 10<sup>-4</sup> cm<sup>3</sup> (STP) / (cm<sup>2</sup>s) at 150°C. The CO<sub>2</sub> flux decrease from 110°C to 150°C was presumably due to the reduction of water retention in the membrane as the temperature increased. At 110°C and 220 psia, the CO<sub>2</sub> flux was 3.47 X 10<sup>-3</sup> cm<sup>3</sup> (STP) / (cm<sup>2</sup>s), which was equivalent to 1.55 X 10<sup>-3</sup> mol / (m<sup>2</sup>s). The higher flux at 220 psia than that at 430 psia was due to the same reasons described earlier in the chapter. The CO<sub>2</sub> permeability as a function of temperature is also plotted in Fig. 5.7.

Fig. 5.8 shows that CO<sub>2</sub>/H<sub>2</sub> and CO<sub>2</sub>/N<sub>2</sub> selectivities decreased as temperature increased. This might be explained by the fact that the transport of H<sub>2</sub> and N<sub>2</sub> was not affected by the facilitated transport, thus not affected significantly by the water retention in the membrane. As temperature increased, the permeabilities of H<sub>2</sub> and N<sub>2</sub> were not significantly affected, while the permeability of CO<sub>2</sub> decreased significantly as shown in Fig. 5.7. Therefore, the overall CO<sub>2</sub>/H<sub>2</sub> and CO<sub>2</sub>/N<sub>2</sub> selectivities decreased as temperature increased.

#### 5.3.4 Effects of permeate pressure on separation performance

In an attempt to improve the CO<sub>2</sub> transport properties, the effects of permeate pressure on CO<sub>2</sub> permeability and CO<sub>2</sub>/H<sub>2</sub> selectivity were investigated using a free-standing membrane with a thickness of 97 μm. The permeate pressures were varied from 16.7 to 44.1 psia, while the feed pressure was maintained at 220 psia. The temperature was maintained at 110°C.

As illustrated in Fig. 5.9, the CO<sub>2</sub> permeability increased as the permeate pressure increased. Since a higher permeate pressure resulted in a higher water partial pressure on the permeate side, water transfer across the membrane was then decreased with the reduced driving force. It was very important for the membrane to maintain enough water content for enhancing the diffusion of solutes and the reaction of CO<sub>2</sub> with the carriers in the membrane. However, the higher water content in the membrane might cause a more swollen membrane structure, which enhanced the H<sub>2</sub> flux and thus decreased the CO<sub>2</sub>/H<sub>2</sub> selectivity. Therefore, an optimal permeate pressure has to be chosen for the tradeoff between permeability and selectivity. In addition, a high permeate CO<sub>2</sub> pressure may be attractive for synthesis gas purification process to integrate with the following CO<sub>2</sub> sequestration step.

Feed pressure (psia)	CO <sub>2</sub> permeability (Barrer)	CO <sub>2</sub> /H <sub>2</sub> selectivity
70	1628	35.8
95	1345	33.1
100	1073	52.8
220	756	42.3
440	391	24.8

Table 5.4: Summary of key data at 110°C (Feed: 20% CO<sub>2</sub> and 80% H<sub>2</sub>).

### 5.3.5 Summary of key data

The key data at 110°C from the CO<sub>2</sub> removal experiments are listed in Table 5.4. As listed in this table, the CO<sub>2</sub> permeability reduced from 1629 to 391 Barrers as the feed pressure increased from 70 to 440 psia. However, the CO<sub>2</sub>/H<sub>2</sub> selectivity was at least 24.8 or higher. At the feed pressure of 220 psia, the CO<sub>2</sub> permeability was 756 Barrers and the CO<sub>2</sub>/H<sub>2</sub> selectivity was 42.3 whereas at the feed pressure of 440 psia, the CO<sub>2</sub> permeability was 391 Barrers and the CO<sub>2</sub>/H<sub>2</sub> selectivity was 24.8.

Membrane	T (°C)	CO <sub>2</sub> partial pressure (psia)	Feed gas composition	P <sub>CO2</sub> (Barrer)	α (CO <sub>2</sub> /H <sub>2</sub> )
Poly(ethylene glycol) diacrylate and poly(ethylene glycol) methyl ether acrylate copolymer (Lin et al., 2006b)	-20	250	80% CO <sub>2</sub> , 20% H <sub>2</sub>	410	31
	35			440	9.1
Dimethylglycine-Li/PVA (Tee et al., 2006)	90	3.53	20% CO <sub>2</sub> , 40% H <sub>2</sub> , 40% N <sub>2</sub>	1700	50
AIBA-K/polyallylamine/PVA in this work (Figs. 5.1 and 5.2)	110	13.9	20% CO <sub>2</sub> , 80% H <sub>2</sub>	1628	35.8
		44.0		756	42.3
		88.0		391	24.8
AIBA-K/polyallylamine/PVA in this work (Figs. 5.7 and 5.8)	110	44.0	20% CO <sub>2</sub> , 40% H <sub>2</sub> , 40% N <sub>2</sub>	803	143
		88.0	250	29.7	

Table 5.5: Comparison of separation performance with membranes reported in the literature (Lin et al., 2006b; Tee et al., 2006).

When the results shown in Figs 5.1, 5.2, 5.7, and 5.8 were compared with the results reported in the literature (Lin et al., 2006b) and our previous results (Tee et al., 2006) as shown in Table 5.5, the results from this work are gratifying in terms of working temperature and separation performance at such a high feed pressure. The improvement in the working temperature could be attributed to better crosslinking of PVA as the polymer matrix. The high permeability and selectivity were presumably attributed to two reasons: (1) better microporous support, since GE E500A, GE A1, and NL-2 microporous polysulfone supports had much higher mechanical strength than the BHA microporous Teflon support used in our previous work and (2) better carriers, since the membranes contained both AIBA-K and  $\text{KHCO}_3\text{-K}_2\text{CO}_3$  as the mobile carriers and poly(allylamine) as the fixed carrier. Thus, the polymeric membranes that we have synthesized have the potential for a wider range of application, including synthesis gas purification, at higher temperatures and/or higher pressures.

#### 5.4 Conclusions

The  $\text{CO}_2$  permeability and  $\text{CO}_2/\text{H}_2$  selectivity for synthesis gas were investigated using the synthesized facilitated transport  $\text{CO}_2$ -selective membranes. The effects of feed pressure, type of microporous support, temperature, and permeate pressure on transport properties were investigated with a simulated synthesis gas containing 20% of  $\text{CO}_2$  and 80% of  $\text{H}_2$ .

(1) The synthesized membranes showed best CO<sub>2</sub> permeability and CO<sub>2</sub>/H<sub>2</sub> selectivity at 110°C. At a feed pressure of 220 psia, the CO<sub>2</sub> permeability and CO<sub>2</sub>/H<sub>2</sub> selectivity reached 756 Barrers and 42, respectively, whereas at a feed pressure of 440 psia, the CO<sub>2</sub> permeability was 391 Barrers and the CO<sub>2</sub>/H<sub>2</sub> selectivity was about 25.

(2) The CO<sub>2</sub> permeability and CO<sub>2</sub>/H<sub>2</sub> selectivity decreased with increasing feed pressure, which can be explained with the carrier saturation phenomenon and the decrease of water content in the feed stream at higher pressures.

(3) Both CO<sub>2</sub> permeability and CO<sub>2</sub>/H<sub>2</sub> selectivity reduced as temperature increased within the temperature range of 110 – 180°C, which was presumably due to the reduction of water retention in the membrane as temperature increased.

(4) One membrane was also investigated with a feed gas consisting of 20% of CO<sub>2</sub>, 40% of H<sub>2</sub>, and 40% of N<sub>2</sub>. At 110°C, the CO<sub>2</sub> fluxes were 3.47 X 10<sup>-3</sup> and 2.81 X 10<sup>-3</sup> cm<sup>3</sup> (STP) / (cm<sup>2</sup>s) at 220 psia and 430 psia, respectively.

(5) The overall gratifying results obtained were presumably attributed to the improvement in crosslinking, higher strength microporous supports, and better carriers.

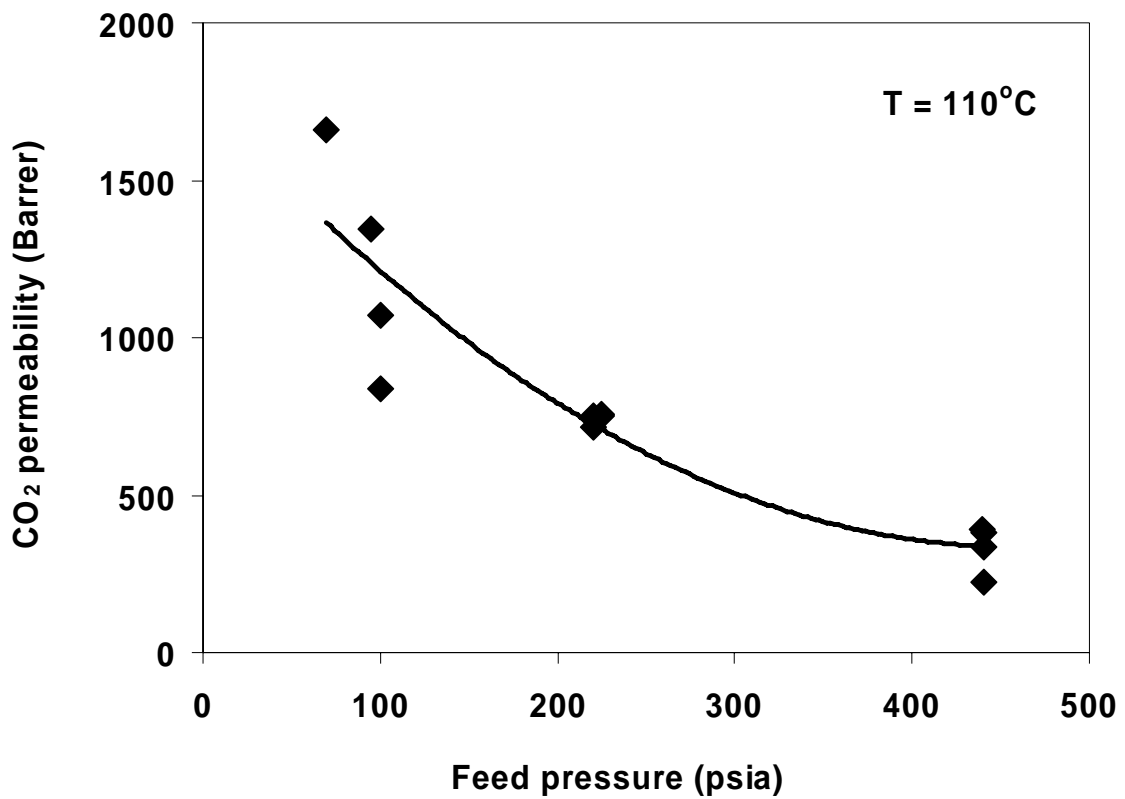


Figure 5.1: Effect of feed pressure on CO<sub>2</sub> permeability.

At 110°C, sweep pressure ~ 15 psia.

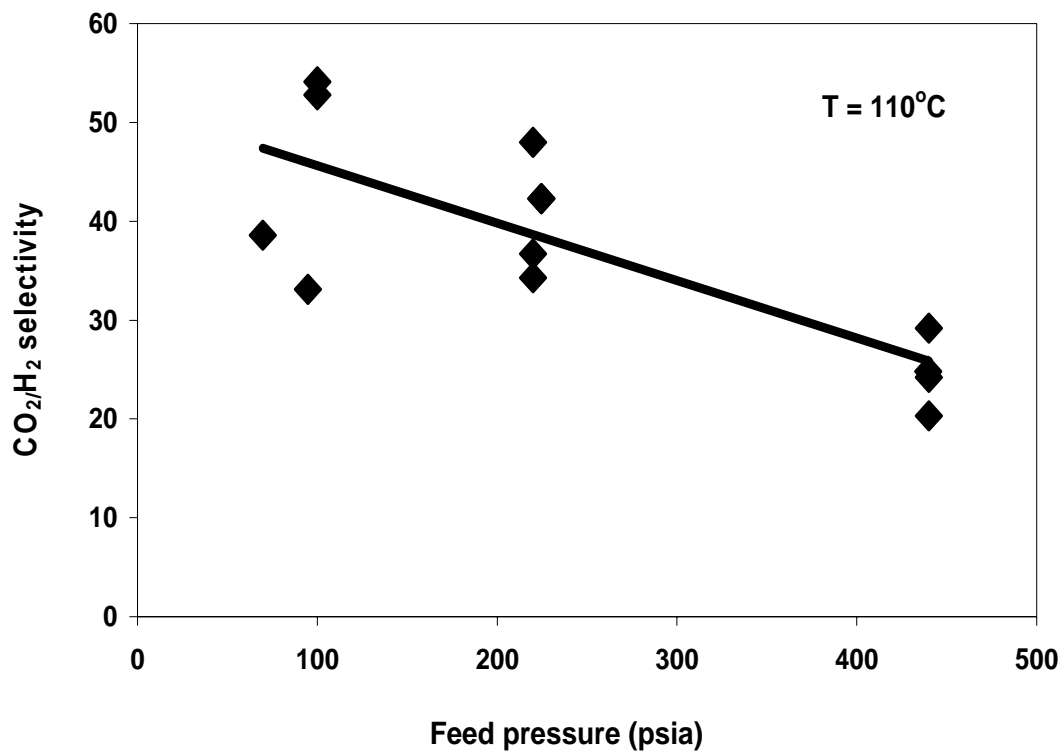


Figure 5.2: Effect of feed pressure on CO<sub>2</sub>/H<sub>2</sub> selectivity.

At 110°C, sweep pressure ~ 15 psia.

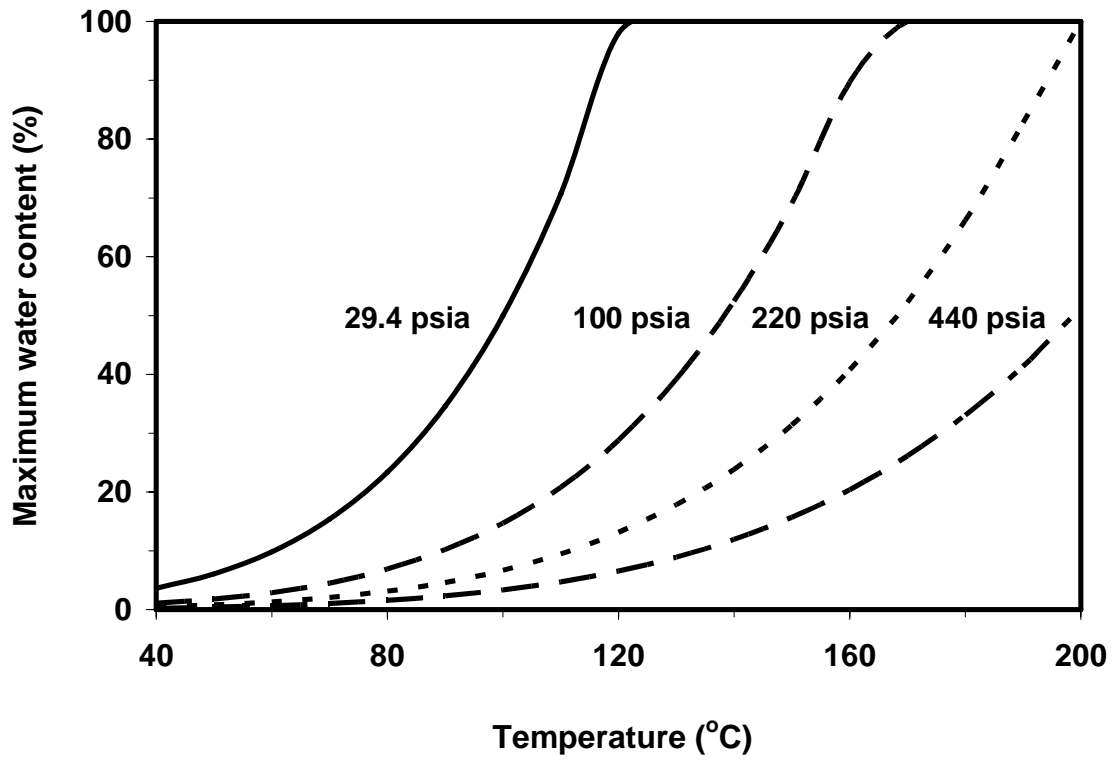


Figure 5.3: Maximum water content vs. temperature.

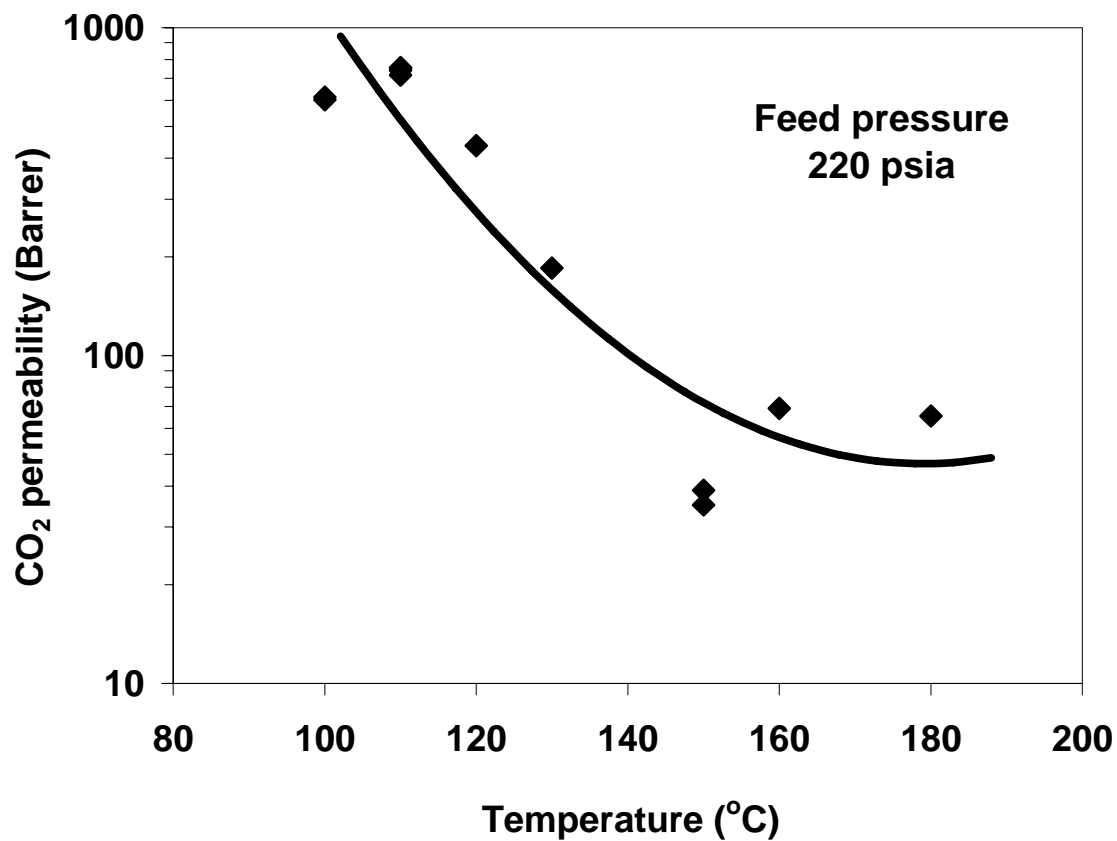


Figure 5.4: Effect of temperature on CO<sub>2</sub> permeability.  
Feed pressure ~ 220 psia, sweep pressure ~ 15 psia.

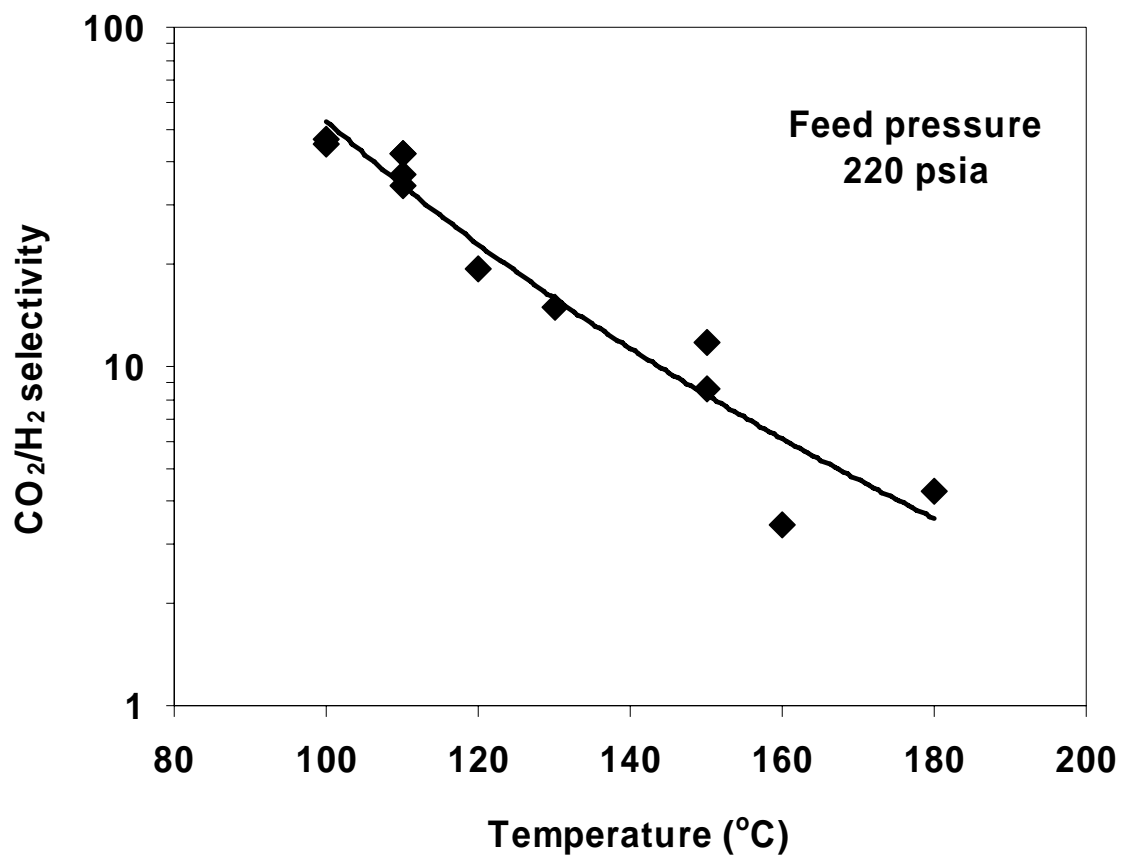


Figure 5.5: Effect of temperature on CO<sub>2</sub>/H<sub>2</sub> selectivity.  
Feed pressure ~ 220 psia; sweep pressure ~ 15 psia.

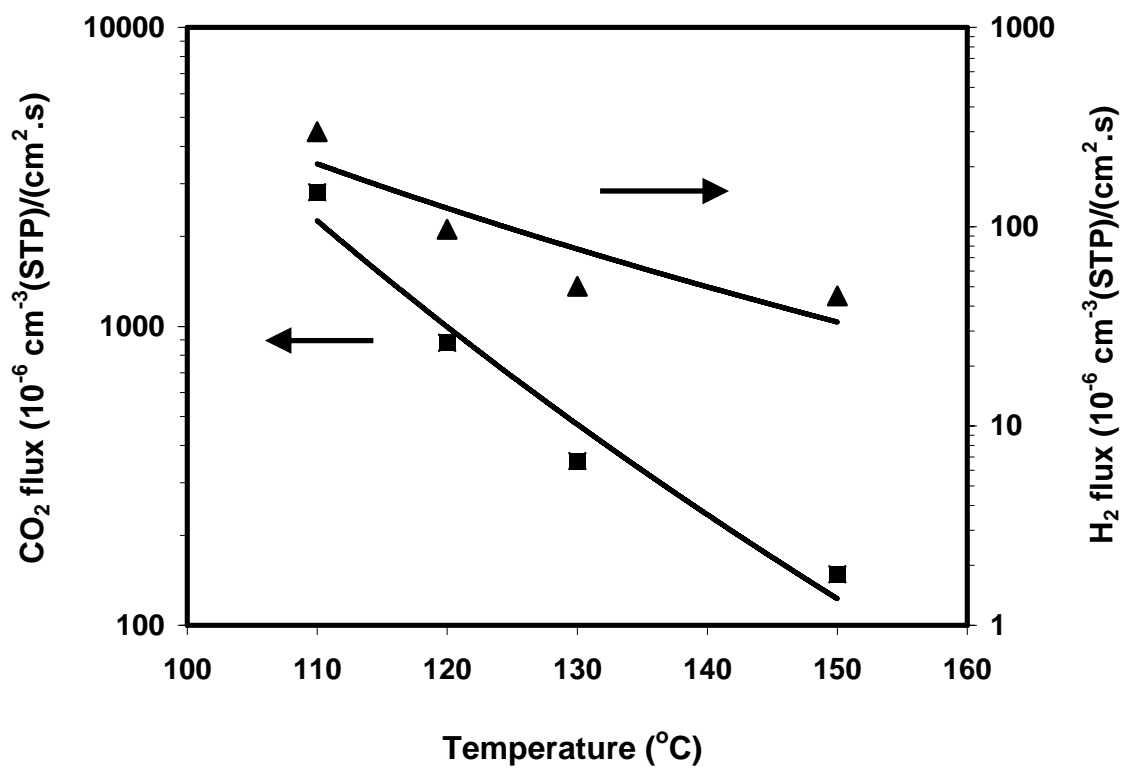


Figure 5.6: Effect of temperature on CO<sub>2</sub> flux and H<sub>2</sub> flux.

Feed gas: CO<sub>2</sub> 19.7 %, H<sub>2</sub> 39.4 %, and N<sub>2</sub> 40.9%; feed pressure ~ 230 psia; sweep pressure ~ 16 psia.

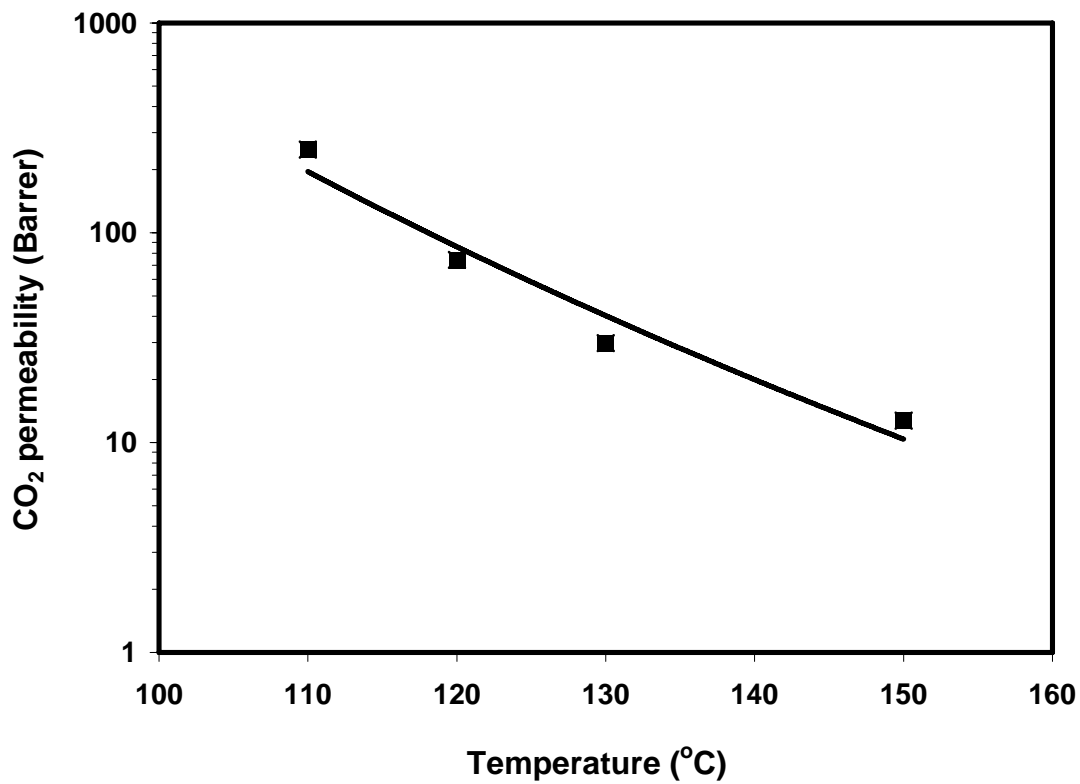


Figure 5.7: Effect of temperature on CO<sub>2</sub> permeability.

Feed gas: CO<sub>2</sub> 19.7 %, H<sub>2</sub> 39.4 %, and N<sub>2</sub> 40.9%; feed pressure ~ 230 psia; sweep pressure ~ 16 psia.

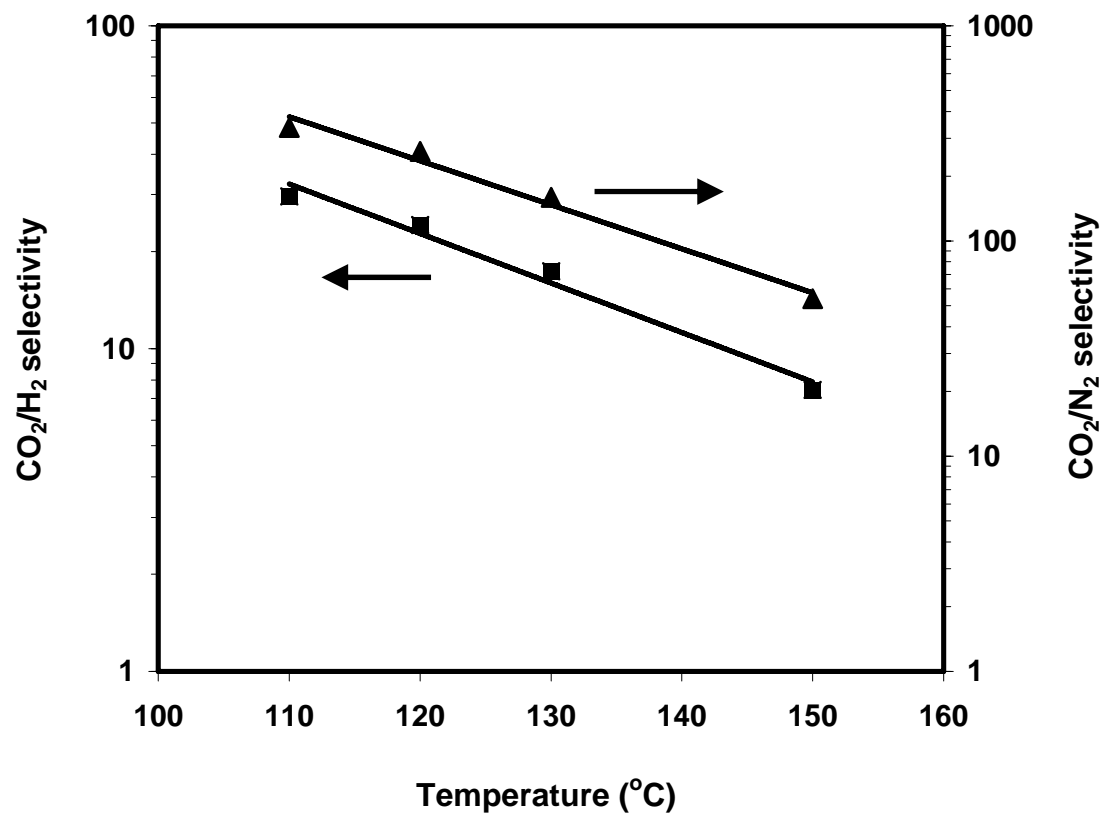


Figure 5.8: Effect of temperature on CO<sub>2</sub>/H<sub>2</sub> and CO<sub>2</sub>/N<sub>2</sub> selectivities.  
 Feed gas: CO<sub>2</sub> 19.7 %, H<sub>2</sub> 39.4 %, and N<sub>2</sub> 40.9%; feed pressure ~ 230 psia; sweep pressure ~ 16 psia.

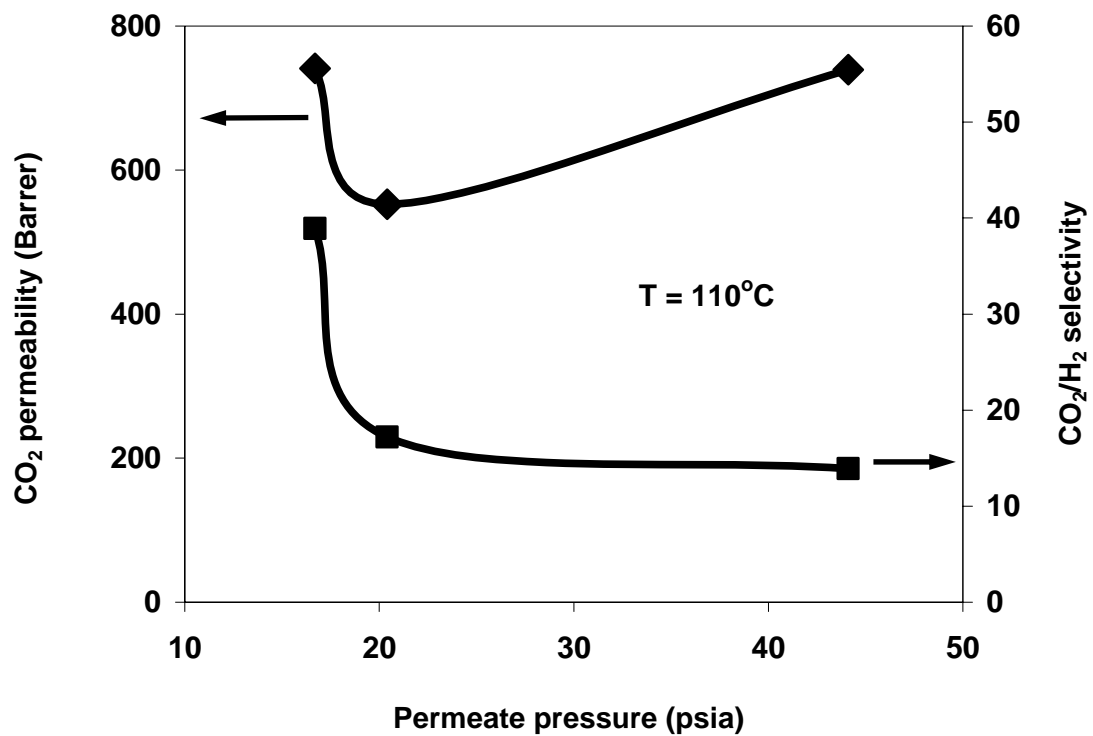


Figure 5.9: Effects of permeate pressure on CO<sub>2</sub> permeability and CO<sub>2</sub>/H<sub>2</sub> selectivity. At 110°C, feed pressure = 220 psia.

## CHAPTER 6

### SUMMARY AND FUTURE WORK

#### 6.1 Summary

In the present work, new CO<sub>2</sub>-selective membranes were synthesized and their applications for hydrogen processing were investigated. The applications included H<sub>2</sub> purification for fuel cells and synthesis gas purification.

In order to enhance CO<sub>2</sub> transport across membranes, facilitated transport membranes with mobile carriers and fixed-site carriers were prepared. The effects of crosslinking, membrane composition, feed pressure, water content, and temperature on transport properties were investigated. The synthesized CO<sub>2</sub>-selective membranes have shown a high CO<sub>2</sub> permeability and a good CO<sub>2</sub>/H<sub>2</sub> selectivity from 25 to 170°C. One type of these membranes showed a CO<sub>2</sub> permeability of 8000 Barrers (1 Barrer = 10<sup>-10</sup> cm<sup>3</sup> (STP).cm / (cm<sup>2</sup>.s.cm.Hg)) and a CO<sub>2</sub>/H<sub>2</sub> selectivity of 290 at 110°C. This membrane had a CO<sub>2</sub> permeability of 1200 Barrers and a CO<sub>2</sub>/H<sub>2</sub> selectivity of 33 even at 170°C. The stability of the membranes was also studied at 130°C and a feed pressure of 30 psia. Both the CO<sub>2</sub> permeability and CO<sub>2</sub>/H<sub>2</sub> selectivity remained stable for a period of 10 days. The applications of the synthesized membranes were demonstrated in a CO<sub>2</sub>-removal experiment, in which the CO<sub>2</sub> concentration in the retentate was decreased from 17% to 10 – 1000 ppm. In comparison with our previous results and the results reported

in the literature, the results obtained in the present study were superior. These gratifying results were presumably attributed to the improvement in crosslinking and better CO<sub>2</sub> transport carriers.

With such membranes, two approaches were developed to reduce the CO concentration of synthesis gas to meet the requirement of proton-exchange membrane fuel cells. One approach was using CO<sub>2</sub>-selective water gas shift (WGS) membrane reactors, in which both the low-temperature water gas shift reaction and the CO<sub>2</sub>-removal took place. In the CO<sub>2</sub>-selective membrane reactor, the CO concentration was successfully reduced from 1.0 % to less than 10 ppm. A H<sub>2</sub> concentration greater than 50% (on the dry basis) was achieved at various flow rates of a simulated autothermal reformat. Another approach used a process combining the CO<sub>2</sub>-removal membrane with a subsequent water gas shift reaction. In this process, with more than 99.5% of CO<sub>2</sub> in the synthesis gas removed by the membrane, the reversible WGS reaction was shifted forward so that the CO concentration was decreased from 1.2% to less than 10 ppm (dry), which met the requirement for proton-exchange membrane fuel cells. The WGS reactor had a gas hourly space velocity of 7650 h<sup>-1</sup> at 150°C, and the H<sub>2</sub> concentration in the outlet was more than 54.7% (on the dry basis). These two processes increased the yield of H<sub>2</sub> instead of losing H<sub>2</sub> and CO<sub>2</sub> was easily concentrated on the low-pressure side of the membrane and thus was ready for sequestration, in comparison with methanation, preferential oxidation, and pressure swing adsorption. The cost of the synthesized membranes is expected to be low as low-cost starting materials were used (vs. the cost of the H<sub>2</sub>-selective membranes based on precious metals, such as palladium and palladium alloy membranes).

The applications of the synthesized CO<sub>2</sub>-selective membranes for high-pressure synthesis gas purification were also studied. CO<sub>2</sub>/H<sub>2</sub> separation at feed pressures higher than 200 psia and temperatures ranging from 100 to 150°C were investigated by using the membranes. The effects of feed pressure, type of porous support, temperature, and permeate pressure were investigated using a simulated synthesis gas containing 20% carbon dioxide and 80% hydrogen. The membranes synthesized showed the best CO<sub>2</sub> permeability and CO<sub>2</sub>/H<sub>2</sub> selectivity at 110°C. At a feed pressure of 220 psia, the CO<sub>2</sub> permeability and CO<sub>2</sub>/H<sub>2</sub> selectivity reached 756 Barrers and 42, respectively, whereas at a feed pressure of 440 psia, the CO<sub>2</sub> permeability was 391 Barrers and the CO<sub>2</sub>/H<sub>2</sub> selectivity was about 25.

## 6.2 Future work

As described above, many accomplishments have been achieved in the course of this dissertation. However, there are several possible areas that were not fully explored, and some could serve as areas for future investigation. The first of these is to understand the transport mechanism of the synthesized membranes. The synthesized membranes contained two types of mobile carriers, AIBA-K and K<sub>2</sub>CO<sub>3</sub>/KHCO<sub>3</sub> (converted from KOH), and one type of fixed-site carrier, poly(allylamine). Our preliminary results showed that KOH contributed more to the CO<sub>2</sub> transport than AIBA-K and that the mobile carriers were more effective than the fixed-site carrier in the CO<sub>2</sub> transport. However, an in-depth quantitative analysis has not been conducted. As we have discussed in the dissertation, water played a critical role in our facilitated transport membranes. Yet, the adsorption of water in the membranes has not been fully understood.

A much better understanding of the synthesized membranes could be achieved if the quantitative analysis can be conducted to analyze the role of each carrier and water in the transport mechanism.

An unmet challenge was to incorporate some chemicals into the membranes to maintain the water content in the membrane at higher temperatures. As we described earlier, both CO<sub>2</sub> flux and CO<sub>2</sub>/H<sub>2</sub> selectivity decreased with increasing temperature, which was presumably attributed to the loss of water at higher temperatures. Therefore, to incorporate some chemicals into the membranes to maintain the water content in the membrane at higher temperatures is a logical step to improve the membrane performance. Al<sub>2</sub>(SO<sub>4</sub>)<sub>3</sub> was tried without success due to its low solubility in water and PVA solution. More chemicals need to be explored to achieve this goal.

The synthesized membranes used poly(vinyl alcohol) as the polymer matrix for the membranes due to its good compatibility with both mobile and fixed carriers, high hydrophilicity, and good film forming ability. However, poly(vinyl alcohol) has a glass transition temperature around 65 – 80°C, which makes it difficult to maintain thermal stability at temperatures more than 200°C, even with crosslinking. Our synthesized membranes maintained their thermal stability only up to 170°C. Therefore, polymers with higher glass transition temperatures and high hydrophilicity are needed for the membrane matrix in order to improve the performance of synthesis gas purification.

## **APPENDIX A**

### **MEMBRANE COMPOSITION AND MEMBRANE SEPARATION DATA**

Membrane	Z2004-1-92	
Membrane composition	50.0 wt% PVA / 18.3 wt% KOH / 20.7 wt% AIBA-K / 11.0 wt% poly(allylamine)	
PVA solution	Poly(vinyl alcohol)	8.802 g
	Water	52.201 g
Crosslinking agent		
(equivalent to a crosslinking degree of 60 mol%)	Formaldehyde solution (37 wt%)	4.890 g
Crosslinking catalyst	KOH	3.520 g
	Water	5.2 g
Poly(allylamine) aqueous solution	Poly(allylamine) / methanol solution	36.7 cm <sup>3</sup>
	Water	11.2 g
AIBA-K solution	2-Aminoisobutyric acid	2.861 g
	KOH	1.601 g
	Water	5.433 g

Table A.1: Casting solution composition of a formaldehyde-crosslinked membrane.

Membrane	Z2005-1-24	
Membrane composition	50.0 wt% PVA / 18.3 wt% KOH / 20.7 wt% AIBA-K / 11.0 wt% poly(allylamine)	
PVA solution	Poly(vinyl alcohol)	2.202 g
	Water	11.439 g
Crosslinking agent		
(equivalent to a crosslinking degree of 15 mol%)	Glutaraldehyde solution (50 wt%)	0.372 g
Crosslinking catalyst	KOH	0.195 g
	Water	2.256 g
Poly(allylamine) aqueous solution	Poly(allylamine) / methanol solution	8.9 cm <sup>3</sup>
	Water	3.967 g
AIBA-K solution	2-Aminoisobutyric acid	0.702 g
	KOH	1.022 g
	Water	4.168 g

Table A.2: Casting solution composition of a glutaraldehyde-crosslinked membrane.

Membrane	Z2004-1-45	
Membrane composition	55.0 wt% PVA / 20.0 wt% KOH / 25.0 wt% AIBA-K	
PVA solution	Poly(vinyl alcohol)	4.408 g
	Water	27.856 g
Crosslinking agent		
(equivalent to a crosslinking degree of 20 mol%)	Maleic anhydride	0.989 g
Crosslinking catalyst	KOH	0.306 g
	Water	2.650 g
AIBA-K solution	2-Aminoisobutyric acid	1.708 g
	KOH	2.511 g
	Water	5.121 g

Table A.3: Casting solution composition of a maleic anhydride-crosslinked membrane.

Experiment	Z2004-1-99	
PVA solution	Poly(vinyl alcohol)	3.305 g
	Water	25.555 g
Crosslinking agent		
(equivalent to a crosslinking degree of 4.0 mol%)	Divinyl sulfone	0.179 g
Crosslinking catalyst	KOH	0.493 g
	Water	4.306 g

Table A.4: Solution composition of crosslinking PVA with divinyl sulfone.

Time (Hour)	T (°C)	Water rate (cm <sup>3</sup> /min)		Feed p (psia)	Sweep p (psia)	$\alpha$ (CO <sub>2</sub> /H <sub>2</sub> )	Permeability (Barrer)	Permeance (GPU)
		Feed	Sweep					
24.6	110	0.03	0.03	29.7	15.6	165.6	1020.6	64.19
25.3	110	0.03	0.03	29.7	15.6	172.8	1035.7	65.14
17.2	130	0.03	0.09	29.8	15.6	178.3	712.2	44.79
19.2	130	0.03	0.09	29.8	15.6	217.4	743.8	46.78
14.3	170	0.09	0.09	29.7	15.6	3.7	370.5	23.30
19.7	170	0.09	0.09	29.7	15.6	4.4	371.3	23.36

Membrane: Z2004-1-45 on BHA Teflon support; test: U1-2004-2-18; feed gas: H<sub>2</sub> 58.27 %, CO<sub>2</sub> 3.12 %, CO 1.05 %, and N<sub>2</sub> 37.56 %.

Membrane composition: 55 wt% PVA (20 mol% maleic anhydride crosslinked 55 minutes), 25.0 wt% AIBA-K, 20.0 wt% KOH; membrane thickness = 15.9  $\mu$ m.

Table A.5: Separation results of a maleic acid-crosslinked membrane at various temperatures.

Time (Hour)	T (°C)	Water rate (cm <sup>3</sup> /min)		Feed p (psia)	Sweep p (psia)	$\alpha$ (CO <sub>2</sub> /H <sub>2</sub> )	Permeability (Barrer)	Permeance (GPU)
		Feed	Sweep					
19.6	110	0.03	0.03	29.7	15.6	794.8	1861.6	44.01
22.8	110	0.03	0.03	29.7	15.6	790.1	2143.9	50.68
8.6	130	0.03	0.09	29.8	15.6	230.0	2519.2	59.55
9.3	130	0.03	0.09	29.8	15.6	554.9	2281.6	53.94
11.6	150	0.03	0.15	29.7	15.6	142.5	865.1	20.45
12.3	150	0.03	0.15	29.7	15.6	132.0	831.5	19.66
17.2	170	0.03	0.09	29.8	15.6	68.4	584.9	13.83
19.2	170	0.03	0.09	29.8	15.6	72.3	608.8	14.39

Membrane: Z2004-1-47 on BHA Teflon support; test: U1-2004-2-20; feed gas: H<sub>2</sub> 58.27 %, CO<sub>2</sub> 3.12 %, CO 1.05 %, and N<sub>2</sub> 37.56 %.

Membrane composition: 55 wt% PVA (20 mol% glutaraldehyde crosslinked two hours), 25.0 wt% AIBA-K, 20.0 wt% KOH; membrane thickness = 42.3  $\mu$ m.

Table A.6: Separation results of a glutaraldehyde-crosslinked membrane at various temperatures.

T (°C)	Water rate (cm <sup>3</sup> /min)		$\alpha$ (CO <sub>2</sub> /H <sub>2</sub> )	Permeability (Barrer)	Permeance (GPU)
	Feed	Sweep			
100	0.03	0.03	212.6	6568.5	254.6
100	0.03	0.03	206.0	6621.4	256.6
100	0.03	0.03	205.7	6489.1	251.5
110	0.03	0.03	270.2	5913.9	229.2
110	0.03	0.03	277.3	5932.8	230.0
110	0.03	0.03	291.0	6011.3	233.0
120	0.03	0.03	261.5	4119.7	159.7
120	0.03	0.03	257.4	3788.2	146.8
120	0.03	0.03	269.8	3815.7	147.9
130	0.03	0.03	193.3	2466.3	95.6
130	0.03	0.03	181.7	2216.5	85.9
130	0.03	0.03	197.8	2721.9	105.5
140	0.03	0.03	122.3	1464.8	56.8
140	0.03	0.03	125.3	1481.1	57.4
140	0.03	0.03	126.2	1605.4	62.2
140	0.06	0.06	159.0	2986.4	115.8
140	0.06	0.06	161.4	3003.6	116.4
140	0.06	0.06	168.3	3119.8	120.9
150	0.06	0.06	101.3	1862.2	72.2
150	0.06	0.06	98.7	1787.6	69.3
150	0.06	0.06	97.9	1888.6	73.2

Membrane: Z2003-1-30 on BHA Teflon support; test: U1-2002-93; feed pressure = 31.7 psia; sweep pressure = 15.7 psia, feed gas: 20% CO<sub>2</sub>, 40% H<sub>2</sub>, and 40% N<sub>2</sub>.

Membrane composition: 45 wt% PVA (60 mol% formaldehyde crosslinked), 25.7 wt% AIBA-K, 18.3 wt% KOH, and 11.0 wt% poly(allylamine); membrane thickness = 25.8  $\mu\text{m}$ .

Continued

Table A.7: Separation results of a formaldehyde-crosslinked membrane at various temperatures.

Table A.7 continued

150	0.09	0.09	82.4	2538.0	98.4
150	0.09	0.09	80.4	2547.1	98.7
150	0.09	0.09	78.5	2519.4	97.7
160	0.09	0.09	63.3	1723.9	66.8
160	0.09	0.09	65.3	1759.8	68.2
160	0.09	0.09	63.6	1717.7	66.6
160	0.12	0.12	69.9	2154.0	83.5
160	0.12	0.12	69.2	2175.9	84.3
160	0.12	0.12	61.8	2042.3	79.2
170	0.12	0.12	53.2	1654.4	64.1
170	0.12	0.12	52.6	1643.2	63.7
170	0.12	0.12	51.1	1620.2	62.8
180	0.12	0.12	10.1	1451.8	56.3

Time (Hour)	T (°C)	Water Rate (cm <sup>3</sup> /min)		Feed p (psia)	Sweep p (psia)	$\alpha$ (CO <sub>2</sub> /H <sub>2</sub> )	Permeability (Barrer)	Permeance (GPU)
		Feed	Sweep					
14.4	110	0.03	0.03	29.3	15.6	288.7	889.4	17.90
15.2	110	0.03	0.03	29.3	15.6	305.9	901.9	18.15
13.6	130	0.03	0.09	28.8	15.6	176.7	1344.5	27.05
24.8	130	0.03	0.09	28.8	15.6	176.9	1323.6	26.63

Membrane: Z2004-1-73 on BHA Teflon support; test: U1-2004-2-45; feed gas: 21.53% CO<sub>2</sub>, 41.90% H<sub>2</sub>, and 36.57% N<sub>2</sub>; gas flow rate = 60/30 cm<sup>3</sup>/min.

Membrane composition: 50 wt% PVA (60 mol% formaldehyde crosslinked 21.8 hours), 29.0 wt% AIBA-K, 10.0 wt% KOH, and 11% polyallylamine; membrane thickness = 49.7  $\mu$ m.

Table A.8: Separation results of a formaldehyde-crosslinked membrane.

Time (Hour)	T (°C)	Water rate (cm <sup>3</sup> /min)		Feed p (psia)	Sweep p (psia)	$\alpha$ (CO <sub>2</sub> /H <sub>2</sub> )	Permeability (Barrer)	Permeance (GPU)
		Feed	Sweep					
18.3	110	0.03	0.03	29.5	14.7	78.2	806.5	24.29
19.0	110	0.03	0.03	29.5	14.7	78.9	789.9	23.79
20.5	130	0.03	0.09	29.3	14.7	78.2	944.0	28.43
21.6	130	0.03	0.09	29.3	14.7	78.4	696.7	20.99
13.1	150	0.02	0.12	29.1	14.7	37.1	524.9	15.81
13.9	150	0.02	0.12	29.1	14.7	37.0	511.5	15.41
32.1	150	0.02	0.12	29.1	14.7	26.6	461.3	13.90
32.9	150	0.02	0.12	29.1	14.7	38.6	549.3	16.54

Membrane: Z2004-1-77; test: U1-2004-2-49; feed gas: 21.53% CO<sub>2</sub>, 41.90% H<sub>2</sub>, and 36.57% N<sub>2</sub>.

Membrane composition: 50 wt% PVA (60 mol% formaldehyde crosslinked 21.5 hours), 24.8 wt% AIBA-K, 14.2 wt% KOH, and 11.0 wt% polyallylamine; membrane thickness = 33.2  $\mu$ m.

Table A.9: Separation results of a formaldehyde-crosslinked membrane at various temperatures

Time (Hour)	Feed p (psia)	Sweep p (psia)	$\alpha$ (CO <sub>2</sub> /H <sub>2</sub> )	$\alpha$ (CO <sub>2</sub> /N <sub>2</sub> )	Permeability (Barrer)	Permeance (GPU)
16.4	29.5	15.7	246.1	1009.8	4753.9	78.32
17.2	29.5	15.7	238.2	1360.6	4711.7	77.62

Membrane: Z2004-1-67-1; test: U1-2004-2-51; feed gas: 21.53% CO<sub>2</sub>, 41.90% H<sub>2</sub>, and 36.57% N<sub>2</sub>; T = 110°C; water rate = 0.03 / 0.03 cm<sup>3</sup>/min.

Membrane composition: 50 wt% PVA (60 mol% formaldehyde crosslinked 17.7 hours), 20.7 wt% AIBA-K, 18.3 wt% KOH, and 11.0 wt% polyallylamine; membrane thickness = 60.7  $\mu$ m.

Table A.10: Separation results of a formaldehyde-crosslinked membrane.

Time (Hours)	T (°C)	Water Rate (cm <sup>3</sup> /min)		Feed p (psia)	Sweep p (psia)	$\alpha$ (CO <sub>2</sub> /H <sub>2</sub> )	Permeability (Barrers)	Permeance (GPU)
		Feed	Sweep					
10.6	110	0.03	0.03	30.4	15.8	222.1	1701.6	45.62
20.2	110	0.03	0.03	30.4	15.8	213.2	1764.0	47.29
14.6	130	0.03	0.09	29.1	15.2	173.1	1396.0	37.43
15.4	130	0.03	0.09	29.1	15.2	175.2	1421.8	38.12
9.2	150	0.02	0.12	29.0	15.2	2.6	1432.0	38.39

Membrane: Z2004-1-81, test: U1-2004-2-57; feed Gas: 21.53% CO<sub>2</sub>, 41.90% H<sub>2</sub>, 36.57% N<sub>2</sub>.

Membrane composition: 50 wt% PVA (60 mol% formaldehyde crosslinked 18 hours), 20.7 wt% AIBA-K, 18.3 wt% KOH, and 11.0 wt% polyethylenimine; membrane thickness: 37.3  $\mu$ m.

Table A.11: Separation results of a formaldehyde-crosslinked membrane containing polyethylenimine at various temperatures.

T (°C)	Water rate (cm <sup>3</sup> /min)		Gas flow rate feed / sweep (cm <sup>3</sup> /min)	$\alpha$ (CO <sub>2</sub> /H <sub>2</sub> )	$\alpha$ (CO <sub>2</sub> /N <sub>2</sub> )	Permeability (Barrers)	Permeance (GPU)
	Feed	Sweep					
110	0.03	0.03	60 / 30	290.0	2057.8	6119.4	88.94
110	0.03	0.03	60 / 30	295.2	1565.9	5784.8	84.08
120	0.03	0.03	60 / 30	214.5	524.8	3562.5	51.78
120	0.03	0.03	60 / 30	213.5	521.1	3701.6	53.80
130	0.03	0.03	60 / 30	134.3	282.7	2250.2	32.71
130	0.03	0.03	60 / 30	137.2	561.2	2248.6	32.68
130	0.03	0.06	60 / 30	194.2	639.4	3749.7	54.50
130	0.03	0.06	60 / 30	208.2	324.1	3881.4	56.42
140	0.03	0.03	60 / 30	108.0	306.1	1661.3	24.15
140	0.03	0.03	60 / 30	95.1	215.7	1394.5	20.27
150	0.03	0.03	60 / 30	56.2	132.5	979.7	14.24
150	0.03	0.03	60 / 30	53.8	144.5	1003.3	14.58
150	0.02	0.09	30 / 30	95.7	277.9	1698.9	24.69
150	0.02	0.09	30 / 30	105.8	274.5	1853.8	26.95
160	0.02	0.12	30 / 30	65.8	205.4	1294.2	18.81
160	0.02	0.12	30 / 30	65.6	189.6	1302.1	18.93
170	0.02	0.15	30 / 30	33.9	73.4	1197.9	17.41
170	0.02	0.15	30 / 30	33.3	68.6	1233.5	17.93
180	0.02	0.15	30 / 30	7.9	12.0	1000.3	14.54
180	0.02	0.15	30 / 30	6.3	8.9	1084.0	15.76

Membrane: Z2004-1-114-2 on BHA Teflon support; test: U1-2004-2-89; feed pressure = 28.2 – 28.9 psia; sweep pressure = 15.5 psia, feed gas: CO<sub>2</sub> 20 %, H<sub>2</sub> 40 %, and N<sub>2</sub> 40 %. Membrane composition: 50 wt% PVA (60 mol% formaldehyde crosslinked), 20.7 wt% AIBA-K, 18.3 wt% KOH, and 11.0 wt% poly(allylamine); membrane thickness = 68.8  $\mu\text{m}$ .

Table A.12: Separation results of a formaldehyde-crosslinked membrane at various temperatures.

Membrane	Z2006-1-124	
Membrane composition	50.0 wt% PVA / 18.3 wt% KOH / 20.7 wt% AIBA-K / 11.0 wt% poly(allylamine)	
PVA solution	Poly(vinyl alcohol)	3.300 g
	Water	17.451 g
Crosslinking agent		
(equivalent to a crosslinking degree of 15 mol%)	Glutaraldehyde solution (50 wt%)	0.568 g
Crosslinking catalyst	KOH	0.244 g
	Water	2.527 g
Poly(allylamine) aqueous solution	Poly(allylamine) / methanol solution	13.4 cm <sup>3</sup>
	Water	3.854 g
AIBA-K solution	2-Aminoisobutyric acid	1.049 g
	KOH	1.601 g
	Water	5.573 g

Table A.13: Casting solution composition of a glutaraldehyde-crosslinked membrane for high-pressure CO<sub>2</sub>/H<sub>2</sub> separation.

T (°C)	Saturated steam pressure (KPa) (Smith, Van Ness, and Abbott; 2005)	Maximum water rate for a dry gas flowrate of 30 cm <sup>3</sup> /min* (cm <sup>3</sup> /min)			
		29.4 psia	100 psia	220 psia	440 psia
40	7.375	0.0008	0.0002	0.0001	0.0001
50	12.340	0.0014	0.0004	0.0002	0.0001
60	19.920	0.0022	0.0006	0.0003	0.0001
70	31.160	0.0035	0.0010	0.0005	0.0002
80	47.360	0.0052	0.0015	0.0007	0.0004
90	70.110	0.0078	0.0023	0.0010	0.0005
100	101.330	0.0112	0.0033	0.0015	0.0008
110	143.270	0.0159	0.0047	0.0021	0.0011
120	198.540	0.0220	0.0065	0.0029	0.0015
130	270.130	no limit	0.0088	0.0040	0.0020
140	361.380	no limit	0.0118	0.0054	0.0027
150	476.000	no limit	0.0155	0.0070	0.0035
160	618.060	no limit	0.0201	0.0092	0.0046
170	792.020	no limit	no limit	0.0117	0.0059
180	1002.700	no limit	no limit	0.0148	0.0074
190	1255.100	no limit	no limit	0.0186	0.0093
200	1554.900	no limit	no limit	no limit	0.0115

\* The flowrate is calibrated at 101.3 KPa and 20°C.

Table A.14: Maximum water rate for a dry gas flowrate of 30 cm<sup>3</sup>/min.

Time (h)	T (°C)	Feed p (psia)	$\alpha$ (CO <sub>2</sub> /H <sub>2</sub> )	$\alpha$ (CO <sub>2</sub> /N <sub>2</sub> )	CO <sub>2</sub> permeability (Barrer)	CO <sub>2</sub> permeance (GPU)	CO <sub>2</sub> flux [10 <sup>-6</sup> cm <sup>3</sup> (STP)/(cm <sup>2</sup> s)]	CO <sub>2</sub> permeance [10 <sup>-7</sup> mol/(m <sup>2</sup> .s.Pa)]
Feed / sweep = 30 / 30 cm <sup>3</sup> /min; water rate = 0.01 / 0.09 cm <sup>3</sup> /min (feed / sweep)								
8.7	110	219.7	37.5	372	364.8	12.16	2002	0.041
13.1	110	219.7	49.0	457	422.6	14.09	2078	0.047
16.9	110	219.7	59.0	515	452.2	15.07	2064	0.050
18.6	110	219.7	67.8	770	453.8	15.13	2052	0.051
4.8	130	429.7	17.6	180	30.1	1.00	373	0.003
5.6	130	429.7	17.1	140	27.0	0.90	336	0.003
5.2	150	429.7	7.3	52.3	11.2	0.37	143	0.001
6.0	150	429.7	7.6	55.4	11.9	0.40	153	0.001
Feed / sweep = 60 / 60 cm <sup>3</sup> /min; water rate = 0.02 / 0.18 cm <sup>3</sup> /min (feed / sweep)								
24.2	110	220.7	137.6	1264	833.9	27.80	3602	0.093
25.0	110	220.7	149.0	1187	771.8	25.73	3334	0.086
4.8	110	429.7	28.7	330	247.4	8.25	2790	0.028
5.6	110	429.7	30.6	344	251.9	8.40	2824	0.028
8.9	120	429.7	24.0	296	73.8	2.46	890	0.008
9.7	120	429.7	24.3	226	72.1	2.40	873	0.008

Membrane: Z2006-1-124-2; test: U1-2005-1-161; feed gas: CO<sub>2</sub> 19.7 %, H<sub>2</sub> 39.4 %, and N<sub>2</sub> 40.9%; sweep pressure: 15.5 – 16.7 psia.

Membrane composition: 50.0 wt% PVA (15.0 mol% glutaraldehyde crosslinked for 110 minutes), 20.7 wt% AIBA-K, 18.3% KOH, and 11.0 wt% polyallylamine on NL-2 microporous support; membrane thickness = 30  $\mu$ m.

Table A.15: Separation results of a glutaraldehyde-crosslinked membrane at high pressures.

Time (h)	T (°C)	Feed p (psia)	Water (sweep, cm <sup>3</sup> /min)	$\alpha$ (CO <sub>2</sub> /H <sub>2</sub> )	CO <sub>2</sub> permeability (Barrer)	CO <sub>2</sub> permeance (GPU)	CO <sub>2</sub> flux [10 <sup>-6</sup> cm <sup>3</sup> (STP)/(cm <sup>2</sup> s)]	H <sub>2</sub> flux [10 <sup>-6</sup> cm <sup>3</sup> (STP)/(cm <sup>2</sup> s)]
5.6	110	64.7	0.09	51.4	666.8	11.11	475	81.50
9.8	120	64.7	0.09	29.4	220.4	3.67	154	38.49
10.6	120	64.7	0.09	27.9	209.8	3.50	147	38.63
5.0	120	99.7	0.09	15.1	94.1	1.57	115	53.69
5.8	120	99.7	0.09	15.2	91.9	1.53	112	52.25
5.0	120	64.7	0.12	22.1	168.1	2.80	119	38.14
5.8	120	64.7	0.12	24.0	173.5	2.89	123	36.39

Membrane: Z2004-1-155-1; test: U1-2004-2-162; feed gas: CO<sub>2</sub> 20.54 %, and H<sub>2</sub> 79.46 %; feed water rate = 0.02 cm<sup>3</sup>/min; sweep pressure: 15.4 – 15.8 psia.

Membrane composition: 50.0 wt% PVA (60.0 mol% formaldehyde crosslinked for 23.5 hours), 20.7 wt% AIBA-K, 18.3% KOH, and 11.0 wt% polyallylamine on BHA Teflon microporous support; membrane thickness ~ 60  $\mu$ m.

Table A.16: Separation results of a membrane on BHA Teflon support at high pressures.

Time (h)	T (°C)	Feed p (psia)	$\alpha$ (CO <sub>2</sub> /H <sub>2</sub> )	CO <sub>2</sub> permeability (Barrer)	CO <sub>2</sub> permeance (GPU)	CO <sub>2</sub> flux [10 <sup>-6</sup> cm <sup>3</sup> (STP)/(cm <sup>2</sup> s)]	H <sub>2</sub> flux [10 <sup>-6</sup> cm <sup>3</sup> (STP)/(cm <sup>2</sup> s)]
5.2	110	69.7	35.8	1367.5	24.55	1050	334.91
6.0	110	69.7	38.6	1394.6	25.04	1056	330.54
4.3	110	94.7	31.2	1036.8	18.61	1175	413.60
5.1	110	94.7	33.1	1007.6	18.09	1123	394.40
6.4	120	94.7	32.9	800.8	14.38	845	291.29
7.2	120	94.7	33.5	825.3	14.82	870	294.63

Membrane: M2005-1-13-3-2; test: U1-2005-1-3; feed gas: CO<sub>2</sub> 20.54 %, and H<sub>2</sub> 79.46 %; water rate = 0.02 / 0.09 cm<sup>3</sup>/min (feed / sweep); sweep pressure: 15.2 – 15.9 psia.

Membrane composition: 50.0 wt% PVA (60.0 mol% formaldehyde crosslinked for 16.0 hours), 20.7 wt% AIBA-K, 18.3% KOH, and 11.0 wt% polyallylamine on E500A microporous polysulfone support; membrane thickness = 55.7  $\mu$ m.

Table A.17: Separation results of a membrane on BHA Teflon support at high pressures.

Time (h)	T (°C)	Feed p (psia)	$\alpha$		Permeability (Barrer)	Permeance (GPU)	Flux [ $10^{-6} \text{cm}^3$ (STP)/( $\text{cm}^2 \text{s}$ )]	
			CO <sub>2</sub> / H <sub>2</sub>	CO <sub>2</sub> / N <sub>2</sub>			CO <sub>2</sub>	H <sub>2</sub>
Gas flow rate = 30 / 30 cm <sup>3</sup> /min; water rate = 0.01 / 0.09 cm <sup>3</sup> /min (feed / sweep)								
8.7	110	219.7	37.5	372.0	364.8	12.16	2002	167.8
13.1	110	219.7	49.0	457.0	422.6	14.09	2078	186.9
16.9	110	219.7	59.0	515.4	452.2	15.07	2064	201.8
18.6	110	219.7	67.8	770.0	453.8	15.13	2052	182.3
4.8	130	429.7	17.6	179.7	31.4	1.05	373	52.33
5.6	130	429.7	17.1	139.5	28.1	0.94	336	48.16
5.2	150	429.7	7.3	52.3	12.3	0.41	143	44.37
6.0	150	429.7	7.6	55.4	13.2	0.44	153	45.45
Gas flow rate = 60 / 60 cm <sup>3</sup> /min; water rate = 0.02 / 0.18 cm <sup>3</sup> /min (feed / sweep)								
24.2	110	220.7	137.6	1264	833.9	27.80	3602	203.4
25.0	110	220.7	149.0	1187	771.8	25.73	3334	173.2
4.8	110	429.7	28.7	330.1	247.4	8.25	2790	305.5
5.6	110	429.7	30.6	344.1	251.9	8.40	2824	294.9
8.9	120	429.7	24.0	295.7	75.1	2.50	890	99.18
9.7	120	429.7	24.3	225.8	73.4	2.45	873	95.07

Membrane: Z2006-1-124-2; test: U1-2005-1-161; feed gas: CO<sub>2</sub> 19.7 %, H<sub>2</sub> 39.4 %, and N<sub>2</sub> 40.9%.

Membrane composition: 50.0 wt% PVA(15.0 mol% glutaraldehyde crosslinked for 110 minutes), 20.7 wt% AIBA-K, 18.3% KOH, 11.0 wt% polyallylamine on NL-2 microporous polysulfone support; membrane thickness = 30  $\mu\text{m}$ .

Table A.18: Separation results of a membrane on NL-2 microporous polysulfone support at high pressures.

## LIST OF REFERENCES

- Aaron, D., and Tsouris, C. (2005), Separation of CO<sub>2</sub> from flue gas: a review, *Sep. Sci. Technol.* 40, 321.
- Ahmed, S., and Krumpelt, M. (2001), Hydrogen from hydrocarbon fuels for fuel cells, *Int. J. Hydrogen Energy* 26, 291.
- Amadeo, N. E., and Laborde, M. A. (1995), Hydrogen production from the low-temperature water-gas shift reaction: kinetics and simulation of the industrial reactor, *Int. J. Hydrogen Energy* 20, 949.
- Armor, J. N. (1998), Applications of catalytic inorganic membrane reactors to refinery products, *J. Membr. Sci.* 147, 217.
- Basile, A., Drioli, E., Santella, F., Violante, V., Capannelli, G., and Vitulli, G. (1996a) A study on catalytic membrane reactors for water gas shift reaction. *Gas Sepa. Puri.* 10, 53.
- Basile, A., Criscuoli, A., Santella, F., and Drioli, E. (1996b), Membrane reactor for water gas shift reaction, *Gas Sep. Purif.* 10, 243.
- Brown, L. F. (2001), A comparative study of fuels for on-board hydrogen production for fuel-cell-powered automobiles, *Int. J. Hydrogen Energy* 26, 381.
- Campbell, J. S. (1977), Influences of catalyst formulation and poisoning on the activity and die-off of low temperature shift catalysts, *Ind. Eng. Chem. Proc. Des. Dev.* 9, 588.
- Criscuoli, A., Basile, A., and Drioli, E. (2000), An analysis of the performance of membrane reactors for the water-gas shift reaction using gas feed mixtures, *Catal. Today* 56, 53.
- Cussler, E. L., Aris, R., and Bhowan, A. (1989), On the limit of facilitated diffusion, *J. Membr. Sci.* 43, 149.
- Dicks, A. L. (1996), Hydrogen generation from natural gas for the fuel cell systems of tomorrow, *J. Power Source* 61, 113.
- Donaldson, T. L., and Lapinas, A. T. (1982), Secondary flux enhancement in two-carrier facilitated transport, *Chem. Eng. Sci.* 37, 715.

Dortmundt, D, and Doshi, K (1999), Recent developments in CO<sub>2</sub> removal membrane technology, UOP LLC.

Fiolitakis, E., Hoffmann, U., and Hoffmann, H. (1980), Application of wavefront analysis for kinetic investigation of water-gas shift reaction, *Chem. Eng. Sci.* 35, 1021.

Ghenciu, A. F. (2002), Review of fuel processing catalysts for hydrogen production in PEM fuel cell systems, *Curr. Opin. Solid State Mater. Sci.* 6, 389.

Giessler, S., Jordan, L., Diniz da Costa, J. C., and Lu, G. Q. (2003), Performance of hydrophobic and hydrophilic silica membrane reactors for the water gas shift reaction, *Sep. Purif. Technol.* 32, 255.

Gottschlich, D. E., Roberts, D. L., and Way, J. D. (1988), A theoretical comparison of facilitated transport and solution-diffusion membrane modules for gas separation, *Gas Sep. Purif.* 2, 65.

Hirayama, Y., Kase, Y., Tanihara, N., Sumiyama, Y., Kusuki, Y., and Haraya, K. (1999), Permeation properties to CO<sub>2</sub> and N<sub>2</sub> of poly(ethylene oxide)-containing and crosslinked polymer films, *J. Membr. Sci.* 160, 87.

Ho, W. S. W., and Sirkar, K. K. (1992) Overview. In *Membrane Handbook*, (W. S. W. Ho, and K. K. Sirkar, eds.), Chapman & Hall, New York, NY, p. 4.

Ho, W. S. W., and Dalrymple, D. C. (1994), Facilitated transport of olefins in Ag<sup>+</sup>-containing polymer membranes, *J. Membr. Sci.* 91, 13.

Ho, W. S. W. Membranes comprising salts of aminoacids in hydrophilic polymers, US Patent 5,611,843 (1997).

Ho, W. S. W. Membranes comprising aminoacid salts in polyamine polymers and blends, US Patent 6,099,621 (2000).

Hong, J., Kang, Y. S., Jang, J., and Kim, U. Y. (1996), Analysis of facilitated transport in polymeric membrane with fixed site carrier 2. Series RC circuit model, *J. Membr. Sci.* 109, 159.

Huang, J., El-Azzami, L., and Ho, W. S. W. (2005), Modeling of CO<sub>2</sub>-selective water-gas-shift membrane reactor for fuel cell, *J. Membr. Sci.* 261, 67.

Jegal, J., and Lee, K. (1999) Nanofiltration membranes based on poly(vinyl alcohol) and ionic polymers, *J. Appl. Polym. Sci.* 72, 1755.

Kang, Y. S., Hong, J., Jang, J., and Kim, U. Y. (1996), Analysis of facilitated transport in solid membranes with fixed site carriers 1. Single RC circuit model, *J. Membr. Sci.* 109, 149.

Keiski, R. L., Desponds, O., Chang, Y. F., and Somorjai, G. A. (1993), Kinetics of the water-gas-shift reaction over several alkane activation and water-gas-shift catalysts, *Appl. Catal. A* 101, 317.

Kim, S. J., Park, S. J., Shin, M., Lee, Y. H., Kim, N. G., and Sun, S. I. (2002), Thermal characteristics of IPNs composed of polyallylamine and chitosan, *J. Appl. Polym. Sci.* 85, 1956.

Koros, W. J., and Mahajan, R. (2000), Pushing the limits on possibilities for large scale gas separation: which strategies, *J. Membr. Sci.* 175, 181.

Kroschwitz, J. I., and Howe-Grant, M., eds. (1995) Encyclopedia of Chemical Technology, 4th ed., Vol. 13, John Wiley & Sons, Inc., New York, NY, p 927.

Kung, H.H., Kung, M.C., and Costello, C.K. (2003) Supported Au catalysts for low temperature CO oxidation, *J. Catal.* 216, 425.

Lambert, J., Shurvell, H., Lightner, D., and Cooks, R. (1998) *Organic Structural Spectroscopy*, Prentice Hall Inc., Upper Saddle River, NJ.

Langevin, D., Pinoche, M., Selegny, E., Metayer, M., and Roux, R. (1993), CO<sub>2</sub> facilitated transport through functionalized cation-exchange membranes, *J. Membr. Sci.* 82, 51.

LeBlanc, O. H., Ward, W. J., Matson, S. L., and Kimura, S.G. (1980), Facilitated transport in ion-exchange membranes, *J. Membr. Sci.* 6, 339.

Ledjeff-Hey, K., Roes, J., and Wolters, R. (2000), CO<sub>2</sub>-scrubbing and methanation as purification system for PEFC, *J. Power Sources* 86, 556.

Li, J., Chen, C., Han, B., Peng, Y., Zou, J., and Jiang, W. (2002) Laboratory and pilot-scale study on dehydration of benzene by pervaporation, *J. Membr. Sci.* 203, 127.

Lin, H., and Freeman, B. D. (2005a), Materials selection guidelines for membranes that remove CO<sub>2</sub> from gas mixture, *J. Mol. Struct.* 739, 57.

Lin, H., and Freeman, B. D. (2005b) Gas and vapor solubility in cross-linked poly(ethylene glycol diacrylate), *Macromolecules* 38, 8394.

- Lin, H., Kai, T., Freeman, B. D., Kalakkunnath, S., and Kalika, D. S. (2005) The effect of cross-linking on gas permeability in cross-linked poly(ethylene glycol diacrylate), *Macromolecules*, 38, 8381.
- Lin, H., Wagner, E. V., Raharjo, R., Freeman, B. D., and Roman, I. (2006a) High-performance polymer membranes for natural-gas sweetening, *Adv. Mater.* 18, 39.
- Lin, H., Wagner, E. V., Freeman, B. D., Toy, L. G., and Gupta, R. P. (2006b) Plasticization-enhanced hydrogen purification using polymeric membranes, *Science* 311, 639.
- Manasilp, A.; and Gulari, E. (2002), Selective CO oxidation over Pt/alumina catalysts for fuel cell applications, *Appl. Catal., B* 37, 17.
- Matsuyama, H., Teramoto, M., and Iwai, K. (1994), Development of a new functional cation-exchange membrane and its application to facilitated transport of CO<sub>2</sub>, *J. Membr. Sci.* 93, 237.
- Matsuyama, H., Teramoto, M., Sakakura, H., and Iwai, K. (1996), Facilitated transport of CO<sub>2</sub> through various ion exchange membranes prepared by plasma graft polymerization, *J. Membr. Sci.* 117, 251.
- Matsuyama, H., Terada, A., Nakagawara, T., Kitamura, Y., and Teramoto, M. (1999), Facilitated transport of CO<sub>2</sub> through polyethylenimine/poly(vinyl alcohol) blend membrane, *J. Membr. Sci.* 163, 221.
- Matsuyama, H., Teramoto, M., Matsui, K., and Kitamura, Y. (2001), Preparation of poly(acrylic acid)/poly(vinyl alcohol) membrane for the facilitated transport of CO<sub>2</sub>, *J. Appl. Polym. Sci.* 81, 936.
- Meisen, A., and Shuai, X. (1997), Research and development issues in CO<sub>2</sub> capture, *Energy Convers. Manage.* 38, Suppl., S37.
- Moe, J. M. (1962), Design of water-gas-shift reactors, *Chem. Eng. Prog.* 58, 33.
- Meldon, J. H., Smith K. A., and Colton C. K. (1977), The effect of weak acids upon the transport of carbon dioxide in alkaline solutions, *Chem. Eng. Sci.* 32, 939.
- Noble, R. D. (1990), Analysis of facilitated transport with fixed site carrier membranes, *J. Membr. Sci.* 50, 207.

- Noble, R. D. (1991), Facilitated transport mechanism in fixed site carrier membranes, *J. Membr. Sci.* 60, 297.
- Noble, R. D. (1992), Generalized microscopic mechanism of facilitated transport in fixed site carrier membranes, *J. Membr. Sci.* 75, 121.
- Oh, S.H., and Sinkevitch, R.M. (1993), Carbon monoxide removal from hydrogen-rich fuel cell feedstreams by selective catalytic oxidation, *J. Catal.* 142, 254.
- Pritchard, J.G. (1970) *Poly(vinyl alcohol), Basic Properties and Uses*, Gordon and Breach Science Publishers, London, UK.
- Quinn, R., Appleby, J. B., and Pez, G. P. (1995), New facilitated transport membranes for the separation of carbon dioxide from hydrogen and methane, *J. Membr. Sci.* 104, 139.
- Quinn, R., and Laciak, D. V. (1997), Polyelectrolyte membranes for acid gas separations, *J. Membr. Sci.* 131, 49.
- Quinn, R., Laciak, D. V., and Pez, G. P. (1997), Polyelectrolyte-salt blend membranes for acid gas separations, *J. Membr. Sci.* 131, 61.
- Salmi, T., and Hakkarainen, R. (1989), Kinetic study of low-temperature water-gas shift reactor over a Cu-ZnO catalyst, *Appl. Catal.* 49, 285.
- Sartori, G., and Savage, D. W. (1983), Sterically hindered amines for CO<sub>2</sub> removal from gases, *Ind. Eng. Chem. Fundam.* 22, 239.
- Sartori, G., Ho, W. S., Savage, D. W., Chludzinski, G. R., and Wiechert, S. (1987), Sterically-hindered amines for acid-gas absorption, *Sep. Purif. Methods* 16, 171.
- Sedmak, G., Hocevar, S., and Levec, J. (2003), Kinetics of selective CO oxidation in excess of H<sub>2</sub> over the nanostructured Cu<sub>0.1</sub>Ce<sub>0.9</sub>O<sub>2-y</sub> catalyst, *J. Catal.* 213, 135.
- Scholander, P. F. (1960), Oxygen transport through hemoglobin solutions, *Science* 131, 585.
- Shin, M., Kim, S. J., Park, S. J., Lee, Y. H., and Sun S. I. (2002), Synthesis and characteristics of the interpenetrating polymer network hydrogel composed of chitosan and polyallylamine, *J. Appl. Polym. Sci.* 86, 498.
- Smith, D. R., and Quinn, J. A. (1979), The prediction of facilitation factors for reaction augmented membrane transport, *AIChE J.* 25, 197.

- Smith, J. M., Van Ness, H. C., and Abbott, M. M. (2005) *Introduction to Chemical Engineering Thermodynamics*, 7th ed.; McGraw-Hill Companies, Inc.: New York, NY.
- Song, C., (2002), Fuel processing for low-temperature and high-temperature fuel cells: Challenges, and opportunities for sustainable development in the 21st century, *Catal. Today* 77, 17.
- Tee, Y. H., Zou, J., and Ho, W. S. W. (2006), CO<sub>2</sub>-selective membranes containing dimethylglycine mobile carriers and polyethylenimine fixed carrier, *J. Chin. Inst. Chem. Engrs.* 37, 37.
- Teramoto, M., Takeuchi, N., Maki, T., and Matsuyama, H. (2001), Gas separation by liquid membrane accompanied by permeation of membrane liquid through membrane physical transport, *Sep. Purif. Technol.* 24, 101.
- Teramoto, M., Takeuchi, N., Maki, T., and Matsuyama, H. (2002), Facilitated transport of CO<sub>2</sub> through liquid membrane accompanied by permeation of carrier solution, *Sep. Purif. Technol.* 27, 25.
- Teramoto, M., Kitada, S., Ohnishi, N., Matsuyama H., and Matsumiya, N. (2004), Separation and concentration of CO<sub>2</sub> by capillary-type facilitated transport membrane module with permeation of carrier solution, *J. Membr. Sci.* 234, 83.
- Tosti, S., Basile, A., Chiappetta, G., Rizzello, C., and Violante, V. (2003), Pd-Ag membrane reactors for water gas shift reaction, *Chem. Eng. J.* 93, 23.
- Twigg, M. V. (1989) *Catalyst Handbook*; Wolfe Publishing Ltd.: London, UK.
- Uemiya, S., Sato, N., Ando, H., and Kikuchi, E. (1991), The water gas shift reaction assisted by a palladium membrane reactor, *Ind. Eng. Chem. Res.* 30, 585.
- U.S. Department of Energy (2005), Emissions of greenhouse gases in the United States 2004, available at <ftp://ftp.eia.doe.gov/pub/oiaf/1605/cdrom/pdf/ggrpt/057304.pdf>, (accessed March 2006).
- Ward, W. J., and Robb, W. L. (1967), Carbon dioxide-oxygen separation: facilitated transport of carbon dioxide across a liquid film, *Science* 156, 1481.
- Ward, W. J. (1970), Analytical and experimental studies of facilitated transport, *AIChE J.* 16, 405.

Way, J. D., Noble, R. D., Reed, D. L., Ginley, G. M., and Jarr, L. A. (1987), Facilitated transport of CO<sub>2</sub> in ion exchange membranes, *AIChE J.* 33, 480.

Way, J. D., and Noble, R. D. (1992), Facilitated transport. In *Membrane Handbook*, (W. S. W. Ho, and K. K. Sirkar, eds.), Chapman & Hall, New York, NY, p. 834.

Wind, J. D., Paul, D. R., and Koros, W. J. (2004), Natural gas permeation in polyimide membranes, *J. Membr. Sci.* 228, 227.

Xue, E., O'Keeffe, M., and Ross, J. R. H. (1996), Water-gas shift conversion using a feed with a low steam to carbon monoxide ratio and containing sulphur, *Catal. Today* 30, 107.

Yamaguchi, T., Boetje, L. M., Koval, C. A., Noble, R. D., and Brown, C. N. (1995), Transport properties of carbon dioxide through amine functionalized carrier membranes, *Ind. Eng. Chem. Res.* 34, 4071.

Yamaguchi, T., Koval, C. A., Noble, R. D., and Bowman, C. N. (1996), Transport mechanism of carbon dioxide through perfluorosulfonate ionomer membranes containing an amine carrier, *Chem. Eng. Sci.* 51, 4781.

Zolandz, R. R., and Fleming, G. K. (1992), Gas permeation. In *Membrane Handbook*, (W. S. W. Ho, and K. K. Sirkar, eds.), Chapman & Hall, New York, NY, p. 27.